PEOPLE'S DEMOCRATIC REPUBLIC OF ALGERIA
Ministry of Higher Education and Scientific Research

University of Amar Telidji - Laghouat

Faculty of Technology
Department of Electrotechnic

MASTER THESIS

DOMAIN: Science & Technology
FIELD: Automatic
SPECIALTY: Automatic and systems

GHOUINI Mohammed Nadhir & **MEDJDEN Abdelsabour Zakaria**

Theme

Flatness-Based Control of Parallel Inverters in a Microgrid

Jury members:

BENDJEDIA Bachir	MCA	President
BENMILOUD Mohammed	MCB	Examiner
BOUGRINE Mohammed Djameleddine	MCB	Examiner
BENALIA Atallah	Pr	Supervisor
BENZOUBIR Mohammed Elamine	PhD Student	Co-Supervisor

2023 / 2024

Acknowledgements

With the help of Almighty God, we were able to accomplish this work, which was carried out within the LACoSERE laboratory and the Electrical Engineering Department at Amar Telidji University of Laghouat.

At the end of this work, we would like to thank our supervisor, Mr. Atallah BENALIA, for your trust in us and your humble approach with us. We are deeply grateful for your immense knowledge and the way you generously share it with us. Your humble nature and patience have made a profound impact on our personal and professional growth. Your guidance has been invaluable, and your ability to lead with such grace and understanding is truly inspiring. Thank you for your unwavering support and for always being there to help us navigate challenges. We hope to continue learning from you and to meet the high standards you set.

We would like to express our heartfelt thanks to Dr.BENMILOUD Mohammed and Dr.BOUGRINE Mohammed Djameleddine for always answering our questions whenever we approached you. Your assistance and support have been invaluable, and we appreciate it so much.

we would like to thank co-supervisor Mr.BENZOUBIR Mohammed Elamine (PhD Student) , for his contribution to this project.

we would like to thank the jury president Mr.BENDJEDIA Bachir

We would also like to thank the members of the jury for accepting to examine our work,Thank you for the constructive remarks, and for your relevant comments.

We express our gratitude to all professors who contributed to our academic journey.

Dedication

Thanks to Allah for granting us success in completing this work.

To my family:

I want to thank my parents, **Seghier** and **Sultana**, for their prayers and for standing by me in everything I did. Your unwavering support has been my foundation.

I would like to thank my brothers, **Tarek** and **Youcef**, and my sisters , **Sarra** and **Imane** and **Soumia**, for their support and encouragement. Your belief in me has been a source of strength.

To my colleagues:

I want to thank my colleague, **Medjden Abelsabour Zakaria**, who was by my side throughout the academic path. Your companionship and support were invaluable.

To my friends:

To my friend, **Harran**, thank you for your encouragement and support in everything.

To everyone who has helped us:

Finally, I thank everyone who supported and encouraged me in completing this thesis.

Ghouini Mohammed Nadhir

Dedication

To my family:

To my dear father,

Before Alzheimer's took hold, you encouraged me to make my diploma, knowledge, and mind my greatest weapons. You might not remember that you are my father and that you told me this, but I will always remember. Your unwavering belief in my potential has been my guiding light and the driving force behind my perseverance.

To my loving mother,,thank you for being strong, thank you for all the help that you have given us, and thank you for teaching us how to be strong and fight during the hard times. Your endless support, nurturing care, and sacrifices have been the bedrock of our family. Your strength and resilience have inspired me every day to strive for excellence.

To my sisters, I am very lucky to have you as my sisters. Thank you for all the love and support. Your constant companionship, understanding, and unwavering support have been a source of joy and motivation in my life.

To my dear friend:

To my dear college friend,GHOUINI Mohammed Nadhir,

We met in the first year of college and have supported each other in our studies despite the challenges. Thank you for that.

With all my love and gratitude,

Medjden Abdelsabour Zakaria

Abstract: Globally, the push toward eco-friendly energy solutions is growing, highlighting the pivotal role of micro-grid technology in facilitating renewable energy integration. This dissertation concentrates on a critical element of AC micro-grid management—specifically, the control of inverters. The main objective of this dissertation is to enhance power quality, enable effective load sharing, and manage circulating currents, to address these challenges, a one-loop, flatness- based control strategy is proposed for the management of a single inverter and multiple inverters in parallel. This control strategy capitalizes on the advantage of state and input variables that can be directly expressed through flat outputs and their derivatives, facilitating precise trajectory generation. This approach notably leverages the inherent advantages of flatness to improve system response and operational efficacy. The study presented in this dissertation could significantly contribute to the fields of micro-grid management and sustainable energy practices.

Key-words: Micro-grid, Flatness-based control, Inverter, Circulating currents.

ملخص :عالميًا، تتزايد الحركة نحو حلول الطاقة الصديقة للبيئة، مما يبرز الدور الحاسم لتكنولوجيا الشبكات الصغيرة في تعزيز دمج الطاقة المستدامة. تركز هذه الرسالة على عنصر حيوي في إدارة شبكات الـ AC الصغيرة—وهو التحكم في المحولات. الهدف الأساسي لهذه الرسالة هو تحسين جودة الطاقة، تسهيل مشاركة الأحمال بفعالية، وإدارة التيارات المتداولة. لمواجهة هذه التحديات، نقترح استراتيجية تحكم مبنية على نظام تحكم واحد مستند إلى التحكم المعتمد على التسطيح لإدارة محول واحد وعدة محولات بالتوازي. تستغل هذه الاستراتيجية فوائد المتغيرات الحالة والمدخلات، التي يمكن التعبير عنها مباشرة من خلال النواتج المسطحة ومشتقاتها، مما يتيح توليد مسارات دقيقة. تستفيد هذه الطريقة بشكل فعال من المزايا الأساسية للتحكم المبني على التسطيح لتعزيز استجابة النظام وكفاءته التشغيلية. الرؤى التي تمت مناقشتها في هذه الرسالة لديها القدرة على

الإسهام بشكل كبير في مجالات إدارة الشبكات الصغيرة وممارسات الطاقة المستدامة.

الكلمات المفتاحية: شبكات صغيرة، التحكم المبني على السطحية، المحول، التيارات المتداولة.

Résumé : À l'échelle mondiale, le mouvement vers des solutions énergétiques respectueuses de l'environnement prend de l'ampleur, soulignant le rôle crucial de la technologie des micro-réseaux dans la promotion de l'intégration de l'énergie renouvelable. Cette thèse se concentre sur un élément essentiel de la gestion des micro-réseaux AC—spécifiquement, le contrôle des onduleurs. L'objectif principal de cette thèse est d'améliorer la qualité de l'énergie, de faciliter le partage de charge efficace, et de gérer les courants circulants, pour relever ces défis, une stratégie de contrôle basée sur une boucle unique et utilisant la commande basée sur la platitude est proposée pour la gestion d'un onduleur unique et de plusieurs onduleurs en parallèle. Cette stratégie tire parti des avantages des variables d'état et d'entrée, qui peuvent être directement exprimées à travers les sorties plates et leurs dérivées, facilitant ainsi la génération de trajectoires précises. Cette approche exploite efficacement les avantages inhérents de la commande basée sur la platitude pour améliorer la réponse du système et l'efficacité opérationnelle. L'étude présentées dans cette thèse pourraient contribuer de manière significative aux domaines de la gestion des micro-réseaux et des pratiques énergétiques durables.

Mots-clés : Micro-réseau, Commande basée sur la platitude, Onduleur, Courants circulants.

Contents

List of Figures

List of Tables

Nomenclature

AC : Alternating Current

C_f : Capacitance of the AC bus

DC : Direct Current

$DERs$: Distributed Energy Resources

FBC : Flatness Based Control

i_a : Phase A Current

i_b : Phase B Current

i_c : Phase C Current

i_{0k} : 0dq component of line currents from the k-th inverter (zero sequence)

i_{d1} : dq component of line currents from the first inverter (d-axis)

i_{dk} : 0dq component of line currents from the k-th inverter (d-axis)

i_{la} : Load Current for Phase A

i_{lb} : Load Current for Phase B

i_{lc} : Load Current for Phase C

i_{Ld} : dq component of load currents (d-axis)

i_{Lq} : dq component of load currents (q-axis)

i_{q1} : dq component of line currents from the first inverter (q-axis)

i_{qk} : 0dq component of line currents from the k-th inverter (q-axis)

L_1 : Inductance of the filter at the output of the first inverter

L_k : Inductance of the filter at the output of the k-th inverter

MGD : Microgrid

r_1 : Resistance of the filter at the output of the first inverter

r_k : Resistance of the filter at the output of the k-th inverter

UPS : Uninterruptible Power Supply

v_a : Phase A Voltage

v_b : Phase B Voltage

v_c : Phase C Voltage

V_{0k} : Control voltage in the Park reference frame for the k-th inverter (zero sequence)

v_{ca} : Line Voltage between Phase C and Phase A

v_{cb} : Line Voltage between Phase C and Phase B

v_{cc} : Line Voltage between Phase C and Phase C

V_{cd} : Park component corresponding to the AC bus capacitor voltage (d-axis)

V_{cq} : Park component corresponding to the AC bus capacitor voltage (q-axis)

V_{d1} : Control voltage in the Park reference frame for the first inverter (d-axis)

V_{dk} : Control voltage in the Park reference frame for the k-th inverter (d-axis)

V_{q1} : Control voltage in the Park reference frame for the first inverter (q-axis)

V_{qk} : Control voltage in the Park reference frame for the k-th inverter (q-axis)

V_{RMS} : Root Mean Square Voltage

General Introduction

Over the decades, awareness of the environmental impacts of fossil fuels has increased. Initially, during the Industrial Revolution, they were noted for causing visible air pollution. By the mid-20th century, the broader consequences, such as increased greenhouse gas emissions and global warming, became clear. This realization led to international efforts to reduce emissions by the late 20 th century[26]. Renewable energy (RE) has since become a key strategy to reduce these emissions and meet growing global energy demands, aligning with environmental and economic goals. Within this framework, Algeria has actively expanded its renewable energy capacity, setting a target of 22,000 MW by 2030, up from an initial goal of 11,000 MW [4], reflecting its commitment to renewable initiatives.

This thesis focuses on autonomous AC microgrids (MGs), which are small, self-sufficient electricity networks composed of distributed generators (DGs) that produce electricity from renewable energy sources (RES) like wind and solar power. The main objective is to develop effective control mechanisms to ensure power sharing and stability in islanded MGs. This involves balancing power supply and demand, maintaining power quality in terms of frequency and voltage, and ensuring the overall robustness and stability of the system.

This thesis was developed as part of the Master's program in Automatic Control at the LACoSERE Laboratory, University of Laghouat. The research is structured into three chapters:

Chapter 1 of this thesis introduces MGs as a key element for electricity production based on DGs. This chapter discusses their advantages and disadvantages, examines various types of MGs, and highlights the essential role and classification of inverters. It then addresses the necessity of parallel inverters, followed by an overview of control strategies. Finally, advanced control strategies are discussed, with special focus on flatness-based control.

In Chapter 2, a three-phase inverter with an LC filter is modeled using Kirchhoff's laws

and Park's transformation to simplify its dynamics. A robust control strategy is implemented through a single-loop controller based on differential flatness control. The performance, stability, and robustness of the inverter are assessed through various tests conducted using MATLAB Simulink and SimPower. These evaluations confirm the effectiveness of the proposed control strategy in controling autonomous inverters, even in the presence of parameter variations.

Building on this foundation, Chapter 3 extends the application of the single-loop control based on flatness approach to an isolated power supply system comprising multiple parallel inverters. Each inverter draws power from a DG source and converts it to AC power, which is subsequently supplied to the AC load. This chapter aims to design a flatness-based controller to ensure equal power sharing among inverters, while addressing parallel operation issues such as circulating currents. A notable advantage of this control method is its ability to achieve a high control bandwidth, which not only mitigates circulating currents but also improves the power quality at the Point of Common Coupling (PCC). The effectiveness of the proposed controller was evaluated through simulation results using MATLAB/Simulink software. All results were thoroughly analyzed and discussed, providing a comprehensive assessment of the system's performance.

Finally, a conclusion summarizes the work and offers some perspectives for future research.

Chapter 1

Microgrid System: Description and Control

1.1 Introduction

With growing concerns about the environment, the world is moving towards cleaner energy solutions. This trend has captivated policymakers and researchers alike,leading to a worldwide effort to create new electrical systems that focus on using renewable energy sources like solar and wind power.

This chapter lays the groundwork for understanding MGs by exploring their advantages, limitations, and operational principles. It delves into the complexities of DC-AC converters (inverters), examining their various types and their roles within MG structures. Finally, the chapter analyzes the diverse control strategies used to control parallel inverters in MGs.

1.2 MGs: A Localized Power Network

A MG represents a localized, self-contained electricity system comprising various distributed energy resources (DERs) and loads, as illustrated in Figure. 1.1. Unlike conventional centralized grids, MGs have the capability to operate in both, autonomous or grid-connected mode, offering increased resilience, flexibility, and reliability. They are commonly found in areas such as communities, campuses, and industrial complexes, where they provide reliable power supply,

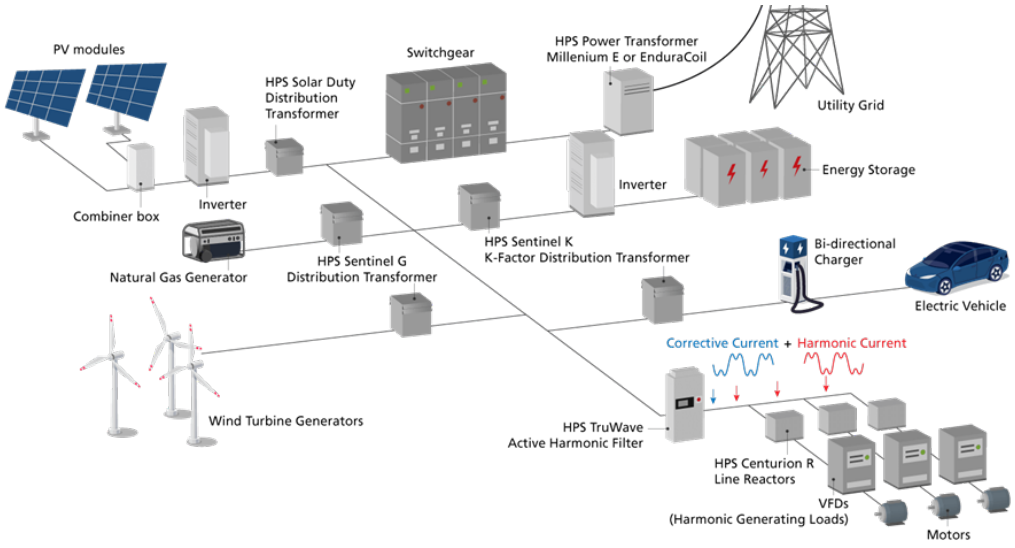

Figure 1.1: Basic structure of a microgrid

integrate renewable energy sources like solar and wind, and support local control and optimization of energy distribution[23]. One of the key advantages of MGs is their ability to continue functioning independently during grid outages, ensuring uninterrupted power supply to critical facilities and enhancing overall energy security. Additionally, MGs contribute to grid stability and reliability by providing ancillary services such as frequency regulation and voltage support. As the demand for cleaner, more resilient energy solutions grows, MGs are increasingly being recognized as a viable and valuable component of the modern energy landscape, offering benefits to both communities and utilities alike[13].

1.3 Advantages and disadvantages of MGs

1.3.1 advantages of MGs

The emergence of MGs is driven by several key advantages they offer over traditional grid systems:

- **Integration of Renewable Energy Sources:** MGs offer a perfect platform for integrating renewable energy sources like solar and wind power. This promotes a cleaner and more sustainable energy future by reducing reliance on fossil fuels and associated greenhouse gas emissions [11].

- **Enhanced Grid Reliability and Resilience:** By providing islanding mode operation, MGs improve overall grid resilience. Critical loads within the MG can remain powered even during widespread outages on the main grid [10].
- **Improved Power Quality:** MGs can regulate voltage and frequency fluctuations, leading to cleaner and more stable power for sensitive equipment. This is particularly beneficial for data centers, hospitals, and other facilities requiring a reliable and high-quality power supply [13].
- **Increased Efficiency and Reduced Losses:** MGs promote efficient energy use through localized generation and consumption. This reduces reliance on long-distance transmission lines, minimizing transmission and distribution losses associated with traditional centralized grids [17].
- **Reduced Reliance on Centralized Generation:** MGs empower communities and critical infrastructure with a degree of energy independence, potentially reducing reliance on centralized power plants [1].

1.3.2 Disadvantages of MGs

Despite their numerous advantages, MGs also have some limitations to consider:

- **Higher Initial Investment Costs:** Setting up a MG can be more expensive compared to traditional grid infrastructure due to the initial costs associated with DERs, control systems, and communication networks [13].
- **Intermittent Renewable Energy Sources:** MGs heavily reliant on renewable sources like solar and wind power may face challenges due to the intermittent nature of these resources. Storage solutions or backup generators might be necessary to ensure consistent power supply [16].
- **Technical Complexity:** MG control systems require sophisticated algorithms to manage power flow, optimize energy use, and ensure seamless transitions between grid-connected and island mode operation. This can add complexity to the overall system design and operation [17].

1.4 Types of MGs

1.4.1 From a Connection Standpoint

Grid-connected MG:

These MGs are connected to the main utility grid and can operate both in grid-connected mode and in islanded mode when disconnected from the main grid during emergencies or for other reasons [13].

Islanded MG:

Islanded MGs are completely disconnected from the main grid and operate independently, relying solely on their internal energy resources to meet local demand. They are designed to maintain power supply during grid outages [2].

1.4.2 From an Operational Configuration Standpoint

AC MG:

AC MGs predominantly use alternating current (AC) for power distribution. They are compatible with most conventional electrical loads and equipment and often employ inverters to integrate renewable energy sources into the grid [13].

DC MG:

DC MGs utilize direct current (DC) for power distribution. They are efficient for certain applications such as data centers, telecommunications facilities, and residential buildings, where DC loads are prevalent, and can directly integrate with DC-based renewable energy sources and energy storage systems [2].

Hybrid MG:

Hybrid MGs combine both AC and DC components, allowing for flexible energy management and optimization. They leverage the advantages of both AC and DC systems and are suitable for diverse applications ranging from remote communities to urban settings [13].

1.5 Definition of an Inverter

An inverter is an electrical device that converts direct current (DC) into alternating current (AC). It is commonly used in various applications such as solar photovoltaic systems, wind turbines, electric vehicles, and uninterruptible power supplies (UPS). In renewable energy systems, inverters play a crucial role in converting the DC power generated by solar panels or wind turbines into AC power that can be fed into the electrical grid or used to power AC loads. In addition to conversion, inverters may also provide functions such as voltage regulation, frequency control, and grid synchronization.[24]

1.6 Classification of inverters

1.6.1 Grid following inverters

Grid-following inverters are a control strategy for inverter-based energy sources that synchronize their output with the grid's voltage and frequency. These inverters are current sources that track the grid angle and magnitude to inject or absorb active and reactive power. They depend on the grid to provide a stable voltage and frequency reference and cannot operate in islanded or off-grid mode.[21]

1.6.2 Grid forming inverters

Grid-forming inverters are a crucial technology for integrating more renewable energy sources into the grid and ensuring its reliability and stability. They refer to the ability of an inverter-based energy source, such as solar, wind, or batteries, to provide voltage and frequency support to the grid, especially during disturbances or outages. Grid-forming inverters can operate independently or in coordination with other sources, and they can help restore the grid after a blackout. Their capability to autonomously establish grid parameters makes them essential for the transition to a more renewable energy-driven grid.[21]

1.7 Parallel Inverters

1.7.1 The purpose of using parallel inverters

In a grid-connected context, utilizing a single inverter presents significant challenges, particularly in the provision of reactive energy and the maintenance of stable voltage and frequency during peak demand periods. The reliance on a single inverter can lead to potential reliability issues, as any malfunction or shutdown can disrupt the entire microgrid operation. Furthermore, maintenance tasks become more complex, as downtime for a single inverter can halt all dependent processes. To address these challenges effectively, a parallel arrangement of inverters offers a practical solution, see Figure. 1.2. This approach not only increases the power capacity but also significantly enhances system reliability. The implementation of parallel inverters provides several key benefits, including improved system resilience in the event of a failure of one or more units, and simplified maintenance planning without compromising overall system operation. In summary, the deployment of parallel inverters mitigates the risks associated with relying on a single unit, ensuring continuous operation and efficient maintenance in grid-connected applications.

However, the use of parallel inverters introduces its own set of challenges, The next section will discuss this.

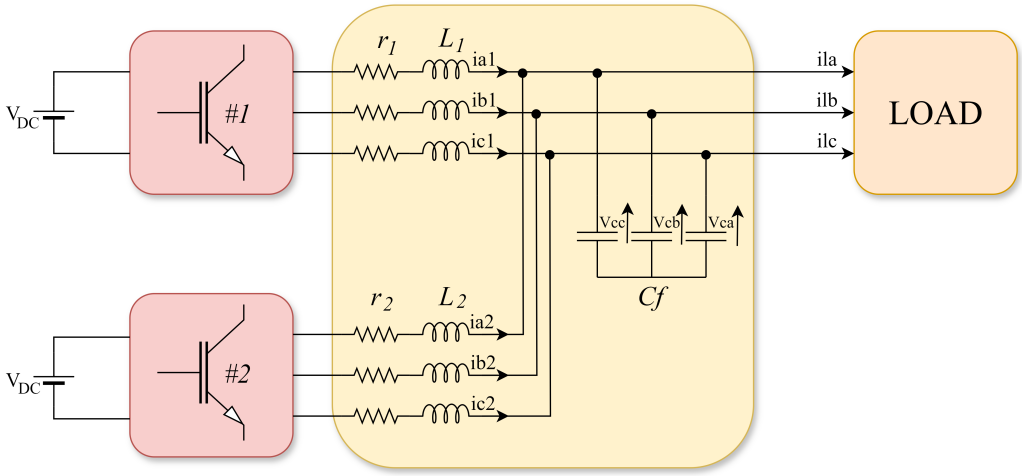

Figure 1.2: Circuit structure for the 2-parallel connected inverters

1.7.2 Challenges of using parallel inverters

While parallel inverters offer significant advantages, they also present several challenges that must be addressed to ensure reliable and efficient operation. These challenges include:

- **Circulating Currents:** Unwanted currents flowing between inverters can cause increased losses and potential damage [27].
- **Synchronization:** Ensuring all inverters operate in phase is crucial to avoid power quality issues [15].
- **Load Sharing:** Achieving proportional load distribution among inverters to prevent overloading and inefficiencies [12].
- **System Stability:** Maintaining stability in the overall power system, especially under varying load conditions [6].
- **Control Complexity:** Advanced control strategies are required, increasing system design complexity and cost. The control of parallel inverters in AC microgrids involves various strategies, generally categorized into centralized and decentralized approaches.
  More advanced techniques, such as droop control and flatness-based control, are also utilized to enhance performance and reliability; [17][11]

1.8 MG Control Strategies

In the realm of MG control, various methodologies are employed to regulate the distributed energy resources and ensure grid stability. Two common approaches are centralized control and decentralized control.

Centralized Control: In this structure, a central controller (the master) oversees and coordinates the actions of subordinate controllers (the slaves). This method allows for centralized decision-making, streamlining control processes and ensuring consistency in system operations. However, master-slave control can face challenges with scalability and increased communication demands, particularly in larger MG systems. These issues can lead to communication overheads and reduced efficiency as the system scales up[19].

Decentralized Control: Centralized control involves a single controller managing the entire MG operation, providing a cohesive approach to system regulation. In contrast, decentralized control distributes control tasks across multiple controllers, enhancing system resilience through redundancy. However, decentralized control may necessitate sophisticated coordination algorithms to ensure seamless operation[23].

1.9 Advanced Control Strategies: Flatness-Based Control

In order to facilitate the analysis and control of nonlinear systems, automation engineers have always sought to simplify complex models to linear models that are easy to study. A flatness approach proposed in 1992 by Fliess et al. [7], allowing the dynamic behavior of a system to be parameterized in a simple way, based on variables called linearizing (or flat) output. The system is then linearizable by dynamic looping using the flat outputs and a finite number of their derivatives. Figure. 1.3 shows the correspondence between the flat outputs and the state variables.

FBC achieves robust control by combining feed-forward and feedback components, leveraging the principles of differential flatness. Consider the nonlinear system:

$$\dot{x} = f(x, u) \tag{1.1}$$

where $x \in \mathbb{R}^n$ is the state and $u \in \mathbb{R}^m$ is the input.

Definition: The system is deferentially flat iff, the flat output $y \in \mathbb{R}^m$ can be defined as:

$$y = \varphi_y(x, u, \dot{u}, \ldots, u^l) \tag{1.2}$$

Such that:

$$\begin{cases} x = \varphi_x(y, \dot{y}, \ldots, y^r) \\ u = \varphi_u(y, \dot{y}, \ldots, y^{r+1}) \end{cases} \tag{1.3}$$

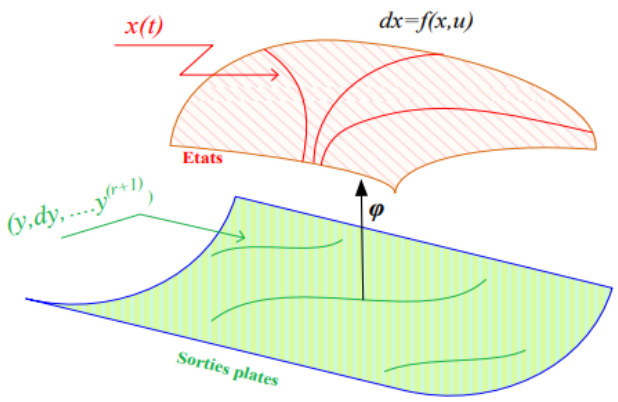

Figure 1.3: The correspondence between the trajectories of flat outputs and those of state variables.

Locally satisfying:

$$\text{rank}(\varphi_y) = m, \quad \text{rank}(\varphi_x) = n, \quad \text{rank}(\varphi_u) = m.$$

Given a desired trajectory $y_d(t)$, the corresponding feed-forward control (open-loop control) can be explicitly generated from:

$$u_f = \varphi_u(y_d(t), \dot{y}_d(t), \ldots, y_d^{r+1}(t)). \tag{1.4}$$

However, real systems experience perturbations and parameter variations, necessitating feedback mechanisms to compensate for these effects. FBC incorporates feedback to address deviations caused by disturbances, including parameter variations and external perturbations. Unlike traditional control strategies that rely on disturbance feedback, flat controllers use reference feedback, reducing the impact of noise. This approach enhances FBC's robustness against erroneous feedback measurements, making it highly effective in practical implementations.

The overall control law is given by:

$$u_f = \varphi_u(y_d(t), \dot{y}_d(t), \ldots, v). \tag{1.5}$$

1.9.1 Trajectory Planning for Flat Systems

The concept of flatness provides a robust solution to a significant challenge in control theory concerning trajectory planning. The primary aim of trajectory planning is to devise a closed-loop control law to guide a given system from a known initial state to a desired final state, as illustrated in Figure 1.4. For flat systems, the key approach to solving the planning problem involves initially conducting planning for the equivalent linear system and then mapping back to the original system using endogenous coordinate transformations[25][7].

The core objective of trajectory planning is to determine the control vector $u(t)$ over a finite time horizon T to steer the system from the initial state $x(0)$ to the desired final state $x(T)$.

$$x(0) = A(y(0), \ldots, y^{(n)}(0))$$

$$x(T) = A(y(T), \ldots, y^{(n)}(T))$$

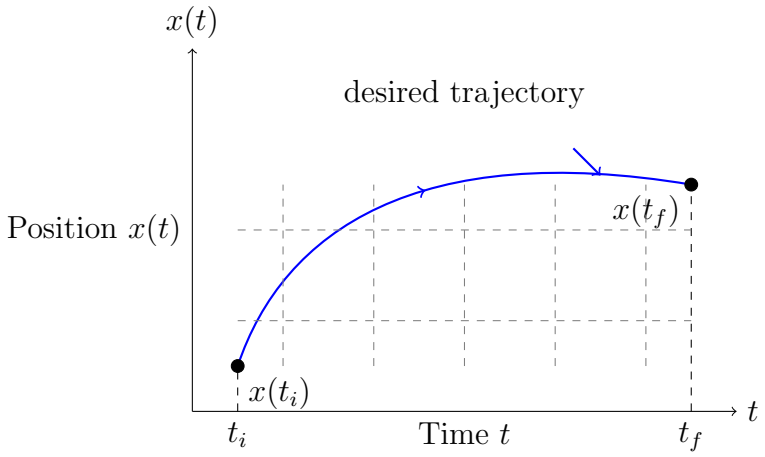

Figure 1.4: Desired trajectory between two equilibrium points (t_i,$x(t_i)$) and (t_f,$x(t_f)$).

1.9.2 Tracking: feedback linearization

In preceding discussions, our emphasis has been on the development of open-loop trajectories, under the assumptions of perfect knowledge of the system model and exact initial condition determination. Well-structured reference open-loop trajectories (x_r, u_r) typically result in the system closely approximating the desired trajectory. However, to effectively manage environmental disturbances and accommodate minor model uncertainties, robust tracking of constrained

open-loop trajectories necessitates the integration of feedback control mechanisms. Incorporating feedback control not only ensures stability but also enhances the approach's resilience to uncertainties and disturbances[7][25].

Where we have defined $y^{r+1} = \gamma$. The additional control $\gamma \in \mathbb{R}^n$ is given by the equation

$$0 = \left(\gamma_i - y_{di}^{r+1}(t)\right) + \sum_{j=0}^{r} k_{ij} \cdot \left(y_i^{(r-j)}(t) - y_{di}^{(r-j)}(t)\right) + k_{i(r+1)} \int \left(y_i(\tau) - y_{di}(\tau)\right) d\tau \tag{1.6}$$

For $i = 1 \cdots m$ and where we have noted by $y_i^{(j)}(t) = \frac{d^j y(t)}{dt^j}$ and $y_{di}^{(k)}(t) = \frac{d^j y_d(t)}{dt^j}$. The equation (1.6) can be put in matrix form.

$$0 = \left(\gamma - y_d^{r+1}(t)\right) + KE + K_{r+1} \int \left(y_i(\tau) - y_{di}(\tau)\right) d\tau$$

where $E^T = \begin{bmatrix} (y_i^r(t) - y_{di}^r(t) & \cdots & (y_i^r(t) - y_{di}^r(t) \end{bmatrix}$ and $K = [k_{ij}] \in \mathbb{R}^{m \times (r+1)}$. From (1.6), the dynamic error for each component of the flat output is given by

$$0 = e_i^{r+2} + \sum_{j=0}^{r} k_{ij} \cdot e_i^{(r-j+1)} + k_{(r+1)j} \cdot e_i \tag{1.7}$$

The characteristic of this linear dynamic is

$$0 = \left(s^{r+2} + k_{i0} s^{r+1} + \cdots + k_{i(r-1)} s^2 + k_{ir} s + k_{i(r+1)}\right) \cdot e_i \tag{1.8}$$

Its dynamic depends on the choice of the controller parameters polynomial k_{ij}. By matching these parameters to a desired one, we can compute these controller parameters.

In the preceding development of the controller, the reference trajectory should be given or generated. In real applications, we should generate the reference trajectory based on the desired behavior. We propose to use a low pass filter of appropriate order to plan the reference trajectory of the flat output that links an initial value noted $y_{di}(t_0)$ at the initial time t_0 and

the desired value noted y_{diset}. Thus, the trajectory of each component $y_{di}(t)$ is defined by

$$y_{di}(t) = y_{di}(t_0) + \mathcal{L}^{-1}\left\{F_i(s)\left(y_{diset} - y_{di}(t_0)\right)(s)\right\} \quad i = 1, \cdots, m \tag{1.9}$$

Where $F_i(p)$ is a stable transfer function with $F_i(0) = 1$ with appropriate dynamics.

1.10 Advantages of Flatness Control

Simplified Controller Design: Flatness-based control simplifies controller design by transforming system dynamics into a form where outputs are explicitly expressed in terms of inputs and their derivatives. This reduces controller complexity and facilitates easier implementation[7].

Precise Trajectory Tracking: By directly controlling flat outputs, flatness-based controllers achieve accurate trajectory tracking, even in the presence of disturbances. This enables superior performance compared to traditional methods, especially in complex systems[7].

Robustness to Parameter Variations: Flatness-based control inherently handles parameter variations and model uncertainties with minimal impact on performance. This robustness makes it suitable for real-world applications where uncertainties are common[7].

Reduced Computational Complexity: Transforming system dynamics into a flat output space simplifies nonlinearities and reduces computational complexity. This results in faster control loop execution times and efficient computation of control actions, ideal for real-time applications.

1.10.1 Key Steps in Flatness-Based Control Design for Dynamic Systems

In summary, we can outline the following key steps in flatness-based control design for dynamic systems:

1. **Verification of Flatness**: This initial step entails confirming the differential flatness property of the system. Essential to this process is defining the flat output vector, ensuring that (1.1), (1.2), and (1.3) can be computed from the system dynamics.

2. **Reference Trajectory Generation**: Subsequent to verifying flatness, attention shifts to establishing the desired behavior of the flat output vector. Equation (1.9) serves as a fundamental tool for generating the desired trajectories of the flat output.

3. **Feedback Design**: To enable the flat outputs to effectively track the desired trajectories amid uncertainties or external perturbations, feedback mechanisms are employed. This critical stage involves selecting an appropriate closed dynamic system based on the desired error dynamics outlined in (1.8).

1.11 Conclusion

In this chapter, we introduced MGs, emphasizing their importance in enhancing power system reliability, resilience, and renewable energy integration, despite their control challenges. We discussed inverters, differentiating between grid-following and grid-forming types, and noted the role of parallel inverters in boosting capacity and reliability. We also briefly touched on MG control strategies, including the promising flatness-based control method for managing complex systems As we conclude this chapter, we have laid the foundation for a comprehensive understanding of MG dynamics and control strategies. The subsequent chapters will delve deeper into the intricacies of MG control, exploring advanced methodologies such as flatness-based control and their implications for the efficient operation of AC MGs.

Chapter 2

FBC of Three-Phase Inverter connected to LC Filter

2.1 Introduction

As discussed in the previous chapter, the foundational concepts of microgrids and the pivotal role of inverters have been established. Additionally, an advanced control strategy known as flatness-based control was introduced. Building on this foundation, this chapter focuses on controlling a three-phase inverter connected to an LC filter by applying a single one-loop flatness-based control strategy. The primary objective of this stage is to generate a three-phase sinusoidal voltage with a defined amplitude under any load condition. Experimental results under balanced, unbalanced, and nonlinear load conditions are presented in this chapter to validate the proposed control method.

2.2 Three Phase Inverter DC-AC Interface Modelling

The structure of a three-phase inverter as shown in Figure. 2.1 is commonly delineated into two fundamental sections: the inverter bridge and the LC filter, each component is characterized by a mathematical model that captures the complex relationship between the input variables and the corresponding outputs. The inverter bridge governs the conversion of DC power to AC power, while the LC filter serves to mitigate harmonics and enhance the quality of the

output waveform,these mathematical models play a pivotal role in the analysis, design, and optimization of three-phase inverter systems across various applications in power electronics and electrical engineering.

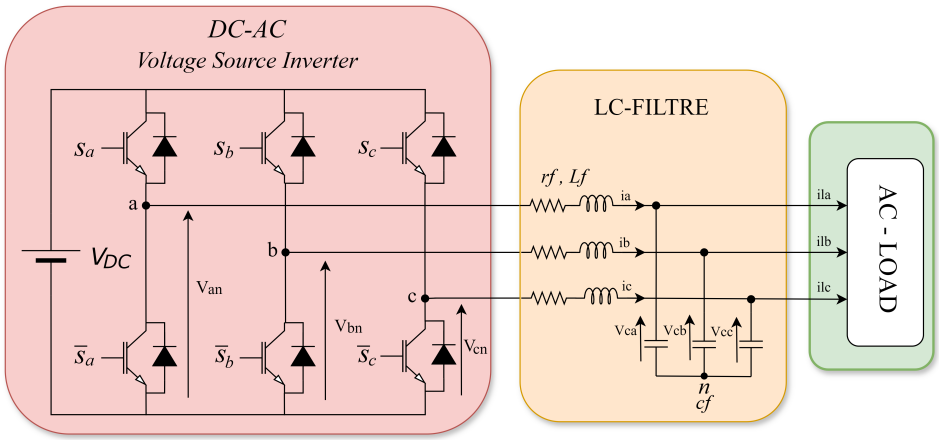

Figure 2.1: Synoptic scheme of three-phase inverter connected to *LC* filter

2.2.1 Inverter's bridge model

Three phase inverter is composed of six switches in total, as illustrated in Figure. 2.2. It should be noted that each pair of switches sharing a "leg," for example S_a and $\overline{S_a}$, are always complementarily switched, meaning they cannot be both open or closed at the same time [3].

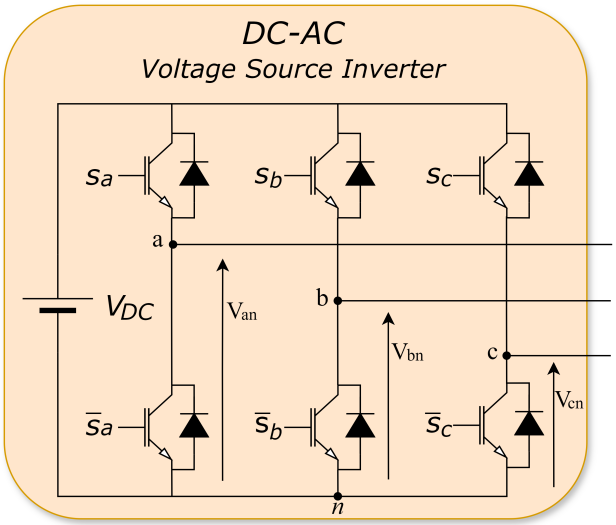

Figure 2.2: Three phase inverter's bridge

Taking that into consideration, and by using Kirchhoff's law we can describe the relationship

between the phase-to-neutral voltages (V_{an}, V_{bn}, V_{cn}) and the upper switches (Sa, Sb, Sc) with the following equation:

$$\begin{bmatrix} V_{an} \\ V_{bn} \\ V_{cn} \end{bmatrix} = \frac{1}{3} V_{DC} \begin{bmatrix} 2 & -1 & -1 \\ -1 & 2 & -1 \\ -1 & -1 & 2 \end{bmatrix} \begin{bmatrix} S_a \\ S_b \\ S_c \end{bmatrix} \tag{2.1}$$

2.2.2 LC Filter Modeling

Figure. 2.1 depicts a three-phase inverter system connected to an LC filter. This section delves into the mathematical modeling of this filter, as shown in Figure 2.3, enabling a precise characterization of the system's behavior.

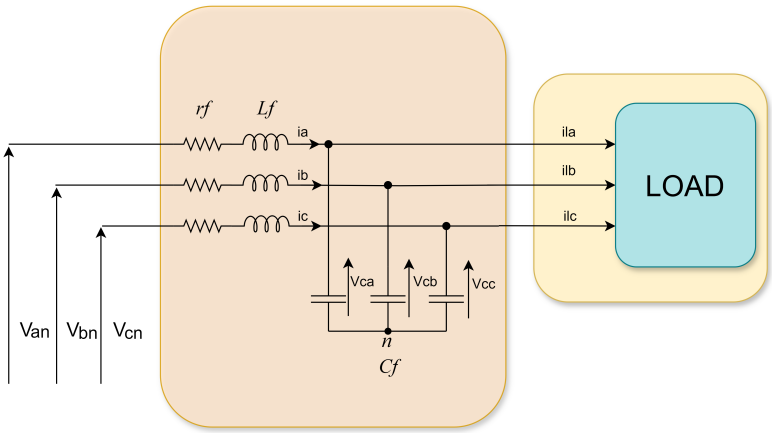

Figure 2.3: LC filter scheme

The mathematical modeling process typically involves applying Kirchhoff's Current Law (KCL) and Kirchhoff's Voltage Law (KVL) to each node in the LC filter circuit. These fundamental circuit analysis techniques establish relationships between voltages and currents at various points.

Using Kirchhoff's laws, the equations that describe the relationships between voltages and currents in the circuit are formulated.

The modelling of the LC filter is divided into two parts :

- In the First part we handle the currents of the first set of inductors.
- The second part will be about the voltage of the capacitors.

The differential equations describing the circuit can be formulated as follows :

$$\begin{cases} v_{ca} + L_f \frac{di_a}{dt} + r_f i_a = V_{an} \\ v_{cb} + L_f \frac{di_b}{dt} + r_f i_b = V_{bn} \\ v_{cc} + L_f \frac{di_c}{dt} + r_f i_c = V_{cn} \end{cases} \tag{2.2}$$

$$\begin{cases} \frac{di_a}{dt} &= (V_{an} - v_{ca} - r_f i_a)\frac{1}{L_f} \\ \frac{di_b}{dt} &= (V_{bn} - v_{cb} - r_f i_b)\frac{1}{L_f} \\ \frac{di_c}{dt} &= (V_{cn} - v_{cc} - r_f i_c)\frac{1}{L_f} \end{cases} \tag{2.3}$$

By applying Kirchhoff's second law, which states that for any node (junction) in an electrical circuit, the sum of currents flowing into that node is equal to the sum of currents flowing out of that node, the behavior of electrical circuits can be systematically analyzed. At node "a", we find

$$i_a = i_{ca} + i_{La}. \tag{2.4}$$

Transitioning to node "b",

$$i_b = i_{cb} + i_{Lb}. \tag{2.5}$$

Finally, at node "c"',

$$i_c = i_{cc} + i_{Lc}. \tag{2.6}$$

Additionally, the equation

$$\frac{dq(t)}{dt} = i(t) \tag{2.7}$$

Describes the rate of change of charge q with respect to time t, which equals the current $i(t)$. Additionally, the charge q on a capacitor is related to the voltage across the capacitor v_c and the capacitance C by the equation

$$q = C \cdot v_c. \tag{2.8}$$

By substituting (2.7) into (2.4), (2.5) and (2.6), the following relationships can be established:

$$\begin{cases} i_a = \frac{dq_a}{dt} + i_{La} \\ i_b = \frac{dq_b}{dt} + i_{Lb} \\ i_c = \frac{dq_c}{dt} + i_{Lc} \end{cases} \tag{2.9}$$

Which means that:

$$\begin{cases} \frac{dq_a}{dt} = i_a - i_{La} \\ \frac{dq_b}{dt} = i_b - i_{Lb} \\ \frac{dq_c}{dt} = i_c - i_{Lc} \end{cases} \tag{2.10}$$

By substituting (2.8) into (2.9), an expression is derived that describes the dynamic relationship between the capacitor voltage derivatives and the currents in the three-phase inverter system:

$$\begin{cases} c_f \cdot \frac{dv_{ca}}{dt} = i_a - i_{La} \\ c_f \cdot \frac{dv_{cb}}{dt} = i_b - i_{Lb} \\ c_f \cdot \frac{dv_{cc}}{dt} = i_c - i_{Lc} \end{cases} \tag{2.11}$$

Therefore:

$$\frac{d}{dt}\begin{pmatrix} v_{ca} \\ v_{cb} \\ v_{cc} \end{pmatrix} = \frac{1}{c_f}\begin{pmatrix} i_a \\ i_b \\ i_c \end{pmatrix} - \frac{1}{c_f}\begin{pmatrix} i_{La} \\ i_{Lb} \\ i_{Lc} \end{pmatrix} \tag{2.12}$$

Following the analysis that led to the solution of (2.12), the voltages across the three capacitors in the system have been successfully established. This crucial step allows for proceeding to the next phase of the analysis, which involves finding the currents flowing through the first set of inductors. From (2.2) and (2.3), it can be concluded that:

$$\frac{d}{dt}\begin{pmatrix} i_a \\ i_b \\ i_c \end{pmatrix} = \begin{pmatrix} \frac{-rf}{L_f} & 0 & 0 \\ 0 & \frac{-rf}{L_f} & 0 \\ 0 & 0 & \frac{-rf}{L_f} \end{pmatrix}\begin{pmatrix} i_a \\ i_b \\ i_c \end{pmatrix} + \frac{1}{L_f}\begin{pmatrix} V_{an} \\ V_{bn} \\ V_{cn} \end{pmatrix} - \frac{1}{L_f}\begin{pmatrix} v_{ca} \\ v_{cb} \\ v_{cc} \end{pmatrix} \tag{2.13}$$

2.3 The Challenge of Three-Phase Analysis

Traditional analysis of three-phase systems involves working with three separate quantities for voltage and current in the a-b-c reference frame[22].

This approach can lead to complex mathematical expressions and challenges in control design. Time-varying phasors offer some simplification, but they rely on approximations that may not be suitable for all scenarios.

2.4 Park's Transformation

Park's transformation addresses the challenges of three-phase analysis by introducing a rotating reference frame ($dq0$). This frame rotates at a specific speed, typically synchronized with the fundamental frequency of the system. The three-phase quantities (a, b, c) are transformed into two orthogonal components (d and q) and a zero-sequence component (0) in the $dq0$ reference frame.
The transformation utilizes two key matrices:

1. Clarke transformation: This first step transforms the three-phase quantities (a, b, c) into a stationary two-phase representation (α, β).

2. Park transformation: This second step converts the stationary $\alpha\beta$ components into the rotating $dq0$ reference frame components (d, q, 0).

2.5 Advantages of the $dq0$ Reference Frame

Employing the $dq0$ reference frame provides several significant benefits for three-phase system analysis and control:

To simplify control and analysis of three-phase systems, employing Park's rotating reference frame has become a prevalent practice. This mathematical transformation, utilizing the Clarke and Park matrices, converts stationary three-phase quantities (abc) into two diphasic components in a rotating frame (dq). This reference frame shift offers several advantages: simplified system equations, decoupling of current/voltage components, and improved performance and

robustness of control laws. The transition to this reference frame is facilitated by the base change matrix P,where $\theta = \omega t + \theta_0$. Here, ω represents the desired electrical pulsation.

$$P = \sqrt{\frac{2}{3}} \begin{pmatrix} \frac{1}{\sqrt{2}} & \frac{1}{\sqrt{2}} & \frac{1}{\sqrt{2}} \\ \cos(\theta) & \cos\left(\theta - \frac{2\pi}{3}\right) & \cos\left(\theta + \frac{2\pi}{3}\right) \\ -\sin(\theta) & -\sin\left(\theta - \frac{2\pi}{3}\right) & -\sin\left(\theta + \frac{2\pi}{3}\right) \end{pmatrix} \tag{2.14}$$

$$\frac{d}{dt}\begin{pmatrix} v_{c0} \\ v_{cd} \\ v_{cq} \end{pmatrix} = \begin{pmatrix} 0 & 0 & 0 \\ 0 & 0 & \omega \\ 0 & -\omega & 0 \end{pmatrix} \begin{pmatrix} v_{c0} \\ v_{cd} \\ v_{cq} \end{pmatrix} + \frac{1}{C_f}\begin{pmatrix} i_0 \\ i_d \\ i_q \end{pmatrix} - \frac{1}{C_f}\begin{pmatrix} i_{L0} \\ i_{Ld} \\ i_{Lq} \end{pmatrix} \tag{2.15}$$

$$\frac{d}{dt}\begin{pmatrix} i_0 \\ i_d \\ i_q \end{pmatrix} = \begin{pmatrix} \frac{-r_f}{L_f} & 0 & 0 \\ 0 & \frac{rf}{L_f} & \omega \\ 0 & -\omega & \frac{-rf}{L_f} \end{pmatrix} \begin{pmatrix} i_0 \\ i_d \\ i_q \end{pmatrix} + \frac{1}{L_f}\begin{pmatrix} V_0 \\ V_d \\ v_q \end{pmatrix} - \frac{1}{L_f}\begin{pmatrix} v_{c0} \\ v_{cd} \\ v_{cq} \end{pmatrix} \tag{2.16}$$

Building upon the understanding of the Park's reference frame transformation, we can now proceed with the mathematical calculations.

Along with

$$\begin{pmatrix} V_0 \\ V_d \\ V_q \end{pmatrix} = \mathbf{P}\begin{pmatrix} V_{an} \\ V_{bn} \\ V_{cn} \end{pmatrix} \quad \text{and} \quad \begin{pmatrix} v_{c0} \\ v_{cd} \\ v_{cq} \end{pmatrix} = \mathbf{P}\begin{pmatrix} v_{ca} \\ v_{cb} \\ v_{cc} \end{pmatrix} \tag{2.17}$$

$$\begin{pmatrix} v_{c0} \\ v_{cd} \\ v_{cq} \end{pmatrix} = \sqrt{\frac{2}{3}} \begin{pmatrix} \frac{1}{\sqrt{2}} & \frac{1}{\sqrt{2}} & \frac{1}{\sqrt{2}} \\ \frac{1}{2} & \cos(\theta) & \cos\left(\theta - \frac{2\pi}{3}\right) \\ \frac{1}{2} & -\sin(\theta) & -\sin\left(\theta - \frac{2\pi}{3}\right) \end{pmatrix} \begin{pmatrix} v_{ca} \\ v_{cb} \\ v_{cc} \end{pmatrix} \tag{2.18}$$

(2.18) yields to

$$\sqrt{\frac{\mathbf{2}}{\mathbf{3}}} \begin{pmatrix} (v_{ca} + v_{cb} + v_{cc})\frac{\mathbf{1}}{\sqrt{\mathbf{2}}} \\ \cos(\theta)v_{ca} + \cos\left(\theta - \frac{2\pi}{3}\right)v_{cb} + \cos\left(\theta + \frac{2\pi}{3}\right)v_{cc} \\ -\sin(\theta)v_{ca} - \sin\left(\theta - \frac{2\pi}{3}\right)v_{cb} - \sin\left(\theta + \frac{2\pi}{3}\right)v_{cc} \end{pmatrix}$$

Accordingly, the following equation can be extracted:

$$\frac{d}{dt}\begin{pmatrix} v_{c0} \\ v_{cd} \\ v_{cq} \end{pmatrix} = \begin{pmatrix} 0 \\ \omega v_{cq} \\ -\omega v_{cd} \end{pmatrix} \tag{2.19}$$

- V_d and V_q represent the d and q components of the voltage in the $dq0$ frame.
- V_a, V_b, and V_c represent the three-phase voltages in the abc frame (phase voltages).
- Both voltages and currents in Park's framework can be transformed using the same basic equation.
- The homopolar components of the inverter's output current ($i_a i_b i_c$), the load current (i_{La}, i_{Lb}, i_{Lc}), and the capacitor current (i_{ca}, i_{cb}, i_{cc}) all register as zero. This outcome stems from the equations:

$$\begin{cases} i_0 &= \frac{i_a+i_b+i_c}{\sqrt{3}} = 0 \\ i_{L0} &= \frac{i_{La}+i_{Lb}+i_{Lc}}{\sqrt{3}} = 0 \\ i_{c0} &= \frac{i_{ca}+i_{cb}+i_{cc}}{\sqrt{3}} = 0 \end{cases}$$

  Even if the elements V_0 and V_{c0} are not zero, they do not affect the transfer of electrical power. Therefore, we only need to consider the following equations for the equivalent two-phase model.

We can then consider only the equivalent two-phase model described by the equations below :

$$\frac{d}{dt}\begin{pmatrix} v_{cd} \\ v_{cq} \end{pmatrix} = \begin{pmatrix} 0 & \omega \\ -\omega & 0 \end{pmatrix}\begin{pmatrix} v_{cd} \\ v_{cq} \end{pmatrix} + \frac{1}{C_f}\begin{pmatrix} i_d \\ i_q \end{pmatrix} - \frac{1}{C_f}\begin{pmatrix} i_{Ld} \\ i_{Lq} \end{pmatrix} \tag{2.20}$$

$$\frac{d}{dt}\begin{pmatrix} i_d \\ i_q \end{pmatrix} = \begin{pmatrix} \frac{-rf}{L_f} & \omega \\ -\omega & \frac{-rf}{L_f} \end{pmatrix}\begin{pmatrix} i_d \\ i_q \end{pmatrix} + \frac{1}{L_f}\begin{pmatrix} v_d \\ v_q \end{pmatrix} - \frac{1}{L_f}\begin{pmatrix} v_{cd} \\ v_{cq} \end{pmatrix} \tag{2.21}$$

2.6 Application of FBC on the three phase inverter connected to LC filter

The application of the flat control strategy described above to the three-phase inverter connected to an LC filter and load (Figure. 2.1) will be explored. The first step is to check the flatness of the inverter by computing the functions φ_y, φ_x, and φ_u. In the following, let $a = \frac{r_f}{L_f}$. The dynamic model of the inverter is given by:

$$\dot{x} = \underbrace{\begin{pmatrix} 0 & w & \frac{1}{C_f} & 0 \\ -w & 0 & 0 & \frac{1}{C_f} \\ \frac{1}{L_f} & 0 & -a & w \\ 0 & -\frac{1}{L_f} & -w & -a \end{pmatrix}}_{A} x + \underbrace{\begin{pmatrix} 0 & 0 \\ 0 & 0 \\ \frac{1}{L_f} & 0 \\ 0 & \frac{1}{L_f} \end{pmatrix}}_{B_1} u + \underbrace{\begin{pmatrix} -\frac{1}{C_f} & 0 \\ 0 & -\frac{1}{C_f} \\ 0 & 0 \\ 0 & 0 \end{pmatrix}}_{B_2} i_L \tag{2.22}$$

The state variables are given by: $x = \begin{pmatrix} v_{cd} & v_{cq} & i_d & i_q \end{pmatrix}^T$, the control variables are represented by: $u = \begin{pmatrix} V_d & V_q \end{pmatrix}^T$, and the inductor currents are denoted as: $i_L = \begin{pmatrix} i_{Ld} & i_{Lq} \end{pmatrix}^T$. According to the control objectives, the candidate flat output vector is proposed to be defined as the voltages capacitors. Specifically, these flat outputs are given by:

$$\begin{cases} y_d = v_{cd} \\ y_q = v_{cq} \end{cases}$$

Thus,

$$y = \begin{pmatrix} y_d \\ y_q \end{pmatrix} = \begin{pmatrix} x_1 \\ x_2 \end{pmatrix} = \begin{pmatrix} \varphi_{y_d}(x) \\ \varphi_{y_q}(x) \end{pmatrix} = \varphi_y(x) \tag{2.23}$$

Note that for the inverter, the flat output depends only on the state of the system. This result is valid for every linear system.The next step involves expressing the state of the system as a function of the flat output and a finite number of its derivatives. Using (2.20), the following expression is obtained:

$$\begin{pmatrix} x_1 \\ x_2 \end{pmatrix} = \begin{pmatrix} v_{cd} \\ v_{cq} \end{pmatrix} = \begin{pmatrix} y_d \\ y_q \end{pmatrix} = \begin{pmatrix} \varphi_{v_{cd}}(y) \\ \varphi_{v_{cq}}(y) \end{pmatrix} = \varphi_x(y) \tag{2.24}$$

The expression of the line currents of the inverter $\begin{pmatrix} x_3 \\ x_4 \end{pmatrix}$ is obtained after differentiating (2.21). Thus, the following expression is obtained:

$$\begin{cases} \dot{y}_d = w \cdot y_q + \frac{1}{C_f} x_3 - \frac{1}{C_f} i_{L_d} \\ \dot{y}_q = -w \cdot y_d + \frac{1}{C_f} x_4 - \frac{1}{C_f} i_{L_q} \end{cases} \tag{2.25}$$

From this last equation, the line current can be expressed as

$$\begin{cases} x_3 = C_f \dot{y}_d - w C_f y_q + I_{Ld} = \varphi_{x_3}(y, \dot{y}) \\ x_4 = C_f \dot{y}_q + w C_f y_d + I_{Lq} = \varphi_{x_4}(y, \dot{y}) \end{cases} \tag{2.26}$$

$$\begin{pmatrix} x_3 \\ x_4 \end{pmatrix} = \begin{pmatrix} i_d \\ i_q \end{pmatrix} = \begin{pmatrix} \varphi_{i_d}(y, \dot{y}) \\ \varphi_{i_q}(y, \dot{y}) \end{pmatrix} = \varphi_x(y) \tag{2.27}$$

The state in terms of the flat output is given by:

$$\begin{pmatrix} x_1 \\ x_2 \\ x_3 \\ x_4 \end{pmatrix} = \begin{pmatrix} \varphi_{x_1}(y) \\ \varphi_{x_2}(y) \\ \varphi_{x_3}(y, \dot{y}) \\ \varphi_{x_4}(y, \dot{y}) \end{pmatrix} = \begin{pmatrix} y_d \\ y_q \\ C_f \dot{y}_d - w C_f y_q + i_{Ld} \\ C_f \dot{y}_q + w C_f y_d + i_{Lq} \end{pmatrix} = \varphi_x(y, \dot{y}) \tag{2.28}$$

The last step concerns the computation of the input in terms of the flat output and its derivatives. This process proceeds by deriving (2.25), leading to:

$$\begin{cases} \ddot{y}_d = w \cdot \dot{y}_q + \frac{1}{C_f} \dot{x}_3 - \frac{1}{C_f} \frac{di_{Ld}}{dt} \\ \ddot{y}_q = -w \cdot \dot{y}_d + \frac{1}{C_f} \dot{x}_4 - \frac{1}{C_f} \frac{di_{Lq}}{dt} \end{cases} \tag{2.29}$$

From (2.25), and (2.26), the expressions $\dot{x}_3$ and $\dot{x}_4$ are given by:

$$\begin{cases} \dot{x}_3 &= -a(C_f\dot{y}_d - wC_f y_q + i_{L_d}) + wC_f\dot{y}_q + wC_f y_d + i_{L_q} + \frac{1}{L_f}V_d - \frac{1}{L_f}y_d \\ \dot{x}_4 &= -wC_f\dot{y}_d - wC_f y_q + i_{L_d} - a(C_f y_q + wC_f y_d + i_{L_q}) + \frac{1}{L_f}V_q - \frac{1}{L_f}y_q \end{cases} \tag{2.30}$$

The current derivative in terms of the flat output is obtained as follows:

$$\begin{pmatrix} \dot{x}_3 \\ \dot{x}_4 \end{pmatrix} = \frac{d}{dt}\begin{pmatrix} i_d \\ i_q \end{pmatrix} = \begin{pmatrix} \varphi_{di_d}(y,\dot{y}) \\ \varphi_{di_q}(y,\dot{y}) \end{pmatrix} \tag{2.31}$$

Substituting (2.30) into (2.25) yields:

$$\begin{cases} \ddot{y}_d = w\dot{y}_q - \dfrac{a}{C_f}(C_f \cdot y_d - wC_f \cdot y_q + i_{L_d}) + \dfrac{w}{C_f}(C_f \cdot y_q + wC_f y_d + i_{L_q}) + \dfrac{1}{L_f C_f}V_d \\ \qquad - \dfrac{1}{L_f C_f}y_d - \dfrac{1}{C_f}\cdot\dfrac{di_{L_d}}{dt} \\ \ddot{y}_q = w\dot{y}_d + \dfrac{1}{C_f}(wC_f \cdot y_d - wC_f y_q + i_{L_d}) - \dfrac{a}{C_f}(C_f \cdot y_q + wC_f y_d + i_{L_q}) + \dfrac{1}{L_f C_f}V_q \\ \qquad - \dfrac{1}{L_f C_f}y_q - \dfrac{1}{C_f}\cdot\dfrac{di_{L_q}}{dt} \end{cases} \tag{2.32}$$

Finally, from this equation, the expression of the input

$$\begin{pmatrix} V_d \\ V_q \end{pmatrix} = \begin{pmatrix} C_f L_f \ddot{y}_d - 2C_f L_f w\dot{y}_q + r_f C_f \dot{y}_d - (1 - w^2 C_f L_f)y_d - wr_f C_f y_q + r_f i_{Ld} - wL_f i_{Lq} + L_f\frac{di_{Ld}}{dt} \\ C_f L_f \ddot{y}_q + 2C_f L_f w\dot{y}_d + r_f C_f \dot{y}_q + (1 - w^2 C_f L_f)y_q + wr_f C_f y_d + r_f i_{Lq} + wL_f i_{Ld} + L_f\frac{di_{Lq}}{dt} \end{pmatrix} \tag{2.33}$$

$$u = \begin{pmatrix} V_d \\ V_q \end{pmatrix} = \begin{pmatrix} \psi_{V_d}(y,\dot{y},\ddot{y}) \\ \psi_{V_q}(y,\dot{y},\ddot{y}) \end{pmatrix} = \psi_u(y,\dot{y},\ddot{y})$$

In summary, the differential flatness conditions expressed in (1.2), (1.3), are verified in (2.23), (2.28), and (2.33) respectively. Thus, the system under study can be considered flat, with the flat output vector $y = \begin{pmatrix} v_{cd} & v_{cq} \end{pmatrix}^T$ associated to the input vector $u = \begin{pmatrix} V_d & V_q \end{pmatrix}^T$.

We have demonstrated that the system under study, presented in Figure. 1.1, can be considered differentially flat. In the next steps, we will present the procedure for synthesizing the feedback control ensuring the tracking of the flat output to its trajectory reference, as well as the algorithm for planning the reference trajectory.

2.7 Trajectory planning

The control objective is to steer the capacitor voltages to their reference point $y_{\text{set}} = \begin{pmatrix} y_{d_{\text{set}}} & y_{q_{\text{set}}} \end{pmatrix}^T$, which corresponds to the original objective of controlling the DC bus. We want to determine a feasible reference trajectory for the flat output for the DC-AC inverter that ensures seamless transitions between initial values and the reference point. From (2.33) and to have continuous control, we need a trajectory of class C^2. Therefore, from (1.9), the reference trajectories associated with the flat outputs are defined in the following equations:

$$\begin{cases} y_d(t) = y_d(t_0) + \mathcal{L}^{-1}\left\{F_1(s)\left(y_{d_{\text{set}}} - y_d(t_0)\right)(s)\right\} \\ y_q(t) = y_q(t_0) + \mathcal{L}^{-1}\left\{F_2(s)\left(y_{q_{\text{set}}} - y_q(t_0)\right)(s)\right\} \end{cases} \tag{2.34}$$

Where $y_d(t_0) = V_{cd}(t_0)$ and $y_q(t_0) = V_{cq}(t_0)$ are respectively the initial capacitor voltages in the dq frame, and $y_{d_{\text{set}}} = V_{cd_{\text{set}}}$ and $y_{q_{\text{set}}} = V_{cq_{\text{set}}}$ are the desired capacitor voltages at time t_0. To ensure the continuity of the generated control, second-order low-pass filters $F_i(p)$, $i = 1, 2$, are used due to their smoothing capability, which ensures seamless transitions, particularly during startup where trajectories are of the 'stop-stop' type. These filters are of the form:

$$\begin{cases} F(s) = \dfrac{1}{(\tau_1 s + 1)^2} = \dfrac{y_d(p)}{(y_{d_{\text{set}}} - y_d(t_0))(p)} \\ F(s) = \dfrac{1}{(\tau_2 s + 1)^2} = \dfrac{y_{d\text{ref}}(s)}{(y_{d1_{\text{set}}} - y_{d1}(t_0))(p)} \end{cases} \tag{2.35}$$

Combining (2.33) and (2.34), yields

$$\begin{cases} y_d(t) = y_d(t_0) + \mathcal{L}^{-1}\left\{\dfrac{1}{(\tau_1 s + 1)^2}\left(y_{d_{\text{set}}} - y_d(t_0)\right)(s)\right\} \\ y_q(t) = y(t_0) + \mathcal{L}^{-1}\left\{\dfrac{1}{(\tau_1 s + 1)^2}\left(y_{q_{\text{set}}} - y_q(t_0)\right)(s)\right\} \end{cases} \tag{2.36}$$

We need to compute $\mathcal{L}^{-1}\left\{\frac{1}{(\tau_1 s+1)^2}\left(y_{d_{\text{set}}} - y_d(t_0)\right)(s)\right\}$ where $\left(y_{d_{\text{set}}} - y_d(t_0)\right)(s)$ is given by

$$y_{d_{\text{consigned}}}(s) = \frac{y_{d_{\text{set}}} - y_d(t_0)}{s}$$

This leads to

$$\begin{cases} y_d(t) = y_d(t_0) + \mathcal{L}^{-1}\left\{\dfrac{y_{d_{\text{set}}} - y_d(t_0)}{s(\tau s+1)^2}\right\} \\ y_q(t) = y_q(t_0) + \mathcal{L}^{-1}\left\{\dfrac{y_{q_{\text{set}}} - y_q(t_0)}{(s(\tau s+1))^2}\right\} \end{cases} \tag{2.37}$$

So for the output in the time domain using the inverse Laplace transform

$$\frac{y_{d_{\text{set}}} - y_d(t_0)}{s(\tau s+1)^2} = \frac{A}{s} + \frac{B}{(s+\frac{1}{\tau})^2} + \frac{c}{s+\frac{1}{\tau}} \tag{2.38}$$

$$F(s) = \frac{1}{s(\tau s+1)^2} = \frac{1}{\tau^2 s(s+\frac{1}{\tau})^2} = \frac{\frac{1}{\tau^2}}{s(s+\frac{1}{\tau})^2} = \frac{A}{s} + \frac{B}{(s+\frac{1}{\tau})^2} + \frac{c}{s+\frac{1}{\tau}}$$

$$\begin{cases} A = y_{d_{\text{set}}} - y_d(t_0)\left[\dfrac{s\frac{1}{\tau^2}}{s(s+\frac{1}{\tau})^2}\right]_{s=0} = y_{d_{\text{set}}} - y_d(t_0) \\ B = \dfrac{1}{0!}\cdot\dfrac{d}{ds}\left[\dfrac{(s+\frac{1}{\tau^2})^2 + \frac{1}{\tau^2}}{s(s+\frac{1}{\tau})^2}\right]_{s=-\frac{1}{\tau}} = -\dfrac{y_{d_{\text{set}}} - y_d(t_0)}{\tau} \\ C = \dfrac{1}{1!}\cdot\dfrac{d}{ds}\left[\dfrac{(s+\frac{1}{\tau^2})^2 + \frac{1}{\tau^2}}{s(s+\frac{1}{\tau})^2}\right]_{s=-\frac{1}{\tau}} = \dfrac{d}{ds}\left[\dfrac{\frac{1}{\tau^2}}{s^2}\right]_{s=-\frac{1}{\tau}} = \dfrac{1}{\tau^2} \end{cases}$$

Hence

$$y(s) = \frac{y_{d_{\text{set}}} - y_d(t_0)}{s} - \frac{y_{d_{\text{set}}} - y_d(t_0)}{\tau\cdot\left(s+\frac{1}{\tau}\right)^2} - \frac{y_{d_{\text{set}}} - y_d(t_0)}{s+\frac{1}{\tau}} \tag{2.39}$$

By putting these results together, the reference trajectories are given by

$$y_{dref_f}(t) = y_{dref}(t_0) + (y_{d_{\text{set}}} - y_{dref}(t_0))\left(1 - e^{-\frac{(t-t_0)}{\tau_1}} - \frac{t-t_0}{\tau_1}\cdot e^{-\frac{(t-t_0)}{\tau_1}}\right) \tag{2.40}$$

$$y_{qref_f}(t) = y_{qref}(t_0) + (y_{q_{\text{set}}} - y_{qref}(t_0))\left(1 - e^{-\frac{(t-t_0)}{\tau_2}} - \frac{t-t_0}{\tau_2}\cdot e^{-\frac{(t-t_0)}{\tau_2}}\right) \tag{2.41}$$

Where t_0 represents the initial time and $y_d(t_0)$ and $y_q(t_0)$ represent the initial value f the capacitor voltage in the dq axis, respectively. τ_1 and τ_2 represent the constant time of the reference trajectory. $y_{d_{\text{set}}}$ and $y_{q_{\text{set}}}$ are the set points of the capacitor voltages. The set points are chosen to be equal to $\sqrt{\frac{3}{2}}V_{\text{rms}}$, where V_{rms} is the root mean square.

The frequency filtering property of (2.38) helps eliminate noise and disturbances, while its

inherent continuity ensures seamless trajectory generation. This approach strikes a balance between computational efficiency and performance, making it suitable for real-time trajectory planning tasks.

2.8 Open Loop Flatness based implementation

Achieving a "stop-stop" trajectory in the open loop, where the system transitions smoothly is tested in this section. To assess the system's inherent ability to accomplish this transition with flatness based open-loop is conducted, as demonstrated in Figure 2.4. This test evaluates the system's capability to track the desired reference trajectory, by utilizing an open-loop approach, the focus remains solely on the system's inherent dynamics, allowing for a clearer understanding of its behavior before introducing the feedback control. We assume that charge is equal to zero.

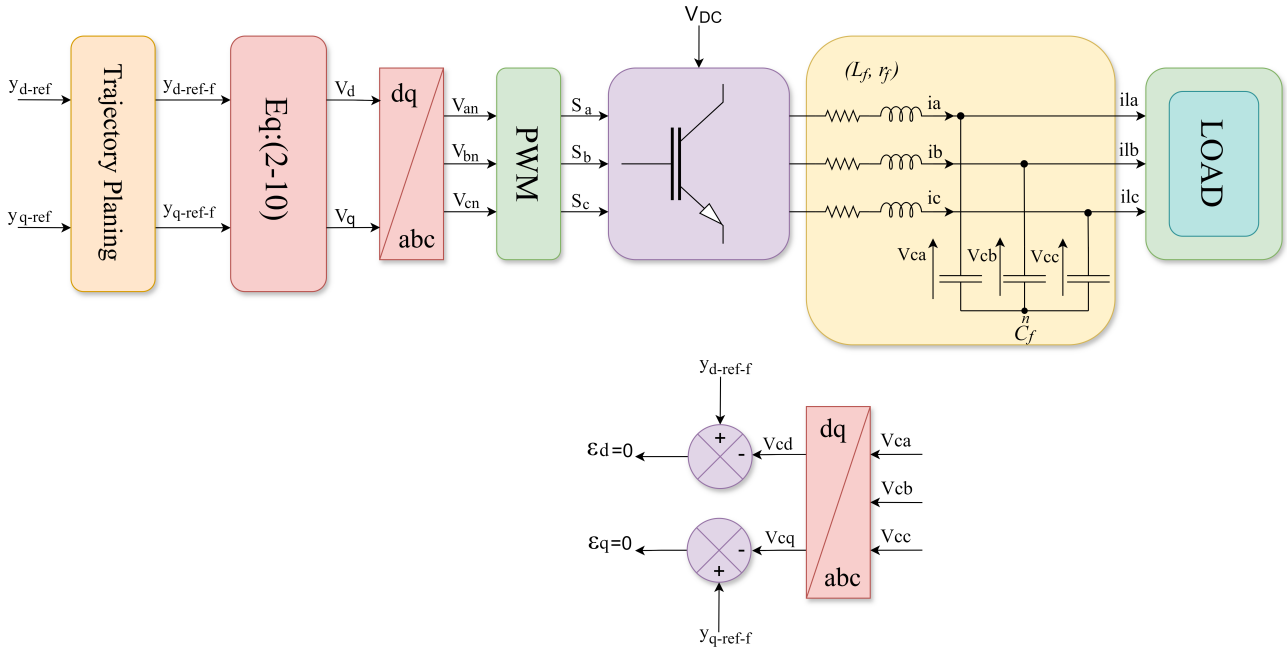

Figure 2.4: Functional block diagram of the proposed control system in open loop

2.9 Open-Loop simulation

The application of a voltage reference step from 0 to 110 V with a fixed load power of 1 kW (resistive) demonstrates the effectiveness of the proposed control system with trajectory

planning. Using MATLAB Simulink SimPower the measured flat outputs (y_d and y_q) precisely follow their reference trajectories during the startup phase, as shown in Figure. 2.5. This confirms the controller's ability to force the system to adhere to predefined paths. The system parameters used in the simulation are listed in Table 2.1.

Table 2.1: Control System Parameters and Controller Gains

Symbol	Parameter Name	Value
r_f	Filter inductive resistance	0.5 Ω
c_f	Filter capacitance	50 μF
L_f	Filter inductance	8 mH
w	Angular frequency	$2\pi \cdot 50$ rad/s
w_n	Cutoff frequency	10000
p_1	Additional pole	7000
ξ	Damping coefficient	0.7

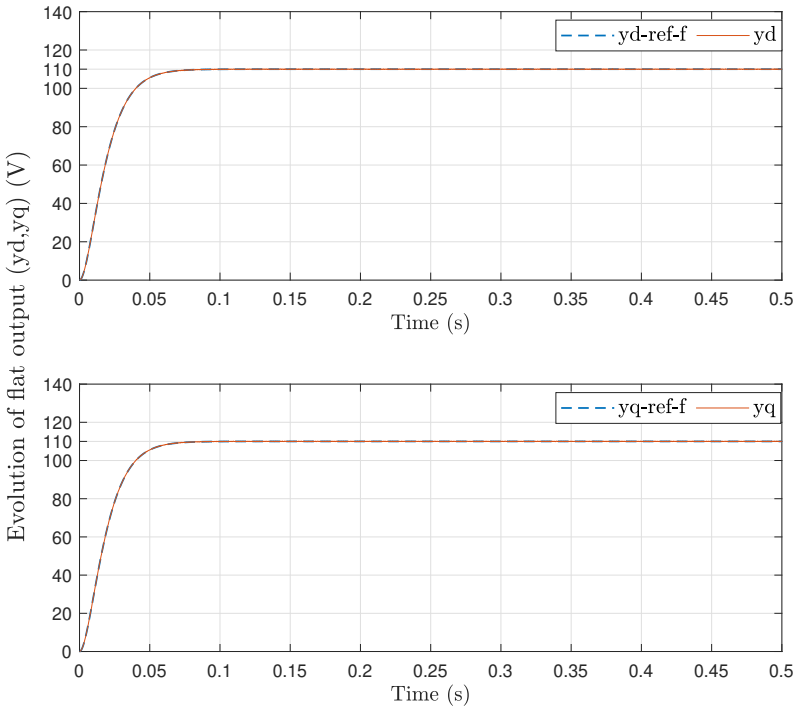

Figure 2.5: Behavior of d-axis and q-axis flat outputs (y_d and y_q) during open-loop startup ($V_{dc} = 400$ V, $V_{\text{eff}} = 110$ V, $P_{\text{Load}} = 1$ kW)

2.10 Trajectory tracking

After ensuring the planning of the reference trajectory, we will now present the synthesis procedure for the control system, ensuring that the flat output tracks its reference. This feedback control design, based on the flatness approach, aims to track the desired flat output reference trajectory while ensuring desired performance and robustness against parameter variations and load changes. This methodology leverages the system's "flat output" to guide it towards the desired reference trajectory.

Recall that our goal is to track the reference trajectory given by (2.38) using the flatness approach. Based on the flatness approach described above and equation (2.33), the control is defined as follows:

To achieve this, we introduce the fictitious control vector[9][8][14], $\gamma = [\gamma_d, \gamma_q]^t$, defined as follows:

$$\ddot{y}_d = \gamma_d$$

$$\ddot{y}_q = \gamma_q$$

The control is defined as follows:

$$\begin{pmatrix} V_d \\ V_q \end{pmatrix} = \begin{pmatrix} \psi_{V_d}(y_{dref_f}(t), y_{qref_f}(t), \dot{y}_{dref_f}(t), \dot{y}_{qref_f}(t), \gamma_d) \\ \psi_{V_q}(y_{qref_f}(t), y_{dref_f}(t), \dot{y}_{qref_f}(t), \dot{y}_{dref_f}(t), \gamma_q) \end{pmatrix} \tag{2.42}$$

$$= \begin{pmatrix} C_f L_f \gamma_d - 2C_f L_f w \dot{y}_{qref_f}(t) + r_f C_f \dot{y}_{dref_f}(t) - (1 - w^2 C_f L_f) y_{dref_f}(t) - w r_f C_f y_{qref_f}(t) + r_f i_{Ld} \\ -w L_f i_{Lq} + L_f \frac{di_{Ld}}{dt} \\ \\ C_f L_f \gamma_q + 2C_f L_f w \dot{y}_{dref_f}(t) + r_f C_f \dot{y}_{qref_f}(t) + (1 - w^2 C_f L_f) y_{qref_f}(t) + w r_f C_f y_{dref_f}(t) + r_f i_{Lq} \\ +w L_f i_{Ld} + L_f \frac{di_{Lq}}{dt} \end{pmatrix} \tag{2.43}$$

The feedback terms γ_d and γ_q is obtained by Equations (2.44):

$$\begin{aligned} 0 &= (\gamma_d - \ddot{y}_{dref_f}) + k_{10}(\dot{y}_d - \dot{y}_{dref_f}) + k_{11}(y_d - y_{dref_f}) + k_{12}\int (y_d - y_{dref_f})d\tau \\ 0 &= (\gamma_q - \ddot{y}_{qref_f}) + k_{20}(\dot{y}_q - \dot{y}_{qref_f}) + k_{21}(y_q - y_{qref_f}) + k_{22}\int (y_q - y_{qref_f})d\tau \end{aligned} \tag{2.44}$$

Integral terms are introduced to ensure zero steady-state errors and compensate for modeling errors and/or uncertainties in parameter values. Each of these equations is equivalent to a third-order equation on the error of the form:

$$\begin{aligned} 0 &= \dddot{e}_d + k_{10}\ddot{e}_d + k_{11}\dot{e}_d + k_{12}e_d \\ 0 &= \dddot{e}_q + k_{20}\ddot{e}_q + k_{21}\dot{e}_q + k_{22}e_q \end{aligned} \tag{2.45}$$

Optimal selection of parameters k_1, k_2, k_3 can be achieved by matching polynomial (2.46) to a characteristic polynomial $p(s)$ given by relation (2.47):

$$p(s) = (s + p_1)(s^2 + 2\xi w_n s + w_n^2) \tag{2.46}$$

$$\begin{aligned} \dddot{\varepsilon}_d - k_1\ddot{\varepsilon}_d - k_2\dot{\varepsilon}_d - k_3\varepsilon_d = 0 \\ \dddot{\varepsilon}_q - k_1\ddot{\varepsilon}_q - k_2\dot{\varepsilon}_q - k_3\varepsilon_q = 0 \end{aligned} \tag{2.47}$$

$$\begin{aligned} k_2 &= k_{10} = k_{20} = -(p_1 + 2\xi_{wn}) \\ k_1 &= k_{11} = k_{21} = -(p_1 + 2\xi_{wn} + w_n^2) \\ k_3 &= k_{12} = k_{22} = -p_1 w_n^2 \end{aligned}$$

The controller (γ_d, γ_q) design process typically involves the following steps shown in Figure. 2.6 :

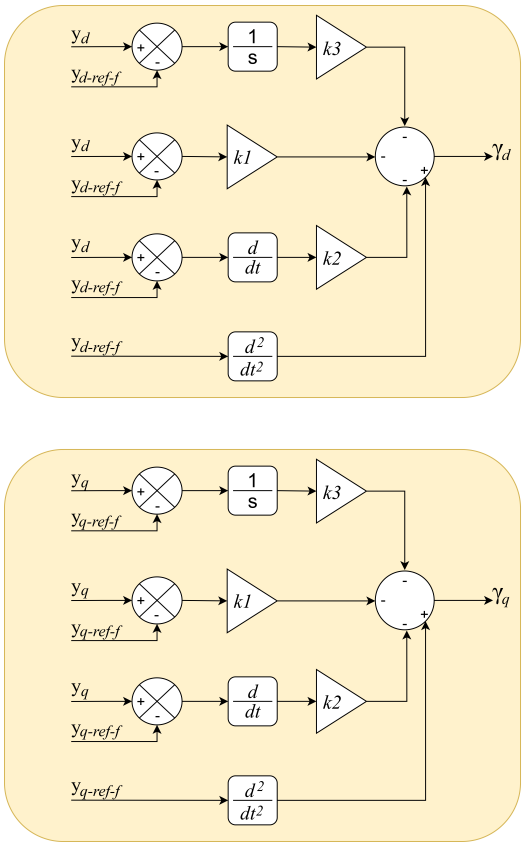

Figure 2.6: Construction γ_d and γ_q

The controller parameters are designed to achieve desired performance in regulation and command tracking. The cutoff frequency is placed to achieve fast rejection of disturbances. The additional pole is set to $\xi \cdot \omega_n$. The numerical values of these parameters are given in Table. 2.1.

Finally, the use of filtered reference outputs $y_{\text{ref}_f} = [y_{d_{\text{ref}_f}}, y_{q_{\text{ref}_f}}]^T$, as well as established control variables $\gamma = [\gamma_d, \gamma_q]^T$, allows for the generation of reference commands associated with the inverter voltages.

$$\psi V_{d_{\text{ref}}} = (y_{d_{\text{ref}_f}}, y_{q_{\text{ref}_f}}, \dot{y}_{d_{\text{ref}_f}}, \dot{y}_{q_{\text{ref}_f}}, \gamma_d) \tag{2.48}$$

$$\psi V_{q_{\text{ref}}} = (y_{d_{\text{ref}_f}}, y_{q_{\text{ref}_f}}, \dot{y}_{d_{\text{ref}_f}}, \dot{y}_{q_{\text{ref}_f}}, \gamma_q) \tag{2.49}$$

The functional diagram of the proposed control is presented in Figure. 2.7.

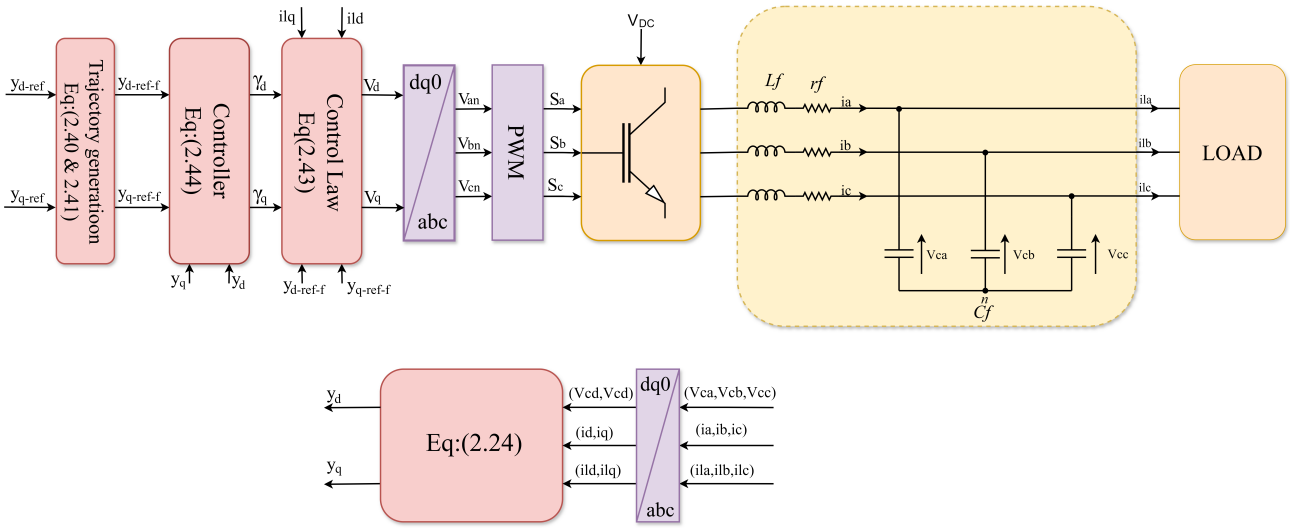

Figure 2.7: Functional Block Diagram of the Proposed Control System

2.11 Simulations results

This section presents the results obtained from a simulation aimed at analyzing the behavior of voltage of the 3-phase system connected to an LC filter under varying load conditions. The simulation focused on the impact of different load types and parameter variations on the voltage characteristics. Additionally, the simulation utilized SimPower, a tool within MATLAB/Simulink environment, to model and analyze the electrical system's performance accurately.

2.11.1 Closed-Loop Control System Implementation and Evaluation

To validate the flatness concept, which allows predicting the system's state variables from flat outputs, we propose demonstrating the system's behavior through simulation during the following phases:

The Startup Phase: The startup phase involves transitioning the system from rest to active operation. It is crucial for setting initial conditions and ensuring controlled stability. This phase observes state variable evolution, tests the system's stability and efficiency, and helps identify potential issues early on.

A Load Transient: A load transient tests the system's response to sudden load changes,

verifying its responsiveness, robustness, and adaptability. This phase ensures that flat outputs accurately predict state evolutions and that the system maintains optimal performance during disturbances.

Figure. 2.8 shows the process of evaluating the results in the ABC reference frame. To achieve this, we first perform an inverse Park transformation to convert the reference values y_d^{ref} and $_q^{ref}$ from the $dq0$ frame back to the ABC frame. Next, we compare these transformed reference values with the actual voltages measured across the capacitor in the ABC frame. This comparison is crucial for assessing the accuracy of the control system. A strong correlation between the reference and actual values indicates that the system accurately follows the desired voltage trajectories, thereby demonstrating effective control and precise trajectory tracking. Figure 2.9 and Figure 2.10 illustrates the behavior of the control input during startup in both open and closed loop .

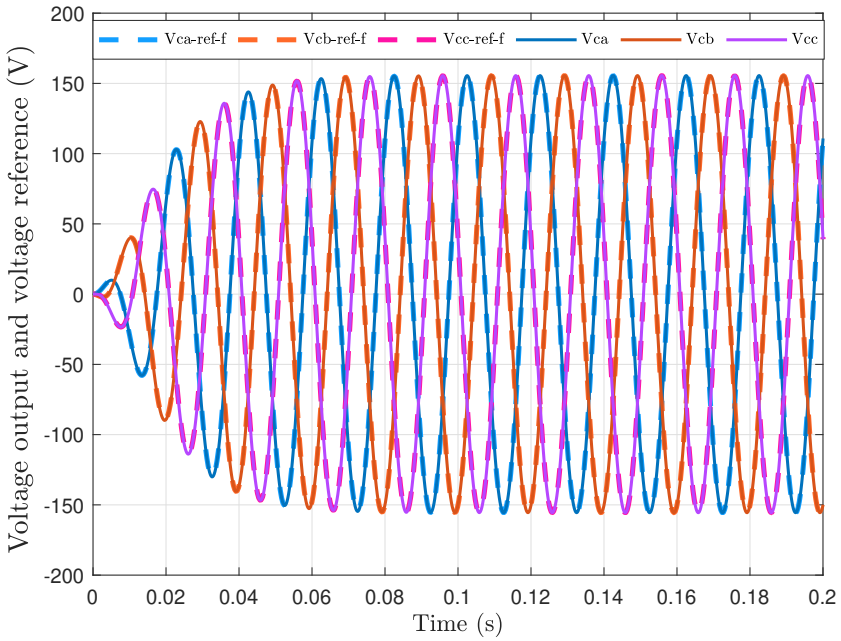

Figure 2.8: Analysis of three-phase line currents (a, b, c) under varying load conditions (0 kW to 1 kW).

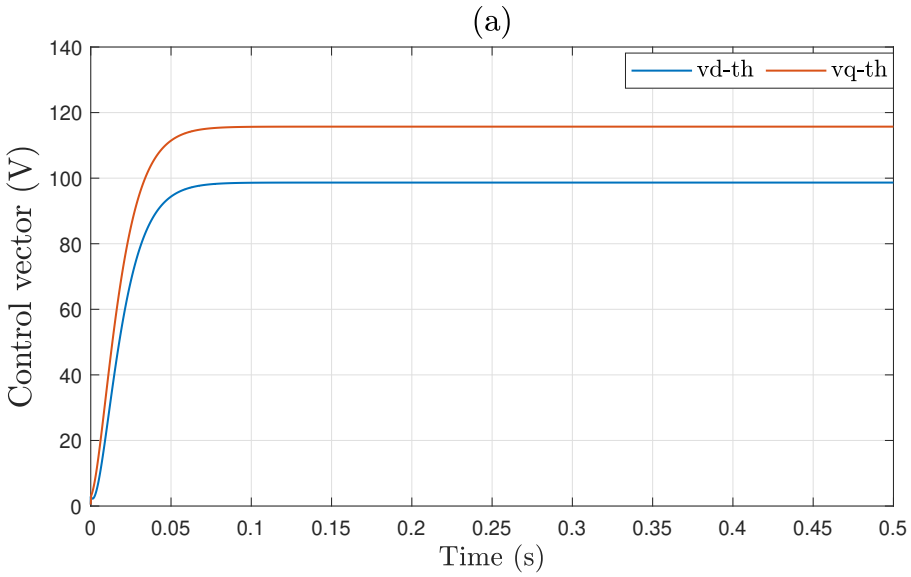

Figure 2.9: Behavior of the Control Input During Startup ($V_{DC} = 400\,\text{V}$, $P_{\text{Charge}} = 1\,\text{kW}$): Open Loop.

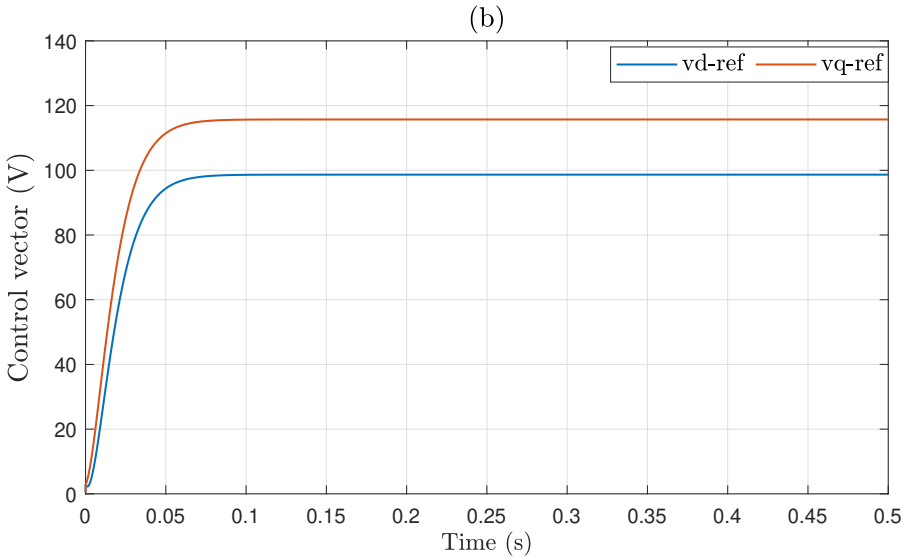

Figure 2.10: Behavior of the Control Input During Startup ($V_{DC} = 400\,\text{V}$, $P_{\text{Charge}} = 1\,\text{kW}$): Closed Loop.

2.12 Validation of the Proposed Control Model

A series of tests were conducted to evaluate the potential of the proposed control strategy:

1. **Energy Quality Test:**
    - The first test focused on checking the quality of the supplied energy.
2. **Response to Changes Test:**
    - The second test examined how the system responds to sudden changes and variations in parameters, providing insight into its robustness and adaptability in different conditions.
3. **Evaluating Robustness Under Dynamic Conditions:**
    - The third test assessed the control strategy's effectiveness in maintaining system stability under various load conditions.

First Test: Energy Quality

Figure. 2.11 shows the voltage and current waveforms on the load side corresponding to phases (a) and (b, c). This method was tested with a nominal resistive load of one kilowatt (1 kW) and an RMS voltage (VRMS) of 110V. The results demonstrate very impressive power quality, with Total Harmonic Distortion (THD) equal to 0.05% in both voltage and current, as depicted in Figure. 2.12 and Figure. 2.13.

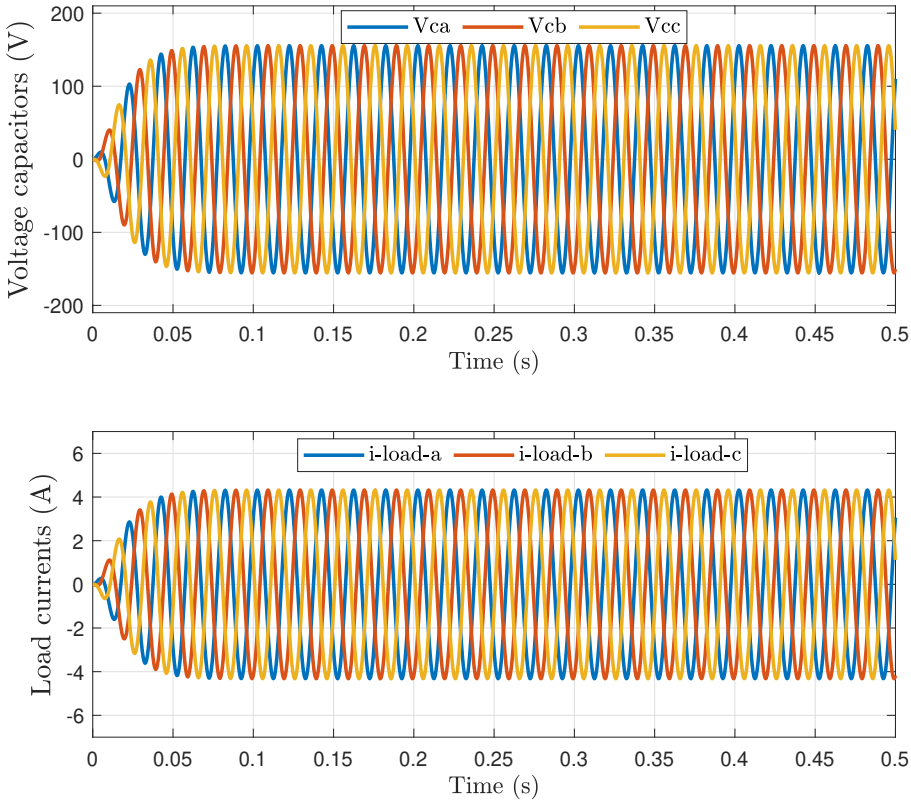

Figure 2.11: Load Side Voltage and Current Measurements During Nominal Operation (1 kW Resistive Load, 110V)

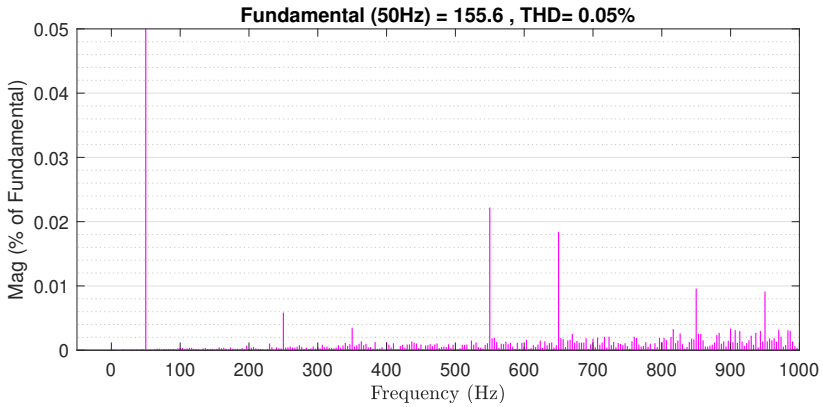

Figure 2.12: Total Harmonic Distortion (THD) of Voltage

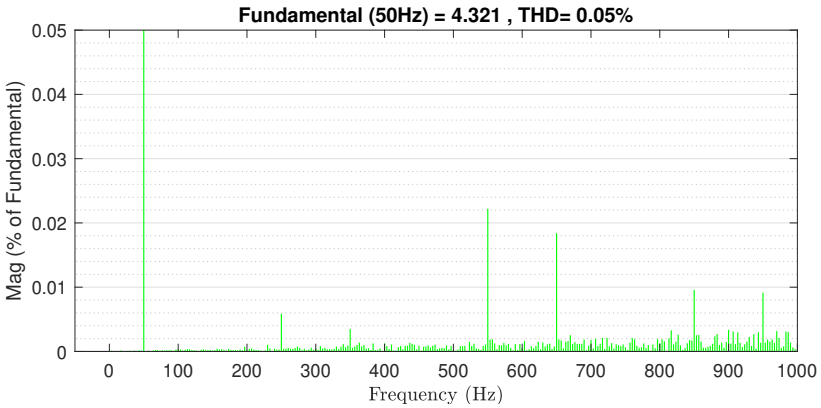

Figure 2.13: Total Harmonic Distortion (THD) of current

To demonstrate the disturbance rejection capabilities, we will supply power to a three phase non-linear load, illustrated in Figure. 2.14. Figure. 2.15 shows the waveforms of the voltages (v_{ca},v_{cb} and v_{cc}) and load currents (i_{La} , i_{Lb} ,i_{Lc}).Additionally, it highlights the Total Harmonic Distortion (THD), which is equal to 3.19%.

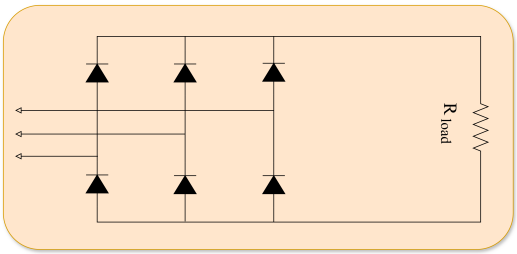

Figure 2.14: Three phase nonlinear load.

Despite the presence of this highly nonlinear load, the system is still able to maintain stable voltage and current waveforms (v_{ca}, v_{cb}, v_{cc}, i_{La}, i_{Lb}, and i_{Lc}). This indicates that the system has mechanisms in place to mitigate the effects of the nonlinear load and maintain the desired output characteristics.

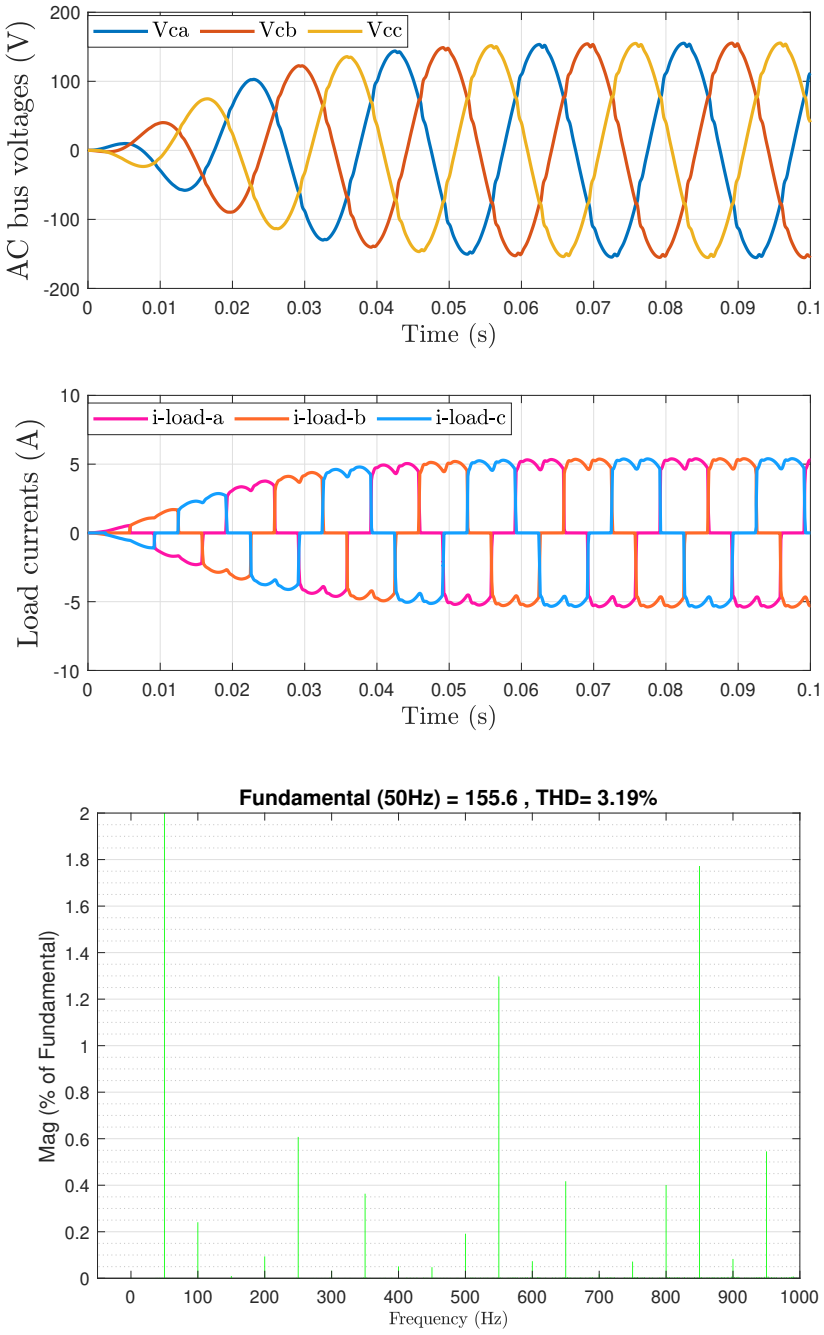

Figure 2.15: Load Side Voltage and Current Measurements During Non-linear Operation (1 kW Load, 110 V_{RMS} AC Bus Voltage) and THD Value of Nonlinear Load.

Second Test: Response to Sudden Changes and Parameter Variations

The assessment of dynamic behavior, demonstrated by a sudden load power change from 0 to 1 kW in 0.1 seconds, is shown in Figure. 2.16. This figure highlights phase (a), representing a single phase within a three-phase inverter system. The waveforms illustrate the voltage and current for this phase during the transient response. Even with this sudden change, the system stabilized very quickly, demonstrating the control strategy's ability to maintain stability and performance under rapid load variations.

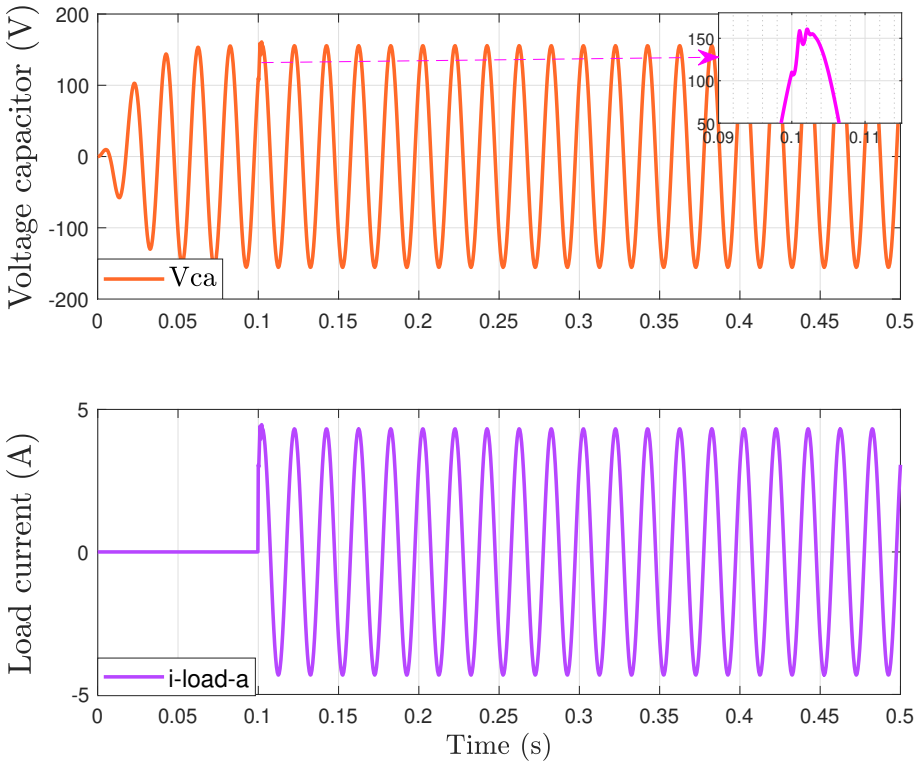

Figure 2.16: Waveforms of the voltage and current of the phase (a) with a rapid variation of the load power.

Figure. 2.17 shows that the measured line currents i_d and i_q closely follow the predicted trajectories ϕ_{id} and ϕ_{iq}, which are calculated using (2.27). This demonstrates that the model accurately predicts the system's current behavior. Figure. 2.18 illustrates the waveform of the load currents, providing insight into their behavior and characteristics.

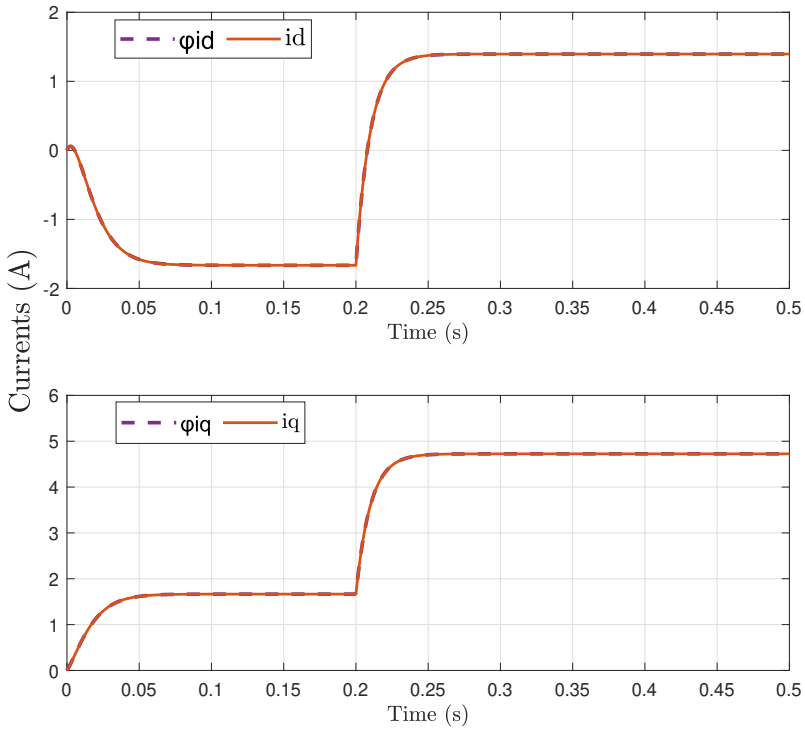

Figure 2.17: Trajectory tracking during a rapid change in load in Line currents.

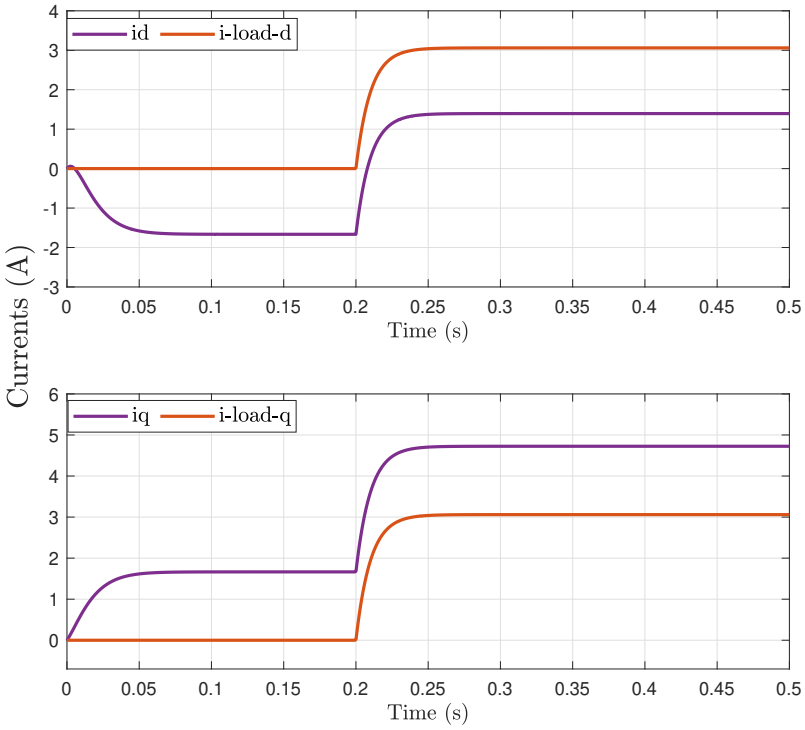

Figure 2.18: Trajectory tracking during a rapid change in load and the resulting variation in load currents.

Evaluating Robustness Under Dynamic Conditions:

A critical aspect of this study is assessing the parametric robustness of the three control approaches. This refers to their ability to maintain performance when encountering unexpected changes in system parameters. To achieve this, we propose a two-pronged approach:

1. **Parameter Variation:**
   - We will introduce variations to the parameters of the LC filter within the system.
   - Specifically, we will simulate two scenarios:
     - **Filter Capacitance (C_f) Variations:**
       * Figure. 2.19 (a) illustrate changes in C_f by $\pm 50\%$.
       * Figure. 2.19 (b) illustrate changes in C_f by $\pm 400\%$.
     - **Inductance (L_n) Errors:**
       * Figure. 2.20 (c) show the inductance value used by the controller with errors of 50%.
       * Figure. 2.20 (d) show the inductance value used by the controller with errors of 250% of its nominal value ($L_n = 1$ mH).
       * Figure 2.21 and Figure 2.22 show the results of C_f by 400% and L_f by 250% in the ABC frame.
2. **Rapid Load Power Change:**
   - In addition to parameter variations, we will simulate a rapid change in load power, as shown in Figure. 2.23.
   - This will involve dynamically adjusting the active load power within the microgrid, ranging from 0 kW (no load) to 12 kW (full load).
   - This rapid change mimics real-world scenarios where power demand fluctuates quickly.
   - The results show that the control approaches effectively handle these dynamic load changes, demonstrating their robustness and adaptability.

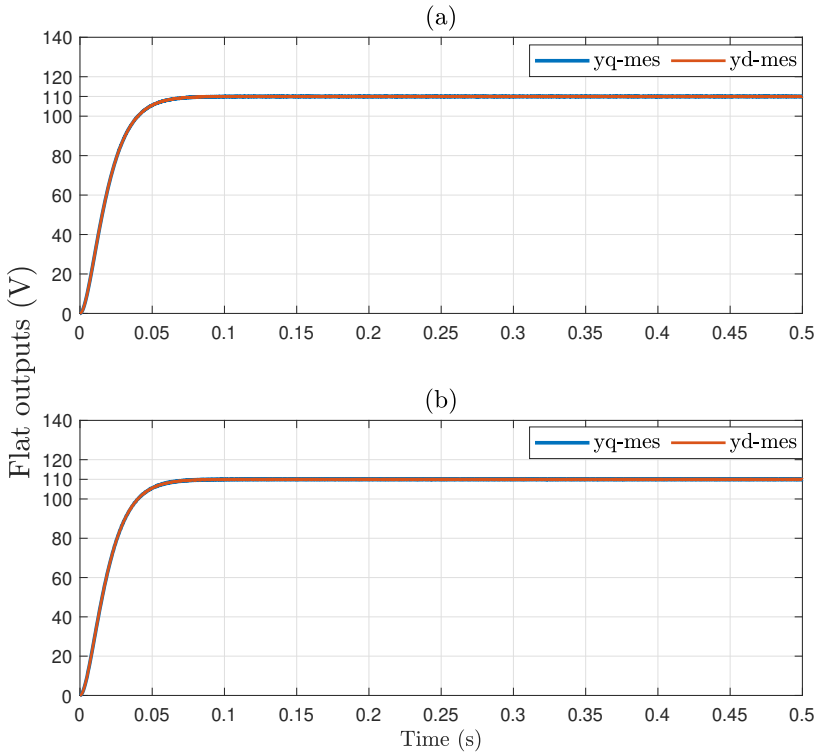

Figure 2.19: Behaviors of y_d and y_q after a Load Step with different values of C_f.

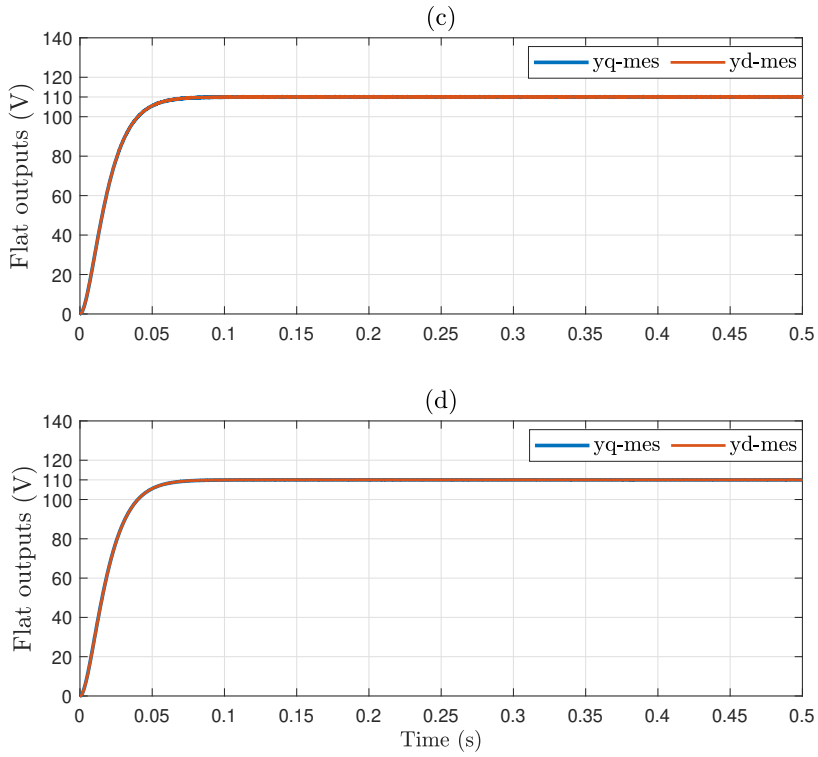

Figure 2.20: Behaviors of y_d and y_q after a Load Step with different values of L_f.

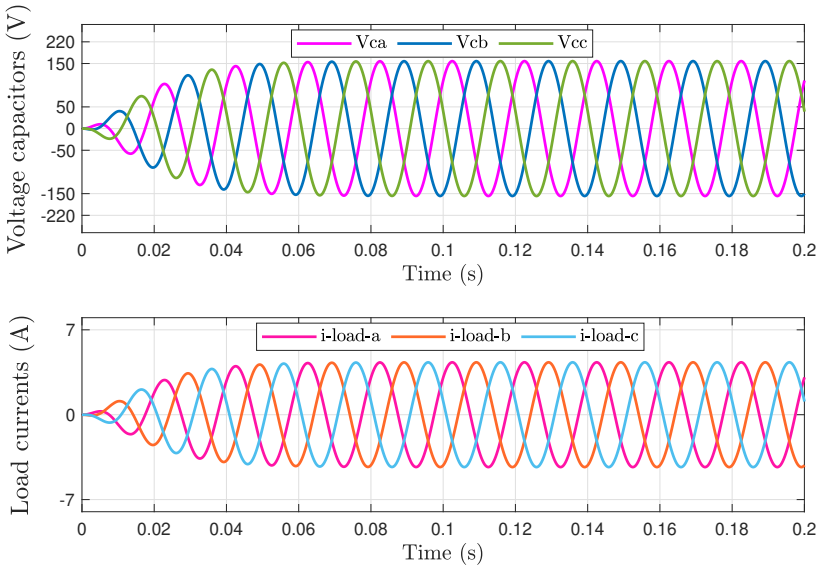

Figure 2.21: Behavior of Load Step with different values of C_f by $\pm 400\%$ in ABC frame

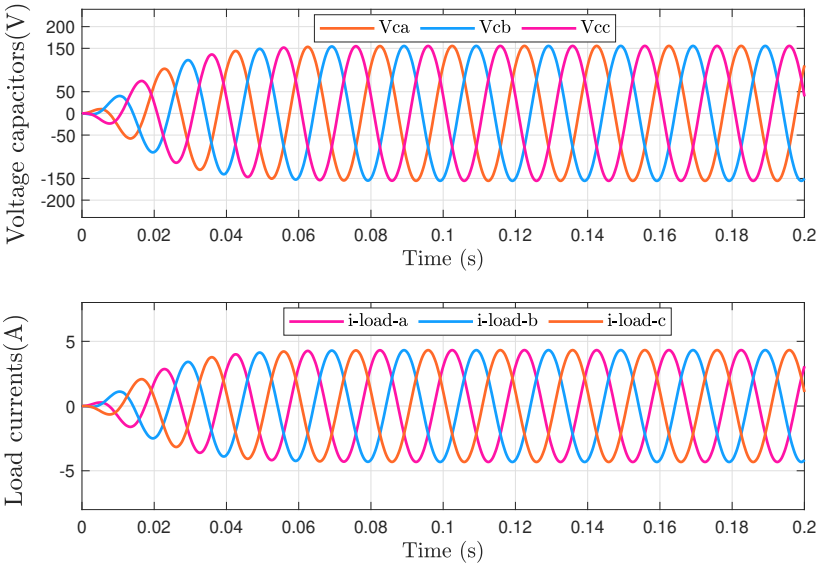

Figure 2.22: Behavior of Load Step with different values of L_f by $\pm 250\%$ in ABC frame

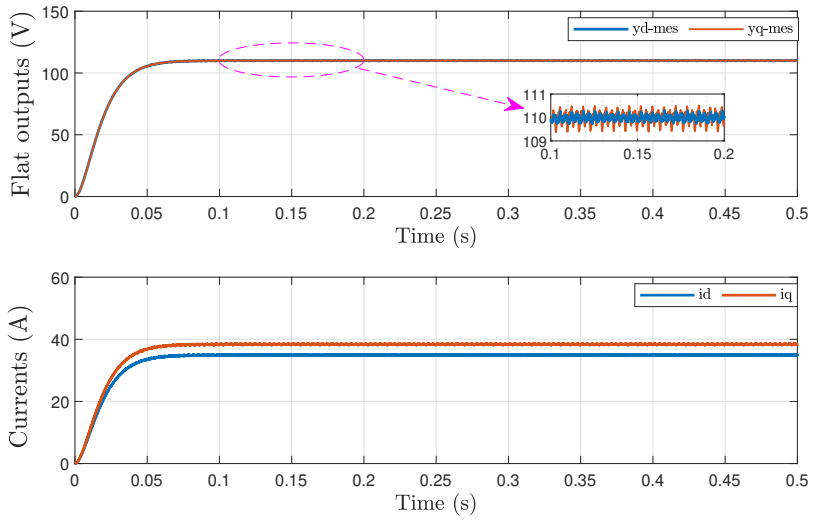

Figure 2.23: Load Side Voltages and Currents (12 kW Resistive Load, Nominal Operation).

2.13 Conclusion

In this chapter, we thoroughly explored the detailed modeling of a 3-phase inverter connected to an LC filter. This endeavor facilitated a comprehensive understanding of the system dynamics through Kirchhoff's laws and Park's transformation, aimed at simplifying system complexities.

Upon establishing a robust model for the inverter, we implemented a flatness-based control strategy. Our initial focus involved verifying the inverter's flatness by computing the functions ϕ_y, ϕ_x, and ϕ_u. Moving forward, we elaborated on the feedback control methodology to ensure precise tracking of the flat output to its reference trajectory and outlined the algorithm for reference trajectory planning. Furthermore, we developed an open-loop control strategy and conducted simulations of a closed-loop system with trajectory tracking to demonstrate the approach's potential,the first test assessed the quality of the supplied energy, ensuring adherence to stringent standards. The second test examined the system's response to transients and parametric variations, providing insights into its robustness and adaptability. Finally, the third test evaluated system stability, examining the control strategy's effectiveness in maintaining stability under varying operating conditions. These comprehensive assessments validated the efficacy of our approach and provided valuable insights into the system's performance in real-world scenarios.

Chapter 3

Flatness-Based Control of AC Microgrid

3.1 Introduction

Building upon the FBC strategies outlined in the previous chapter for a single three-phase inverter connected to an LC filter. This chapter expands the focus to more complex and economically advantageous setup of multiple three-phase inverters connected in parallel within an AC microgrid. Such configurations are increasingly utilized to enhance system capacity, particularly when the capacities of individual switching devices are limited. However, Despite significant advancements in modulation techniques and hardware design for single-phase inverters, as discussed in the previous chapter, scaling these solutions to control parallel inverters remains to be a challenge. This is mainly due to the emergence of circulating currents within the system, which can negatively impact both efficiency and reliability.

This chapter addresses this critical limitation by introducing a novel single-loop FBC that effectively balances currents between parallel inverters and minimizes zero-sequence and circulating current components, maintaining system integrity even in scenarios where one or more inverters might be disconnected. Additionally, the chapter delves into a hierarchical control strategy, designating one inverter as the 'master' to dictate the output voltage, while the remaining inverters function as 'slaves', tasked with regulating currents or power.

3.2 DC/AC interface Case of n inverters in parallel

The power electronics segmentation resulting from the power increase of an electrical installation involves modifying the previous control structure to maintain high dynamic properties while ensuring correct power segmentation in each converter.

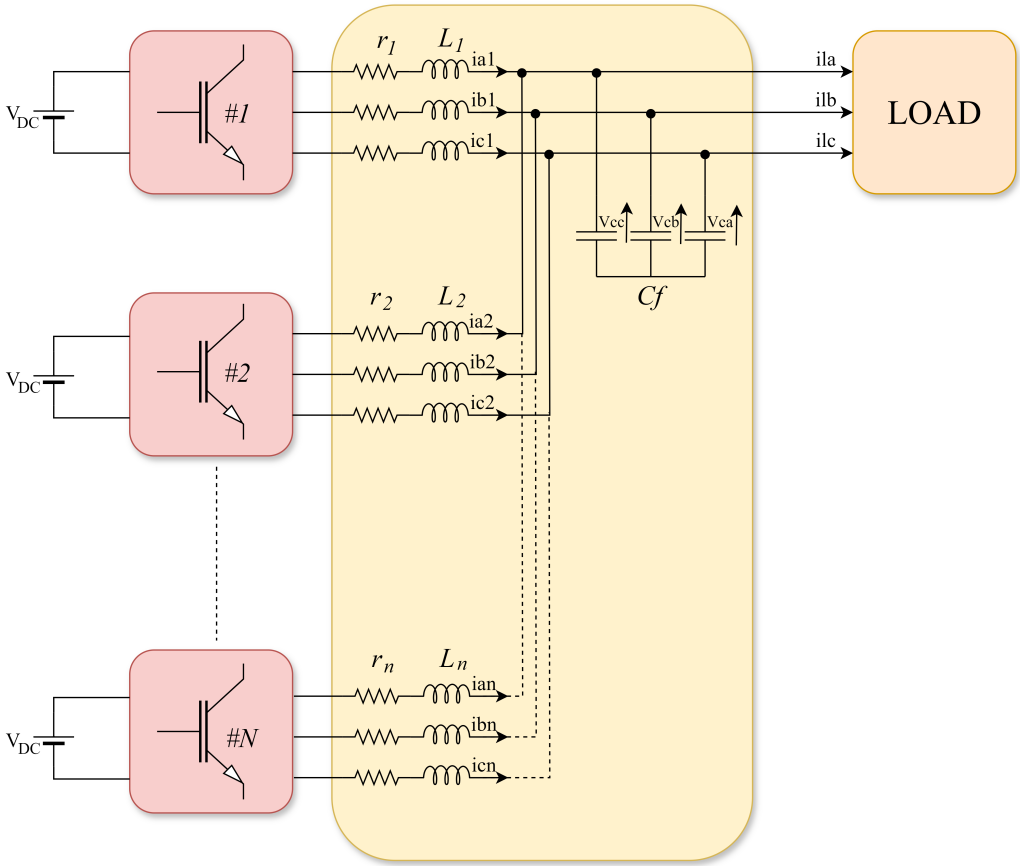

Figure 3.1: DC-to-AC System Architecture: N Parallel Inverters

The DC/AC interface under study consists of n inverters in parallel. As shown in Figure. 3.1, the DC and AC buses are common for all modules. This configuration offers several advantages in terms of reliability and sizing. However, it faces challenges related to interaction between parallel inverters[14][20], leading to circulating currents between parallel branches. When multiple inverters connected to the same DC bus are paralleled, the sum of the output currents of each inverter may not be zero due to differences in physical components and signal distances.

The presence of these circulating currents leads to deteriorated energy quality and decreased component lifespan. Various solutions proposed in the literature focus on modifying pulse width

modulation (PWM) techniques to minimize low-frequency harmonic content[18]. Additionally, combining PWM modifications with physical elements like coupled inductors or common-mode inductances has been suggested[5].

Given the advantages of this topology for autonomous grid power increase, leveraging the properties of differentially flat systems for energy management while ensuring high dynamic properties and controlling homopolar components of inverter currents is proposed. This involves employing a single-loop control structure, establishing a state model, finding its flat output, and designing the control scheme.

For the studied system, the sum of currents absorbed by the load and the sum of currents leaving all n modules are both zero. Similarly, the sum of currents entering the AC bus capacitive filter is zero, assuming DC energy sources are electrically isolated from the AC grid. Consequently, the sum of capacitive currents is zero, and the sum of capacitive voltage values is constant. In this study, assuming initial values of the three capacitive voltages are zero, ensures the homopolar voltage component remains zero.

3.2.1 System Modeling

In a balanced e system depicted in Figure. 3.1, the currents in each phase are mathematically represented as follows:

$$\begin{cases} I_a &= I, \\ I_b &= I\left(-\frac{1}{2} - j\frac{\sqrt{3}}{2}\right), \\ I_c &= I\left(-\frac{1}{2} + j\frac{\sqrt{3}}{2}\right). \end{cases} \tag{3.1}$$

The summation of those current equations yields:

$$I_a + I_b + I_c = I + I\left(-\frac{1}{2} - j\frac{\sqrt{3}}{2}\right) + I\left(-\frac{1}{2} + j\frac{\sqrt{3}}{2}\right) \tag{3.2}$$

$$= I + I(-1) = 0, \tag{3.3}$$

This confirming the principle that the total current in a balanced system is zero, as shown in equation:

$$i_{La} + i_{Lb} + i_{Lc} = 0 \tag{3.4}$$

Extending this principle to the output currents from all n modules in such a system, the combined currents also sum to zero, mathematically expressed as:

$$\sum_{k=1}^{n}(i_{ak} + i_{bk} + i_{ck}) = 0 \tag{3.5}$$

This underscores the inherent stability and efficiency of balanced three-phase electrical systems.

Each inverter within this parallel three-phase system includes a zero-current path, allowing for flexibility in managing zero-sequence currents. Specifically, the zero-sequence current of one inverter can operate freely, while the zero-sequence currents of the remaining $N-1$ inverters are kept as independent state variables. By doing so, the zero-sequence current of the initially free inverter (designated as i_{01}) is negated by the sum of the zero-sequence currents from the other inverters:

$$i_{01} = -\sum_{k=2}^{N} i_{0k} \tag{3.6}$$

To establish the control laws in the continuous domain, the voltage-current model is transformed from the three-phase static frame into the synchronous Park frame. Derivatives of the output voltages in $0dq$ frame with $v_{c0} = 0$ at the common AC bus are obtained as

$$\frac{d}{dt}\begin{pmatrix} v_{cd} \\ v_{cq} \end{pmatrix} = \begin{pmatrix} 0 & \omega \\ -\omega & 0 \end{pmatrix}\begin{pmatrix} v_{cd} \\ v_{cq} \end{pmatrix} + \frac{1}{C_f}\begin{pmatrix} \sum_{k=1}^{n} i_{d_k} \\ \sum_{k=1}^{n} i_{q_k} \end{pmatrix} - \frac{1}{C_f}\begin{pmatrix} i_{Ld} \\ i_{Lq} \end{pmatrix} \tag{3.7}$$

The derivatives of the dq currents of the first inverter as functions of the controlling voltages V_{d1} and V_{q1}, similarly the derivatives of the kth currents of the remaining modules with $k \in \{2, \ldots, N\}$, can be obtained as

$$\frac{d}{dt}\begin{pmatrix} i_{d_1} \\ i_{q_1} \end{pmatrix} = \begin{pmatrix} -\frac{r_f}{L_f} & \omega \\ -\omega & -\frac{r_f}{L_f} \end{pmatrix}\begin{pmatrix} i_{d_1} \\ i_{q_1} \end{pmatrix} + \frac{1}{L_f}\begin{pmatrix} V_{d_1} \\ V_{q_1} \end{pmatrix} - \frac{1}{L_f}\begin{pmatrix} v_{cd} \\ v_{cq} \end{pmatrix} \tag{3.8}$$

The inductive currents of one of the k-th modules remaining, where $k \in \{2, \ldots, n\}$, are:

$$\frac{d}{dt}\begin{pmatrix} i_{0_k} \\ i_{d_k} \\ i_{q_k} \end{pmatrix} = \begin{pmatrix} -\frac{r_k}{L_k} & 0 & 0 \\ 0 & -\frac{r_k}{L_k} & \omega \\ 0 & -\omega & -\frac{r_k}{L_k} \end{pmatrix} \begin{pmatrix} i_{0_k} \\ i_{d_k} \\ i_{q_k} \end{pmatrix} + \frac{1}{L_f}\begin{pmatrix} V_{0_k} \\ V_{d_k} \\ V_{q_k} \end{pmatrix} - \frac{1}{L_f}\begin{pmatrix} v_{c_0} \\ v_{c_d} \\ v_{c_q} \end{pmatrix} \tag{3.9}$$

For the remaining inverters indexed from 2 to n, their individual dq current dynamics are similarly modeled, highlighting the influence of each inverter's specific control voltages alongside shared system voltages on their behavior. where the variables V_{0k}, V_{dk}, and V_{qk} are the controlling voltages of $(N-1)$th inverters.

3.3 PARALLEL INVERTERS CONTROL STRATEGY

3.3.1 Flatness Control of Parallel Inverters System

Control Strategy Using Flat Outputs

The choice of candidate flat outputs in a control system depends significantly on the specific control objectives being pursued. For the system comprising parallel inverters, the voltage and current error vectors between these inverters have been selected as the candidate flat outputs. This decision is geared towards regulating the output AC bus voltage and balancing the currents among the inverters. Such a configuration is expected to enhance dynamic behavior across a variety of conditions, including load perturbations, constant power load systems, and transient states during the switching on or off of any inverter, whether under normal or faulty conditions.

Definition of Candidate Flat Outputs

The candidate flat outputs vector $\mathbf{y}$ is defined as $\mathbf{y} = [\mathbf{y}_c, \mathbf{y}_z]^T$, where the first component $\mathbf{y}_c = [y_d, y_q]^T$ corresponds to the dq voltage capacitors at the output capacitive AC bus of the output LC filter. This is represented mathematically by:

$$\mathbf{y}_c = \begin{pmatrix} y_d \\ y_q \end{pmatrix} \Leftrightarrow \begin{cases} y_d = v_{cd} \\ y_q = v_{cq} \end{cases} \tag{3.10}$$

So:

$$\mathbf{y}_c = \phi_{\mathbf{y}_c}(x) \tag{3.11}$$

The system state vector $(v_{cd}, v_{cq})^T$ is consequently redefined as a function of these flat output vectors, reflecting a direct control linkage.

Current Error Vector as Flat Output

The second part of the flat output vector, $\mathbf{y}_z$, pertains to the current error vector, which encapsulates the differences in current with respect to a reference inverter. This part of the flat output vector is instrumental in minimizing circulating currents and achieving power balance between the reference and all other working kth inverters[14]. Each component y_{zk} for $k \neq i$ in the set $\{2, \ldots, N\}$ is defined as:

$$\mathbf{y}_{z_k} = \begin{pmatrix} z_{0_k} \\ z_{d_k} \\ z_{q_k} \end{pmatrix} = \begin{pmatrix} i_{0_k} \\ i_{d_1} - i_{d_k} \\ i_{q_1} - i_{q_k} \end{pmatrix} = \phi_{\mathbf{y}z_k}(x) \tag{3.12}$$

In (3.11) and (3.12), we validate the initial condition of the flatness theory. Specifically, we confirm that the flat output is selected in terms of the state variables.

$$\mathbf{y} = \phi_{\mathbf{y}}(x) \tag{3.13}$$

Now, it is necessary to verify if the candidate flat output y satisfies the flatness conditions given (1.2) and (1.3). It is evident that (1.2) is satisfied. We only need to express all state variables in terms of the components of the flat output and their successive derivatives.

$$\begin{pmatrix} v_{cd} \\ v_{cq} \end{pmatrix} = \begin{pmatrix} y_d \\ y_q \end{pmatrix} = \begin{pmatrix} \phi_{v_{cd}}(y_d) \\ \phi_{v_{cq}}(y_q) \end{pmatrix} \tag{3.14}$$

From the equation of voltage derivative

$$\frac{d}{dt}\begin{pmatrix} v_{cd} \\ v_{cq} \end{pmatrix} = \begin{pmatrix} 0 & w \\ -w & 0 \end{pmatrix}\begin{pmatrix} v_{cd} \\ v_{cq} \end{pmatrix} + \frac{1}{C_f}\begin{pmatrix} \sum_{k=1}^{n} i_{d_k} \\ \sum_{k=1}^{n} i_{q_k} \end{pmatrix} - \frac{1}{C_f}\begin{pmatrix} i_{Ld} \\ i_{Lq} \end{pmatrix} \tag{3.15}$$

Using (3.10) yields

$$\begin{pmatrix} \dot{y}_d \\ \dot{y}_q \end{pmatrix} = \begin{pmatrix} 0 & w \\ -w & 0 \end{pmatrix} \begin{pmatrix} y_d \\ y_q \end{pmatrix} + \frac{1}{C_f} \begin{pmatrix} i_{d_1} \\ i_{q_1} \end{pmatrix} - \frac{1}{C_f} \begin{pmatrix} i_{Ld} \\ i_{Lq} \end{pmatrix} + \frac{1}{C_f} \begin{pmatrix} \sum_{k=2}^{n} i_{d_k} \\ \sum_{k=2}^{n} i_{q_k} \end{pmatrix} \tag{3.16}$$

The relation between the currents and the flat output $\mathbf{y}_z$ is given by

$$\begin{pmatrix} \sum_{j=2}^{n} i_{d_k} \\ \sum_{j=2}^{n} i_{q_k} \end{pmatrix} = \begin{pmatrix} \sum_{j=2}^{n} (i_{d_1} - z_{d_J}) \\ \sum_{j=2}^{n} (i_{q_1} - z_{q_J}) \end{pmatrix} = (n-1) \begin{pmatrix} i_{d_1} \\ i_{q_1} \end{pmatrix} - \begin{pmatrix} \sum_{j=2}^{n} z_{d_J} \\ \sum_{j=2}^{n} z_{q_j} \end{pmatrix} \tag{3.17}$$

And it entails that

$$\begin{pmatrix} \dot{y}_d \\ \dot{y}_q \end{pmatrix} = \begin{pmatrix} 0 & w \\ -w & 0 \end{pmatrix} \begin{pmatrix} y_d \\ y_q \end{pmatrix} + \frac{1}{C_f} \begin{pmatrix} i_{d_1} \\ i_{q_1} \end{pmatrix} + \frac{(n-1)}{C_f} \begin{pmatrix} i_{d_1} \\ i_{q_1} \end{pmatrix} - \frac{1}{C_f} \begin{pmatrix} \sum_{j=2}^{n} z_{d_J} \\ \sum_{j=2}^{n} z_{q_j} \end{pmatrix} - \frac{1}{C_f} \begin{pmatrix} i_{Ld} \\ i_{Lq} \end{pmatrix} \tag{3.18}$$

Thus, the currents $(i_d, i_q)^T$ are obtained by this equation

$$\begin{pmatrix} i_{d_1} \\ i_{q_1} \end{pmatrix} = \frac{C_f}{n} \begin{pmatrix} \dot{y}_d \\ \dot{y}_q \end{pmatrix} - \frac{1}{n} \begin{pmatrix} 0 & C_f w \\ -w C_f & 0 \end{pmatrix} \begin{pmatrix} y_d \\ y_q \end{pmatrix} + \frac{1}{n} \begin{pmatrix} \sum_{j=2}^{n} z_{d_J} \\ \sum_{j=2}^{n} z_{q_j} \end{pmatrix} + \frac{1}{n} \begin{pmatrix} i_{Ld} \\ i_{Lq} \end{pmatrix} \tag{3.19}$$

The vector $(i_d, i_q)^T$ can be expressed in terms of the flat output and its derivative.

$$\begin{pmatrix} i_{d_1} \\ i_{q_1} \end{pmatrix} = \begin{pmatrix} \phi_{i_{d1}}(y_c, \dot{y}_c, y_z) \\ \phi_{i_{q1}}(y_c, \dot{y}_c, y_z) \end{pmatrix} \tag{3.20}$$

By using (3.12) and (3.19), the expression for the line currents of the remaining inverters k ($k \in \{2, \ldots, n\}$) becomes

$$\begin{pmatrix} i_{0_k} \\ i_{d_k} \\ i_{d_k} \end{pmatrix} = \begin{pmatrix} z_{0_k} \\ \phi_{i_{d1}}(y_c, \dot{y}_c, y_z) - z_{d_k} \\ \phi_{i_{q1}}(y_c, \dot{y}_c, y_z) - z_{q_k} \end{pmatrix} = \begin{pmatrix} \phi_{i_{0k}}(y_z) \\ \phi_{i_{dk}}(y_c, \dot{y}_c, y_z) \\ \phi_{i_{qk}}(y_c, \dot{y}_c, y_z) \end{pmatrix} \tag{3.21}$$

Thus, by incorporating (3.14), (3.20), and (3.21), the expression of the state variables in terms

of the flat output and its derivatives is obtained.

$$x = \phi_x(y_c, \dot{y_c}, y_z) \tag{3.22}$$

Where x represents the state variables. Now, the control vector can be extracted from the equations of the currents derivative. -In the first currents derivative:

$$\frac{d}{dt}\begin{pmatrix} i_{d_1} \\ i_{q_1} \end{pmatrix} = \begin{pmatrix} -\frac{r_1}{L_1} & w \\ -w & -\frac{r_1}{L_1} \end{pmatrix}\begin{pmatrix} i_{d_1} \\ i_{q_1} \end{pmatrix} + \frac{1}{L_1}\begin{pmatrix} V_{d_1} \\ V_{q_1} \end{pmatrix} - \frac{1}{L_1}\begin{pmatrix} y_d \\ y_q \end{pmatrix} \tag{3.23}$$

$$\begin{pmatrix} i_{d_1} \\ i_{q_1} \end{pmatrix} = \frac{C_f}{n}\begin{pmatrix} \dot{y_d} \\ \dot{y_q} \end{pmatrix} - \frac{1}{n}\begin{pmatrix} 0 & C_f w \\ -wC_f & 0 \end{pmatrix}\begin{pmatrix} y_d \\ y_q \end{pmatrix} + \frac{1}{n}\begin{pmatrix} \sum_{j=2}^{n} z_{d_j} \\ \sum_{j=2}^{n} z_{q_j} \end{pmatrix} + \frac{1}{n}\begin{pmatrix} i_{Ld} \\ i_{Lq} \end{pmatrix} \tag{3.24}$$

By deriving this equation, the following is obtained:

$$\frac{d}{dt}\begin{pmatrix} i_{d_1} \\ i_{q_1} \end{pmatrix} = \frac{C_f}{n}\begin{pmatrix} \ddot{y_d} \\ \ddot{y_q} \end{pmatrix} + \frac{1}{n}\begin{pmatrix} 0 & C_f w \\ -wC_f & 0 \end{pmatrix}\begin{pmatrix} \dot{y_d} \\ \dot{y_q} \end{pmatrix} + \frac{1}{n}\begin{pmatrix} \sum_{j=2}^{n} \dot{z_{dJ}} \\ \sum_{j=2}^{n} \dot{z_{qJ}} \end{pmatrix} + \frac{1}{n}\frac{d}{dt}\begin{pmatrix} i_{Ld} \\ i_{Lq} \end{pmatrix} \tag{3.25}$$

Thus, the derivative of the current for the first inverter can be represented as follows

$$\frac{d}{dt}\begin{pmatrix} i_{d_1} \\ i_{q_1} \end{pmatrix} = \begin{pmatrix} \phi_{di_{d1}}(y_c, \dot{y_c}, \ddot{y_c}, y_z, \dot{y_z}) \\ \phi_{di_{q1}}(y_c, \dot{y_c}, \ddot{y_c}, y_z, \dot{y_z}) \end{pmatrix} \tag{3.26}$$

Substituting (3.24) into (3.8) gives

$$\begin{aligned} \frac{d}{dt}\begin{pmatrix} i_{d1} \\ i_{q1} \end{pmatrix} = &\begin{pmatrix} -\frac{C_f \cdot r_1}{L_1 \cdot n}\dot{y_d} + w \cdot \frac{C_f}{n}\dot{y_q} \\ -w \cdot \frac{C_f}{n}\dot{y_d} - \frac{r_1 \cdot C_f}{L_1 \cdot n}\dot{y_q} \end{pmatrix} - \begin{pmatrix} -\frac{C_f \cdot w^2}{n}y_d & -w \cdot \frac{C_f \cdot r_1}{L_1 \cdot n}y_q \\ w \cdot \frac{C_f \cdot r_1}{L_1 \cdot n}y_d & -\frac{w^2 \cdot C_f}{n}y_q \end{pmatrix} + \begin{pmatrix} -\frac{r_1}{L_1 \cdot n}\sum_{j=2}^{n} z_{d_j} + \frac{w}{n}\sum_{j=2}^{n} z_{q_j} \\ -\frac{w}{n}\sum_{j=2}^{n} z_{d_j} - \frac{r_1}{L_1 \cdot n}\sum_{j=2}^{n} z_{q_j} \end{pmatrix} \\ &+ \begin{pmatrix} -\frac{r_1}{L_1 \cdot n}i_{L_d} + \frac{w}{n}i_{L_q} \\ \frac{-w}{n}i_{L_d} - \frac{r_1}{L_1 \cdot n}i_{L_q} \end{pmatrix} + \frac{1}{L_1}\begin{pmatrix} V_{d_1} \\ V_{q_1} \end{pmatrix} - \frac{1}{L_1}\begin{pmatrix} y_d \\ y_q \end{pmatrix} \end{aligned} \tag{3.27}$$

By utilizing the linearity property

$$a\sum_{k=1}^{n} x + b\sum_{k=1}^{n} y = \sum_{k=1}^{n}(ax + by) \tag{3.28}$$

The following can be applied:

$$\frac{d}{dt}\begin{pmatrix} i_{d1} \\ i_{q1} \end{pmatrix} = \begin{pmatrix} -\frac{C_f \cdot r_1}{L_1 \cdot n}\ \dot{y}_d + w \cdot \frac{C_f}{n}\dot{y}_q \\ -w \cdot \frac{C_f}{n}\dot{y}_d - \frac{r_1 \cdot C_f}{n}\dot{y}_q \end{pmatrix} - \begin{pmatrix} -\frac{C_f \cdot r_1 w}{L_1 \cdot n}\ y_q - w^2 \cdot \frac{C_f}{n} y_d \\ w \cdot \frac{C_f \cdot r_1}{L_1 \cdot n} y_d - \frac{w^2 \cdot C_f}{n} y_q \end{pmatrix}$$

$$+ \begin{pmatrix} \sum_{j=2}^{n} \left(\frac{r_1}{L_1 \cdot n} z_{d_J} + \frac{w}{n} z_{q_J} \right) \\ \sum_{j=2}^{n} \left(\frac{w}{n} z_{d_J} + \frac{r_1}{L_1 \cdot n} z_{q_J} \right) \end{pmatrix} + \begin{pmatrix} -\frac{r_1}{L_1 \cdot n}\ i_{L_d} + \frac{w}{n} i_{L_q} \\ -\frac{w}{n}\ i_{L_d} - \frac{r_1}{L_1 \cdot n}\ i_{L_q} \end{pmatrix} + \frac{1}{L_1}\begin{pmatrix} V_{d_1} \\ V_{q_1} \end{pmatrix} - \frac{1}{L_1}\begin{pmatrix} y_d \\ y_q \end{pmatrix} \tag{3.29}$$

From (3.25), the control vector for the first inverter is derived as follows:

$$\begin{pmatrix} V_{d_1} \\ V_{q_1} \end{pmatrix} = L_1 \left[\frac{C_f}{n} \begin{pmatrix} \ddot{y}_d \\ \ddot{y}_q \end{pmatrix} - \frac{1}{n} \begin{pmatrix} C_f \cdot w \cdot \dot{y}_q \\ -C_f \cdot w \cdot \dot{y}_d \end{pmatrix} + \frac{1}{n} \begin{pmatrix} \sum_{j=2}^{n} \dot{z}_{d_J} \\ \sum_{j=2}^{n} \dot{z}_{q_j} \end{pmatrix} + \frac{1}{n}\frac{d}{dt} \begin{pmatrix} i_{Ld} \\ i_{Lq} \end{pmatrix} \right.$$

$$- \begin{pmatrix} -\frac{C_f \cdot r_1}{L_1 \cdot n} \cdot \dot{y}_d + w \cdot \frac{C_f}{n} \cdot \dot{y}_q \\ -w \cdot \frac{C_f}{n} \cdot \dot{y}_d - \frac{r_1 \cdot C_f}{n} \cdot \dot{y}_q \end{pmatrix} + \begin{pmatrix} -\frac{C_f \cdot w^2}{n} \cdot y_d + w \cdot \frac{C_f \cdot r_1}{n L_1} \cdot y_q \\ w \cdot \frac{C_f \cdot r_1}{L_1 \cdot n} \cdot y_d - \frac{w^2 \cdot C_f}{n} \cdot y_q \end{pmatrix} - \begin{pmatrix} \sum_{j=2}^{n} (-\frac{r_1}{L_1 \cdot n} \cdot z_{d_J} + \frac{w}{n} z_{q_J}) \\ \sum_{j=2}^{n} (\frac{-w}{n} z_{d_J} - \frac{r_1}{L_1 \cdot n} \cdot z_{q_J}) \end{pmatrix}$$

$$\left. - \begin{pmatrix} -\frac{r_1}{L_1 \cdot n} \cdot i_{L_d} + \frac{w}{n} i_{L_q} \\ -\frac{w}{n} i_{L_d} - \frac{r_1}{L_1 \cdot n} \cdot i_{L_q} \end{pmatrix} + \frac{1}{L_1} \begin{pmatrix} y_d \\ y_q \end{pmatrix} \right] \tag{3.30}$$

After simplification and utilizing mathematical properties, the equation for the control vector is obtained in the following form:

$$\begin{pmatrix} V_{d_1} \\ V_{q_1} \end{pmatrix} = L_1 \left[\frac{C_f}{n} \begin{pmatrix} \ddot{y}_d \\ \ddot{y}_q \end{pmatrix} - \frac{1}{n} \begin{pmatrix} 2C_f \cdot w \cdot \dot{y}_q \\ -2C_f \cdot w \cdot \dot{y}_d \end{pmatrix} + \frac{1}{n} \begin{pmatrix} \sum_{j=2}^{n} \dot{z}_{d_J} \\ \sum_{j=2}^{n} \dot{z}_{q_j} \end{pmatrix} + \frac{1}{n}\frac{d}{dt} \begin{pmatrix} i_{Ld} \\ i_{Lq} \end{pmatrix} \right.$$

$$+ \frac{1}{n} \begin{pmatrix} C_f \cdot r_1 \cdot \dot{y}_q \\ C_f \cdot r_1 \cdot \dot{y}_d \end{pmatrix} + \frac{1}{n} \left(\frac{C_f \cdot r_1 \cdot w}{L_1} \right) \begin{pmatrix} -y_q \\ y_d \end{pmatrix} + \left(\frac{1}{L_1} - \frac{C_f \cdot w^2}{n} \right) \begin{pmatrix} y_d \\ y_q \end{pmatrix} - \frac{1}{n} \begin{pmatrix} \sum_{j=2}^{n} \left(\frac{-r_1}{L_1} z_{d_j} + w \cdot z_{q_j} \right) \\ \sum_{j=2}^{n} \left(-w \cdot z_{d_j} - \frac{r_1}{L_1} z_{q_j} \right) \end{pmatrix}$$

$$\left. + \frac{1}{n} \begin{pmatrix} \frac{r_1}{L_1} \cdot i_{L_d} - w \cdot i_{L_q} \\ w \cdot i_{L_d} + \frac{r_1}{L_1} \cdot i_{L_q} \end{pmatrix} \right] \tag{3.31}$$

Thus, the control expression of this form is found.

$$\begin{pmatrix} V_{d1} \\ V_{q1} \end{pmatrix} = \begin{pmatrix} \psi_{V_{d1}}(y_c, \dot{y_c}, \ddot{y_c}, y_z, \dot{y_z}) \\ \psi_{V_{q1}}(y_c, \dot{y_c}, \ddot{y_c}, y_z, \dot{y_z}) \end{pmatrix} \tag{3.32}$$

Following the same analysis method, the control vector of the $N-1$ remaining inverters $\forall k \in \{2, \ldots, N\}, k \neq i$ can be obtained as

$$\mathbf{V}_k = \begin{pmatrix} V_{0_k} \\ V_{d_k} \\ V_{q_k} \end{pmatrix} \tag{3.33}$$

The differential equations for the dynamics of the first inverters can be derived from (3.9).

$$\begin{cases} \frac{d}{dt} i_{0_k} & = -\frac{r_k}{L_k} i_{0_k} + \frac{1}{L_k} V_{0_k} - \frac{1}{L_k} v_{c_0}, \\ \frac{d}{dt} \begin{pmatrix} i_{d_k} \\ i_{q_k} \end{pmatrix} & = \begin{pmatrix} 0 & w \\ -w & 0 \end{pmatrix} \begin{pmatrix} i_{d_k} \\ i_{q_k} \end{pmatrix} + \frac{1}{L_k} \begin{pmatrix} V_{d_k} \\ V_{q_k} \end{pmatrix} - \frac{1}{L_k} \begin{pmatrix} v_{c_d} \\ v_{c_q} \end{pmatrix} \end{cases} \tag{3.34}$$

So, by using (3.12), (3.25) and (3.26)

$$\frac{d}{dt} \begin{pmatrix} i_{d_k} + z_{d_k} \\ i_{q_k} + z_{q_k} \end{pmatrix} = \frac{C_f}{n} \begin{pmatrix} \ddot{y_d} \\ \ddot{y_q} \end{pmatrix} + \frac{1}{n} \begin{pmatrix} 0 & C_f w \\ -wC_f & 0 \end{pmatrix} \begin{pmatrix} \dot{y_d} \\ \dot{y_q} \end{pmatrix} + \frac{1}{n} \begin{pmatrix} \sum_{j=2}^{n} \dot{z_{dJ}} \\ \sum_{j=2}^{n} \dot{z_{q}}_J \end{pmatrix} + \frac{1}{n} \frac{d}{dt} \begin{pmatrix} i_{Ld} \\ i_{Lq} \end{pmatrix} \tag{3.35}$$

From this, the following is found:

$$\frac{d}{dt} \begin{pmatrix} i_{d_k} \\ i_{q_k} \end{pmatrix} = \frac{C_f}{n} \begin{pmatrix} \ddot{y_d} \\ \ddot{y_q} \end{pmatrix} + \frac{1}{n} \begin{pmatrix} 0 & C_f w \\ -wC_f & 0 \end{pmatrix} \begin{pmatrix} \dot{y_d} \\ \dot{y_q} \end{pmatrix} + \frac{1}{n} \begin{pmatrix} \sum_{j=2}^{n} \dot{z_{dJ}} \\ \sum_{j=2}^{n} \dot{z_{q}}_J \end{pmatrix} + \frac{1}{n} \frac{d}{dt} \begin{pmatrix} i_{Ld} \\ i_{Lq} \end{pmatrix} - \frac{d}{dt} \begin{pmatrix} z_{d_k} \\ z_{q_k} \end{pmatrix} \tag{3.36}$$

Thus, the relation between the currents of (n-1) inverters and the flat output y and its derivatives

is obtained in the following form:

$$\frac{d}{dt}\begin{pmatrix} i_{0_k} \\ i_{d_k} \\ i_{q_k} \end{pmatrix} = \begin{pmatrix} \phi_{di_{0k}}(\dot{y_z}) \\ \phi_{di_{dk}}(y_c, \dot{y_c}, \ddot{y_c}, y_z, \dot{y_z}) \\ \phi_{di_{qk}}(y_c, \dot{y_c}, \dot{y_c}, y_z, \dot{y_z}) \end{pmatrix} \tag{3.37}$$

According to the second chosen flat output, the following is obtained:

$$z_{0_k} = i_{0_k} \tag{3.38}$$

$$\begin{pmatrix} z_{d_k} \\ z_{d_k} \end{pmatrix} = \begin{pmatrix} i_{d_1} - i_{d_k} \\ i_{q_1} - i_{q_k} \end{pmatrix} \tag{3.39}$$

This leads us to

$$\begin{cases} V_{0_k} = L_k \left(\dot{z}_{0_k} + \frac{r_k}{L_k} z_{0_k} + \frac{1}{L_k} V_{c_0} \right) \\ \\ \frac{d}{dt} \begin{pmatrix} i_{d_1} - z_{d_k} \\ i_{q_1} - z_{q_k} \end{pmatrix} = \begin{pmatrix} -\frac{r_k}{L_k} & w \\ -w & -\frac{r_k}{L_k} \end{pmatrix} \begin{pmatrix} i_{d_1} - z_{d_k} \\ i_{q_1} - z_{q_k} \end{pmatrix} + \frac{1}{L_k} \begin{pmatrix} V_{d_k} \\ V_{q_k} \end{pmatrix} - \frac{1}{L_k} \begin{pmatrix} v_{c_d} \\ v_{c_q} \end{pmatrix} \end{cases} \tag{3.40}$$

By the relation between the second chosen flat output and the currents, and by utilizing (3.34), the following is found:

$$\frac{d}{dt}\begin{pmatrix} i_{d_1} \\ i_{q_1} \end{pmatrix} - \begin{pmatrix} \dot{z}_{d_k} \\ \dot{z}_{q_k} \end{pmatrix} = \begin{pmatrix} -\frac{r_k}{L_k} & w \\ -w & -\frac{r_k}{L_k} \end{pmatrix} \begin{pmatrix} i_{d_1} \\ i_{q_k} \end{pmatrix} - \begin{pmatrix} -\frac{r_k}{L_k} & w \\ -w & -\frac{r_k}{L_k} \end{pmatrix} \begin{pmatrix} z_{d_k} \\ z_{q_k} \end{pmatrix} + \frac{1}{L_k} \begin{pmatrix} V_{d_k} \\ V_{q_k} \end{pmatrix} - \frac{1}{L_k} \begin{pmatrix} v_{c_d} \\ v_{c_q} \end{pmatrix} \tag{3.41}$$

By using (3.24) and (3.25), the following is found:

$$\begin{pmatrix} V_{d_k} \\ V_{q_k} \end{pmatrix} = L_k \left(\frac{C_f}{n} \begin{pmatrix} \ddot{y}_d \\ \ddot{y}_q \end{pmatrix} - \frac{1}{n} \begin{pmatrix} 0 & C_f w \\ -C_f w & 0 \end{pmatrix} \begin{pmatrix} \dot{y}_d \\ \dot{y}_q \end{pmatrix} + \frac{1}{n} \begin{pmatrix} \sum_{j=2}^{n} \dot{z}_{d_j} \\ \sum_{j=2}^{n} \dot{z}_{q_j} \end{pmatrix} + \frac{1}{n} \frac{d}{dt} \begin{pmatrix} i_{Ld} \\ i_{Lq} \end{pmatrix} \right.$$

$$\left. - \begin{pmatrix} \dot{z}_{d_k} \\ \dot{z}_{q_k} \end{pmatrix} - \begin{pmatrix} 0 & -\frac{r_k}{L_k} \\ -\frac{r_k}{L_k} & 0 \end{pmatrix} \begin{pmatrix} \psi_{i_{d1}} \\ \psi_{i_{q1}} \end{pmatrix} - \begin{pmatrix} 0 & -\frac{r_k}{L_k} \\ -\frac{r_k}{L_k} & 0 \end{pmatrix} \begin{pmatrix} z_{d_k} \\ z_{q_k} \end{pmatrix} + \frac{1}{L_k} \begin{pmatrix} y_d \\ y_q \end{pmatrix} \right) \tag{3.42}$$

Thus, the control expression for $\{V_k\}$ is derived in the following form:

$$\mathbf{V}_k = \begin{pmatrix} \psi_{v_{0k}}(y_z, \dot{y_z}) \\ \psi_{v_{dk}}(y_c, \dot{y_c}, \ddot{y_c}, y_z, \dot{y_z}) \\ \psi_{Vq_k}(y_c, \dot{y_c}, \ddot{y_c}, y_z, \dot{y_z}) \end{pmatrix} \tag{3.43}$$

In summary, the three laws of flatness control are verified as follows

The first law, stating the expressibility of state x and control u inputs in terms of flat outputs y,is confirmed by (3.22).

The second law, concerning the differentiability of the flat outputs y and is dependency on state x and inputs u, is upheld by (3.13).

The third law, which involves the parameterization of control inputs u and the expression of state x in terms of the flat output y, is satisfied by (3.32) and (3.43).

3.3.2 Reference Trajectory Definition

To plan the desired trajectory of the candidate flat output y and its components as specified in (1.7) and (1.9), a low-pass second-order filter is employed. This filter helps limit power surges during transient states caused by variations in the voltage reference value V_{rms}. The inputs to these filters are the reference trajectories y_c^{ref} and y_{zk}^{ref}. This formulation ensures that the conditions for the derivatives of the candidate flat output at both the initial time and in steady state are met, requiring these derivatives to be zero at these instants. Therefore, the desired reference trajectory for each component, $y_{\text{ref}} = [y_c^{\text{ref}}, y_z^{\text{ref}}]^T$ for all k in $\{2, \ldots, n\}, k \neq i$, can be modeled as follows:

$$y_{c_{\text{ref\_f}}} = \left[1 - \left(1 + \frac{t - t_{\text{int}}}{\tau_1}\right) e^{-\frac{t-t_{\text{init}}}{\tau_1}}\right] (y_{c_{\text{ref}}} - y_{c_{\text{init}}}) + y_{c_{\text{init}}} \tag{3.44}$$

$$y_{z_{\text{ref\_f}}} = \left[1 - \left(1 + \frac{t - t_{\text{int}}}{\tau_2}\right) e^{-\frac{t-t_{\text{init}}}{\tau_2}}\right] (y_{z_{\text{ref}}} - y_{z_{\text{init}}}) + y_{z_{\text{init}}} \tag{3.45}$$

3.3.3 Flatness-based controller implementation

$$\ddot{y}_d = \gamma_d \tag{3.46}$$

$$\ddot{y}_q = \gamma_q \tag{3.47}$$

This allow an asymptotic convergence of the variables to their respective reference trajectories and can be deduced as:

$$(\ddot{y}_{d_{\text{ref}}} - \gamma_d) + k_{11}(\dot{y}_{d_{\text{ref}}} - \dot{y}_d) + k_{12}(y_{d_{\text{ref}}} - y_d) + k_{13}\int (y_{d_{\text{ref}}} - y_d)d\tau \quad = 0 \tag{3.48}$$

$$(\ddot{y}_{q_{\text{ref}}} - \gamma_q) + k_{11}(\dot{y}_{q_{\text{ref}}} - \dot{y}_q) + k_{12}(y_{q_{\text{ref}}} - y_q) + k_{13}\int (y_{q_{\text{ref}}} - y_q)d\tau \quad = 0 \tag{3.49}$$

The integral term is introduced to ensure zero static error in steady state and compensate the effects introduced by the system modeling errors. For each current error vector y_{zk}, the fictitious control variable $\gamma_{zk} = [\gamma_{z0_k}, \gamma_{zd_k}, \gamma_{zq_k}]^T$ is introduced and expressed in the same way for the output energy vector as:

$$\begin{cases} \dot{z}_{0_k} & = \gamma_{z0_k} \\ \dot{z}_{d_k} & = \gamma_{zd_k} \\ \dot{z}_{q_k} & = \gamma_{zq_k} \end{cases} \forall k \in \{2, ..., N\}. \tag{3.50}$$

Second-order laws are used to ensure that the current error vector y_{zk} follows its planned reference $y_{zk_{ref}}$:

$$(\dot{y}_{zk_{ref}} - \gamma_{zk}) + k_{21}(y_{zk_{ref}} - y_{zk}) + k_{22}\int (y_{zk_{ref}} - y_{zk})d\tau = 0 \tag{3.51}$$

The variable ε is introduced to express dynamics of the error:

$$\begin{aligned} \dddot{\varepsilon}_{yc} + k_{11}\ddot{\varepsilon}_{yc} + k_{12}\dot{\varepsilon}_{yc} + k_{13}\varepsilon_{yc} = 0 \\ \ddot{\varepsilon}_{yz} + k_{21}\dot{\varepsilon}_{yz} + k_{22}\varepsilon_{yz} = 0 \end{aligned} \tag{3.52}$$

Where $\varepsilon_{yc} = y_{c_{ref}} - y_c$ and $\varepsilon_{yz_k} = y_{zk_{ref}} - y_{zk}$.

The parallel system operating point will be stable if the coefficients k_{11}, k_{12}, k_{13}, k_{21}, k_{22} are strictly positive values. The dynamics of the system will be fixed by these gains associated with the control laws.

To determine values of the gain coefficients, a pole placement method is used thanks to a comparison between the characteristic polynomials associated (3.53) with the polynomials (3.52) therefore, the control gains parameters can be defined as:

$$\begin{aligned} p_{yc}(s) &= (s+p_1)\,(s^2+2\xi_{yc}.\omega_{yc}.s+\omega_n^2) \\ p_{yz}(s) &= s^2+2\xi_{yz}.\omega_{yz}.s+\omega_{yz}^2 \end{aligned} \tag{3.53}$$

$$\begin{cases} k_{11} &= 2\xi_c.\omega_{yc}+p_1 \\ k_{12} &= 2\xi_c.\omega_{yc}.p_1+\omega_{yc}^2 \\ k_{13} &= p_{yc}.\omega_{yc}^2 \end{cases} \tag{3.54}$$

$$\begin{cases} k_{21} &= 2\xi_z.\omega_{yz} \\ k_{22} &= \omega_{yz}^2 \end{cases} \tag{3.55}$$

Finaly the close loop control is given by :

$$\begin{aligned} \begin{pmatrix} V_{d_1} \\ V_{q_1} \end{pmatrix} &= \begin{pmatrix} \psi_{Vd1}(y_{c_{reff-f}}, \dot{y}_{c_{ref-f}}, \gamma_c, y_{z_{ref-f}}, \gamma_z) \\ \psi_{Vq1}(y_{c_{ref-f}}, \dot{y}_{c_{ref-f}}, \gamma_c, y_{z_{ref-f}}, \gamma_z) \end{pmatrix} \\ \begin{pmatrix} V_{0_k} \\ V_{d_k} \\ V_{q_k} \end{pmatrix} &= \begin{pmatrix} \psi_{V0k}(y_{zk_{ref-f}}, \gamma_z) \\ \psi_{Vdk}(y_{c_{ref-f}}, \dot{y}_{c_{ref-f}}, \gamma_c, y_{z_{ref-f}}, \gamma_z) \\ \psi_{Vqk}(y_{c_{ref-f}}, \dot{y}_{c_{ref-f}}, \gamma_c, y_{z_{ref-f}}, \gamma_z) \end{pmatrix} \end{aligned} \tag{3.56}$$

3.3.4 simulations and results

To validate the proposed control method, a model based on *MATLAB-Simulink SimPower* has been performed using two parallel inverters,The system parameters and the control gains,experimental validations are listed in Table. 3.1 and Table. 3.2, The schematic diagram of the proposed control system is given in Figure. 3.2.

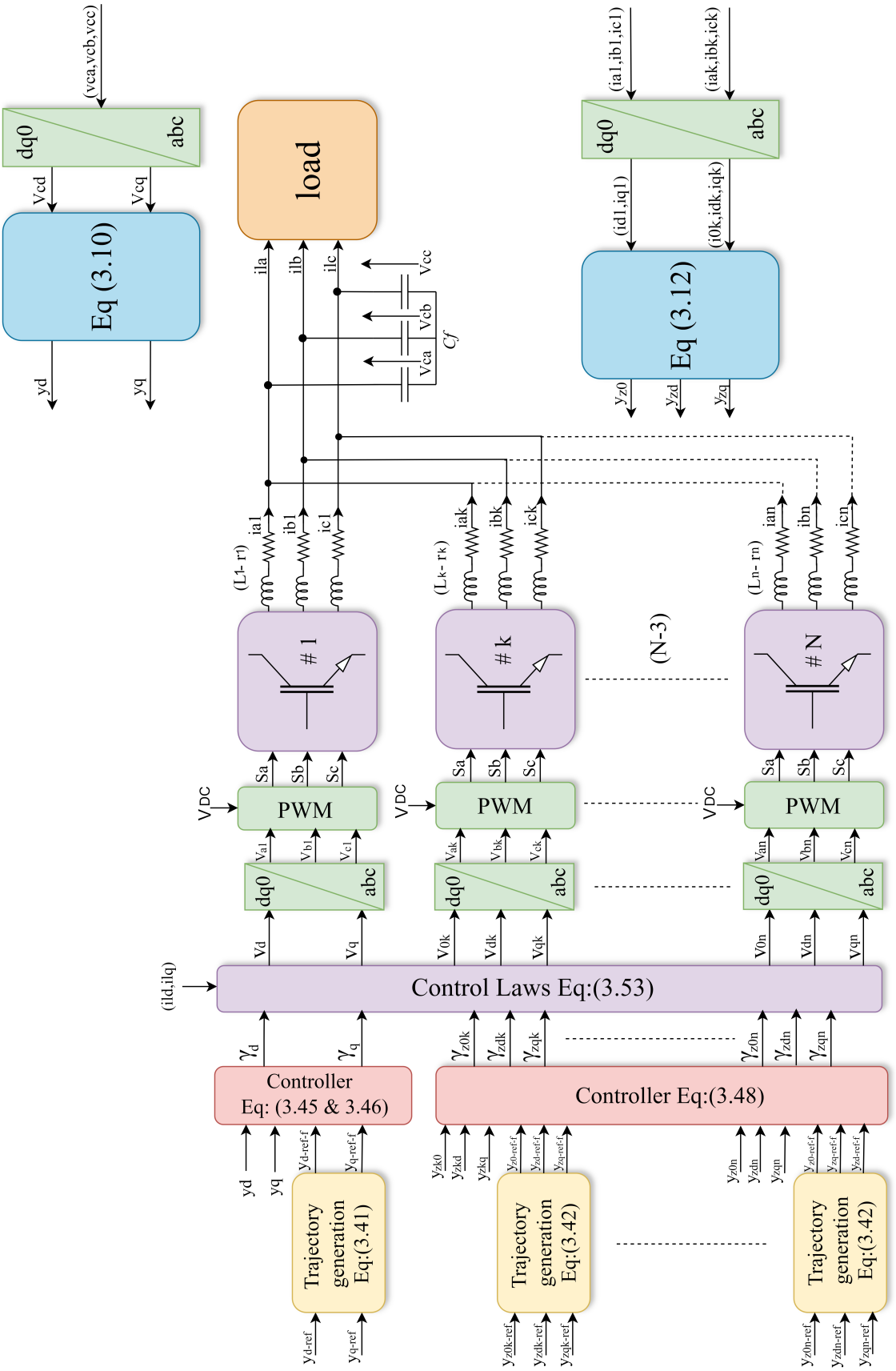

Figure 3.2: Proposed Control Diagram

Table 3.1: Parameters of a two-inverter structure

Parameter	**Value**
Time constants of reference trajectories (τ_1, τ_2)	0.01 ms
Line inductances (L_1)	8 mH
Line resistances (r_1)	0.5 Ω
Capacitance (C_f)	50 μF
Vdc voltage	400 V
Output voltage characteristic	110 V, 50 Hz
Switching frequency (f_{sw})	25 kHz

Table 3.2: Parameter Table of gain values

Parameter	**Value**
Angular frequency (ω_{yc})	6000 rpm
Load speed (ω_{yz})	6000 rpm
Damping ratio (ξ_{yc})	0.7
Load damping ratio (ξ_{yz})	0.7
Pole (p_1)	5000

3.3.5 Concept Verification of Flatness

The test aims to verify two main objectives:

1. **Verification of Flatness**: Demonstrate that the system's behavior can be predicted based on the flat output and its derivatives.

2. **Observing the Transient Response**: Analyze how the system dynamically responds during state transitions.

To verify that the concept of flatness applies to the system being studied, we aim to show that the dynamic behavior of the system, specifically the evolution of the state variables, can

be predicted during the transient regime by using the reference trajectories of the flat output and its successive derivatives. By understanding the expected behavior of the flat output and its derivatives, we can accurately determine the overall system behavior during the transition from one state to another.

Figure. 3.3 illustrates a rapid load change where the system's load power escalates from 0 to 5 kW in a brief period. This scenario is specifically chosen to test the system's response under sudden, significant variations in load.

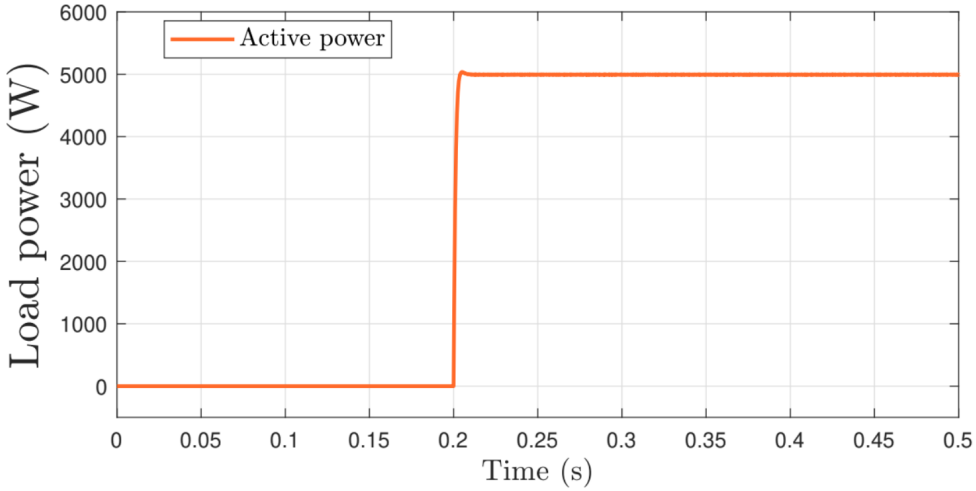

Figure 3.3: Rapid Load Change 0 to 5 kW.

As previously mentioned, the flat output y is illustrated in Figure. 3.4 and Figure. 3.5.

Figure. 3.4 effectively demonstrates that all components of the flat output y_c closely follow their designated reference trajectories, validating the accuracy of the control system in tracking planned paths.

Figure. 3.5 shows the second flat output y_z, whose reference is set to zero to minimize circulation currents. As a result, we observe that the second flat output y_z follows its trajectory effectively.

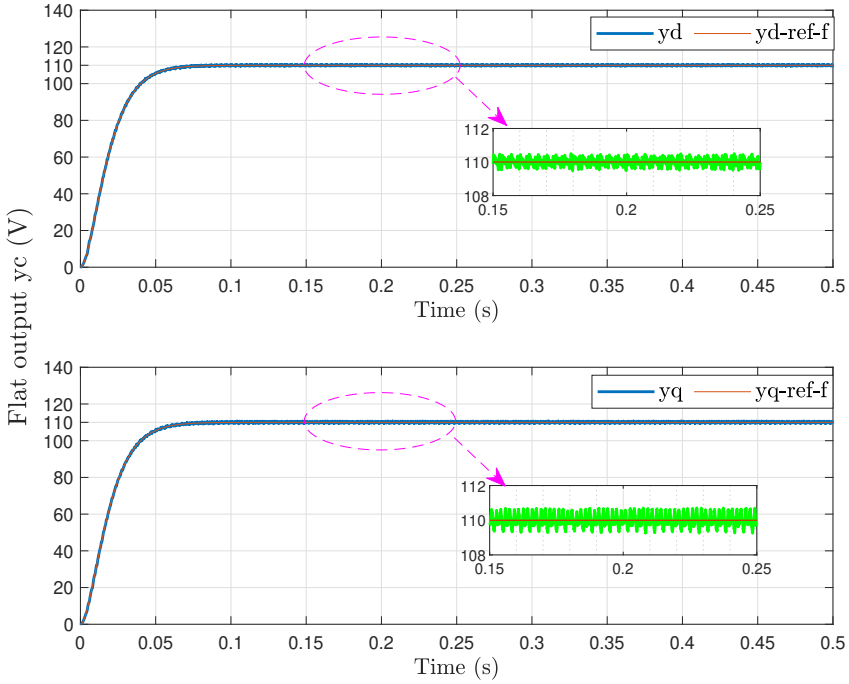

Figure 3.4: Simulation Results: Behavior of Flat Output Components y During a Load Step.

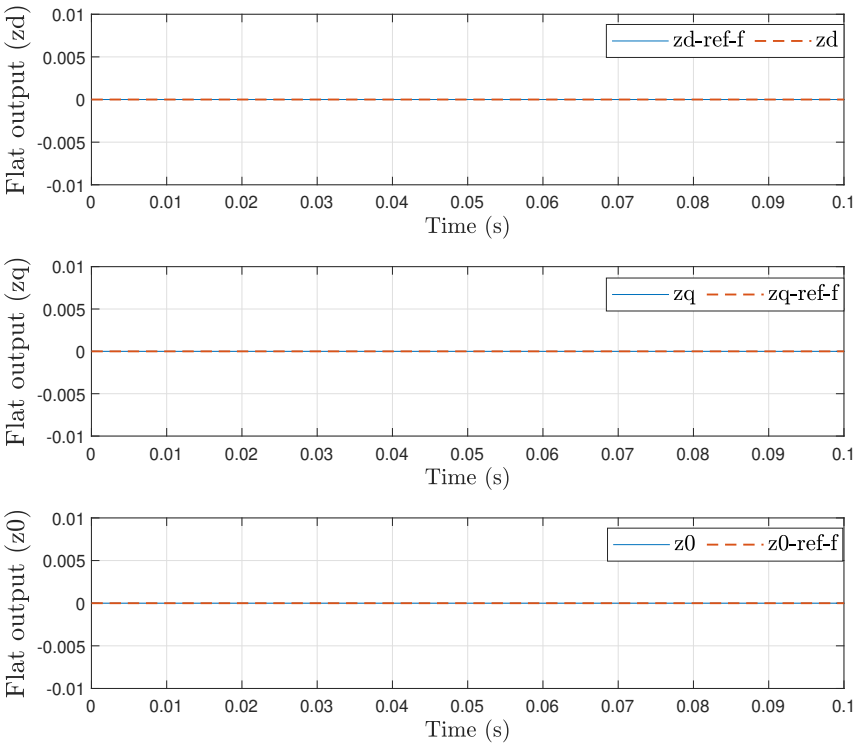

Figure 3.5: Simulation Results: Behavior of Flat Output Components y During a Load Step.

The results depicted in Figure. 3.6 and Figure. 3.7 illustrate that the power sharing between the two inverters is highly precise in active power. This accuracy confirms that the load sharing is effectively achieved, ensuring balanced distribution of power between the inverters.

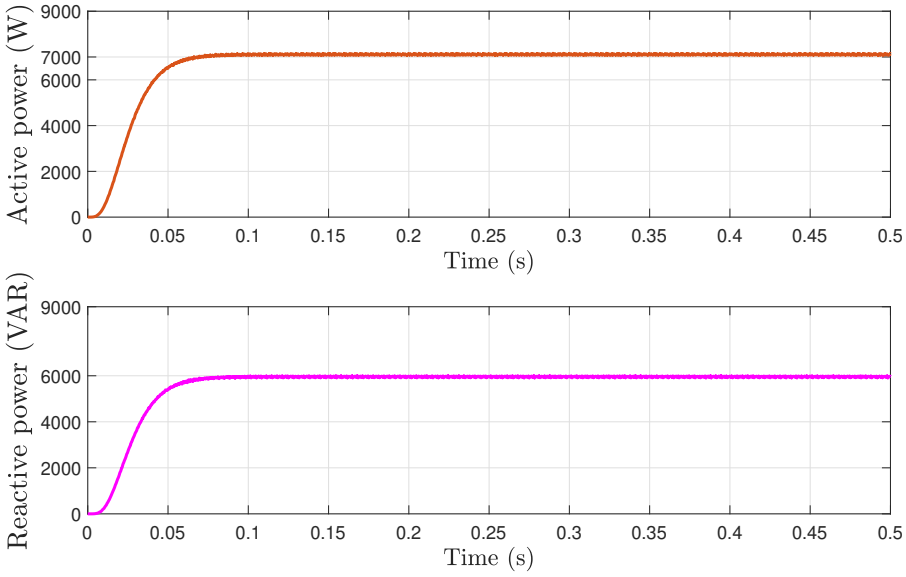

Figure 3.6: Active and Reactive Power.

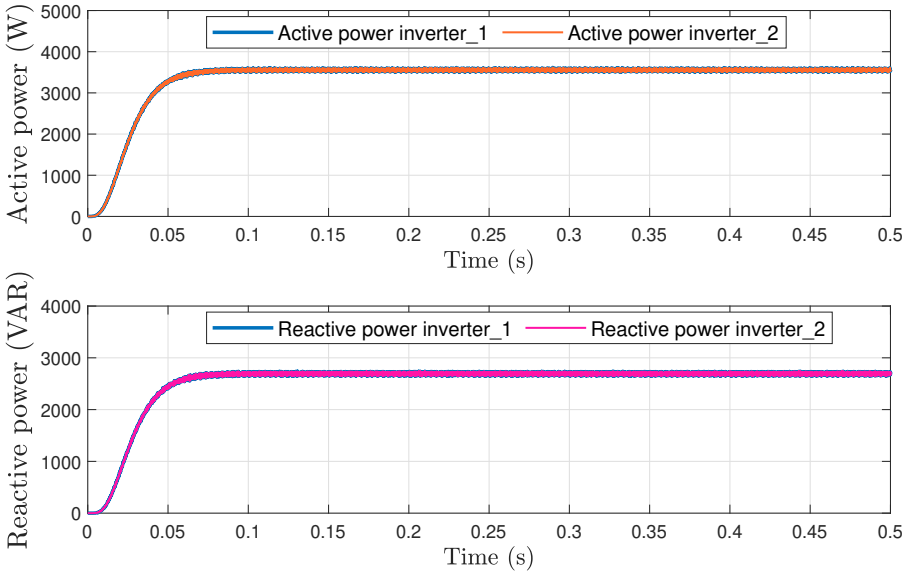

Figure 3.7: Active and Reactive Power of two inverters.

Figure. 3.8 depicts the progression of simulated state variables alongside those determined

through functions specified in (3.14), (3.20) and (3.21), which are computed using the flat output's reference and its derivatives. The state variable trajectories closely adhere to the theoretical paths derived from the reference trajectory associated with the flat output, demonstrating accurate adherence to the modeled behavior.

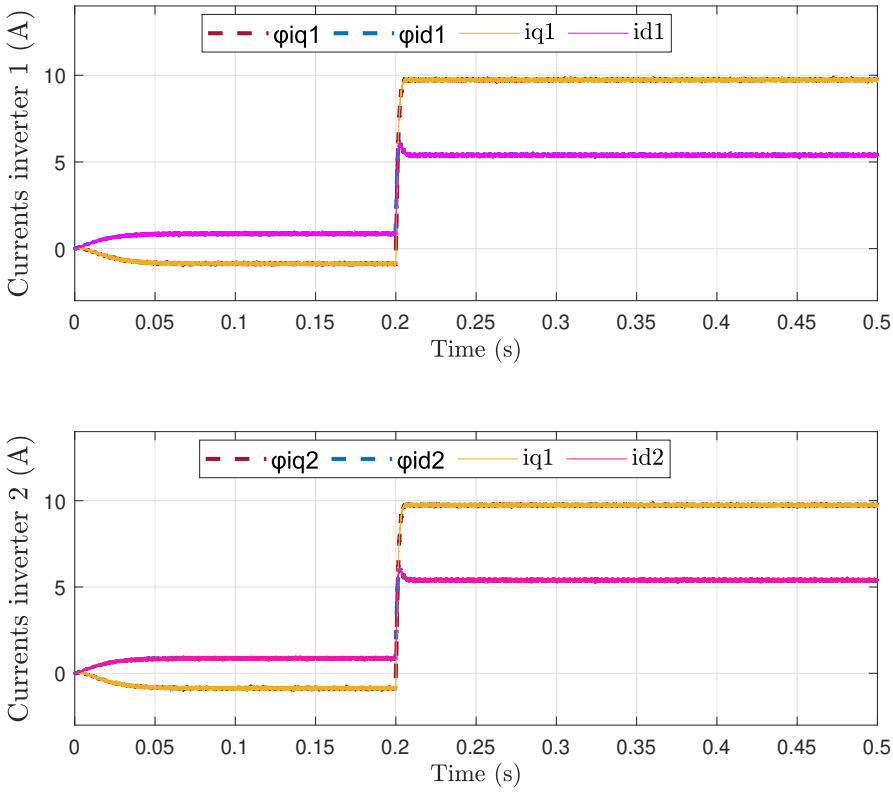

Figure 3.8: Simulation Results: Comparison of Simulated State Variables and Calculated State Variables from Reference Trajectories.

3.3.6 Analysis of Residual Current Behavior in a Three-Phase AC Microgrid Inverter System :

Residual currents, or leakage currents, pose a safety and performance risk in AC microgrids. These unwanted currents flow outside the intended path, often through grounding connections. To assess their behavior and control strategy effectiveness, we analyze three scenarios involving non-ideal inverter conditions:

1. **Identical Inverters (a)**: This baseline case with perfectly matched inverters ideally exhibits minimal to zero residual current.

2. **Non-Identical Inverters with Delay (b)**: A delay introduced in one inverter creates a mismatch, potentially causing residual currents. The control strategy's effectiveness is tested by observing if the dedicated y-z vector corrector can limit these currents. This current remains below $\pm 0.05\,\mathrm{A}$.

3. **Non-Identical Inverters with Parameter Mismatch (c)**: In this case, the inverters are non-identical (similar to Case (b)), but the inductance (L_2) value of the second module is drastically altered to $4\,\mathrm{mh}$, with an additional series resistance of $0.3\,\Omega$. This modification creates a 400% error in the inductance value used by the control algorithm. Despite this significant mismatch, the residual current remains remarkably low, below $\pm 0.3\,\mathrm{A}$. This remarkable outcome underscores the control algorithm's ability to handle parameter uncertainties effectively.

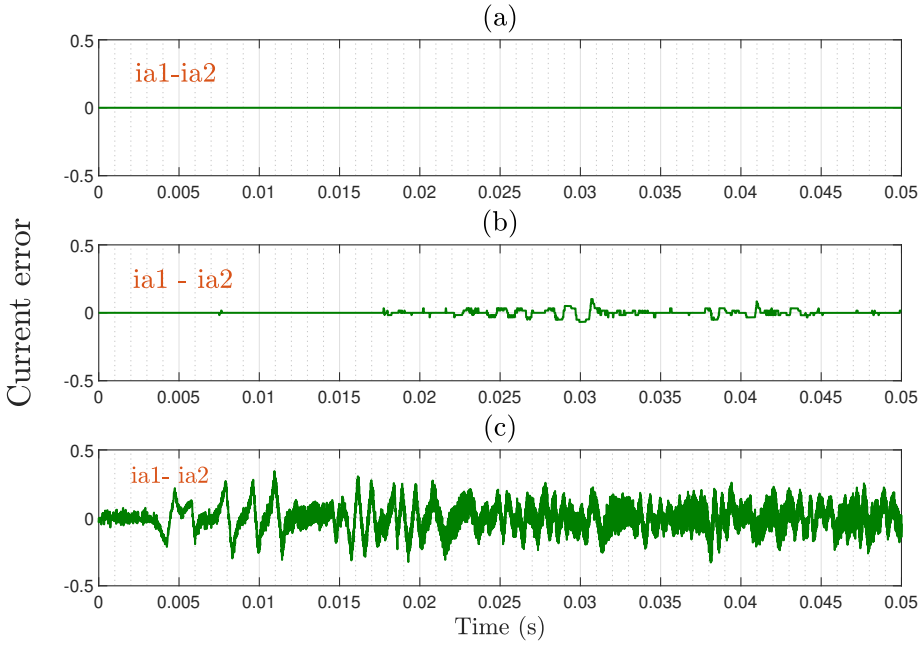

Figure 3.9: Simulation Results: Phase Currents (a1, a2) and Difference Under Load Power of 3.2 kW: Identical(a) vs. Non-Identical Inverters(b) and Parameter Variation (c).

Figure. 3.10 respectively show the behavior of y_z under the test conditions described in case (b). It is observed that the components associated with the vector y_z oscillate around zero with an amplitude of less than $\pm 0.08A$.

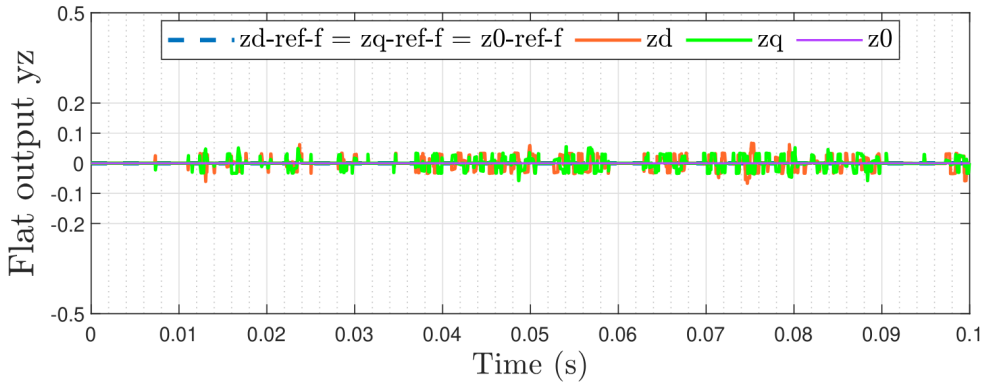

Figure 3.10: Simulation Results:Behavior of Outputs z_d, z_q, and z_0 with $y_{z_{ref}} = 0$.

3.3.7 System Performance

Figure. 3.11 illustrates that the components of the vector y_c adhere to their reference trajectories, facilitating a healthy system startup with a settling time of 2 ms. The second image of the figure proposes to apply a step change from 2 A to 0 A on the reference trajectory of the vector y^z_{ref}. Here, the objective is to demonstrate that the components of the y_z vector accurately follow their designated reference trajectories.

Figure. 3.12 shows the line currents of phases $a1$ and $a2$, as well as their difference, $(i_{a1} - i_{a2})$, in steady state for an active load power of 3.2 kW. The amplitude of the residual current is equal to zero.

Figure. 3.13 displays the voltage and current waveforms for phases a and b, providing critical insights into the system's performance and stability under varying conditions. These waveforms are essential for verifying synchronization and phase behavior, detecting any potential faults or imbalances, and evaluating the effectiveness of control strategies. This analysis confirms that the control system maintains stability and efficiently adapts to operational changes, ensuring reliable system performance. As depicted in Figure. 3.14, the Total Harmonic Distortion (THD) is equal to 0.25, further validating the effectiveness of the control strategies implemented.

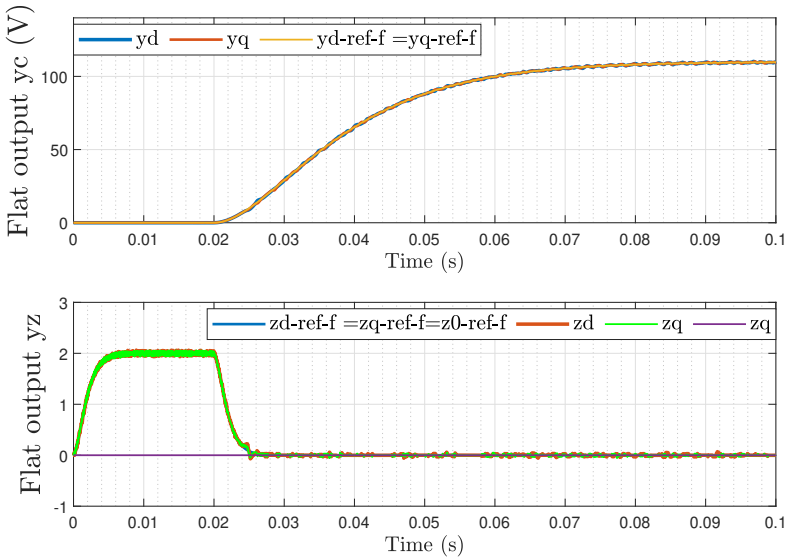

Figure 3.11: Behavior of flat outputs y_d and y_q for a voltage step from 0 to 110V, and behavior of flat outputs z_d, z_q, and z_0 during a step change of y_{ref} from 2 to 0 A.

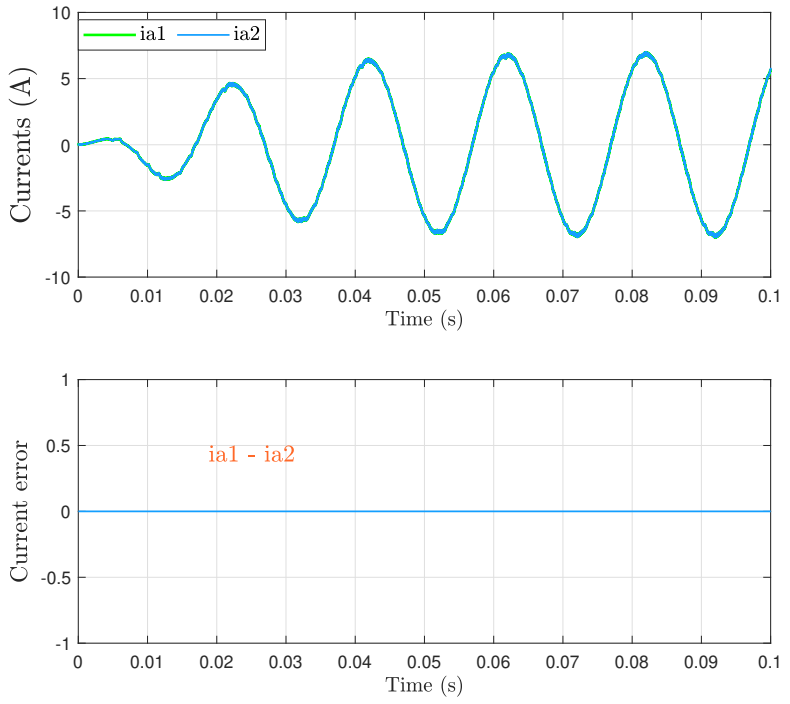

Figure 3.12: line currents of phases $a1$ and $a2$ as well as their difference in steady state, balanced resistive load ($P_{Charge} = 3.2$ kW).

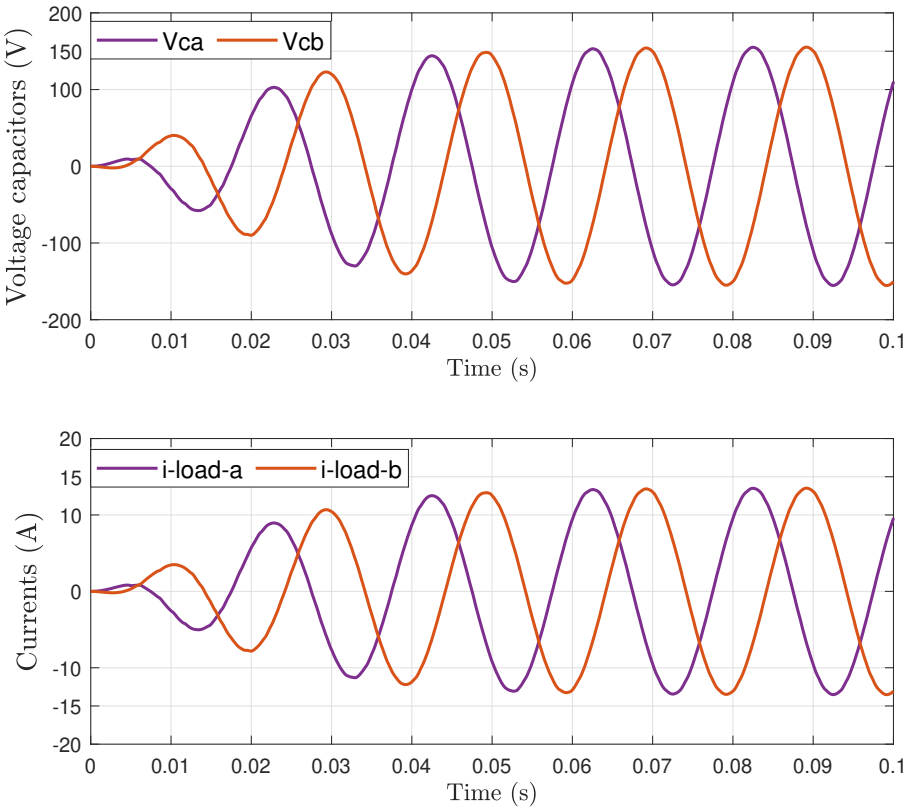

Figure 3.13: Capacitive voltages and load currents in steady state, $P_{Charge} = 3.2$ kW with a regulated AC bus effective voltage of 110 V.

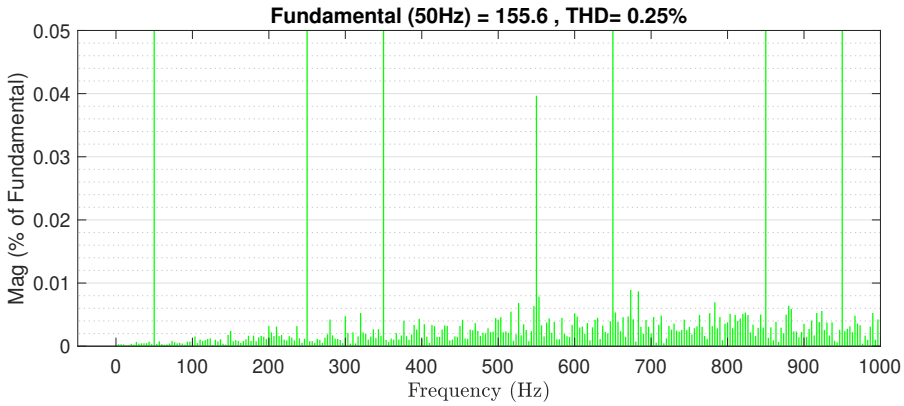

Figure 3.14: Voltage THD of phase a .

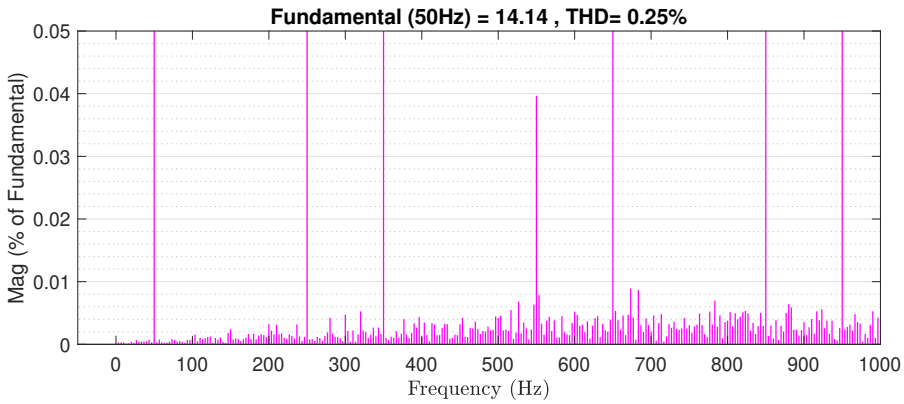

Figure 3.15: Load current THD of phase a.

3.3.8 Dynamic Performance during Load Changes

Figure. 3.16 presents the waveforms of the capacitive voltages and the charging currents for phases (a) and (b) during a step change in active load power from 0 to 3.2 kW. Despite the significant change in load, the waveforms remain stable, demonstrating the system's robustness and effective control.

Figure. 3.17 and Figure. 3.18 respectively show the behavior of the components y_c and y_z during this load variation applied in 4 ms. We observe that the control accurately maintains the reference trajectories of the vectors.

For testing the robustness against parameters uncertainties, the inductor filter $L_{2_{nom}} = 1\,\text{mH}$ is replaced by $L_2 = 4\,\text{mH}$. Figure. 3.19 shows the waveforms of the currents i_{a1}, i_{a2} and their difference $(i_{a1} - i_{a2})$. It can be seen that the control keeps the zero-sequence circulating current below 1 A.

Figure. 3.20 and Figure. 3.21 show the behavior of the proposed control in the case of a nonlinear load consisting of a three-phase diode bridge feeding a resistive load of 3.2 kW.

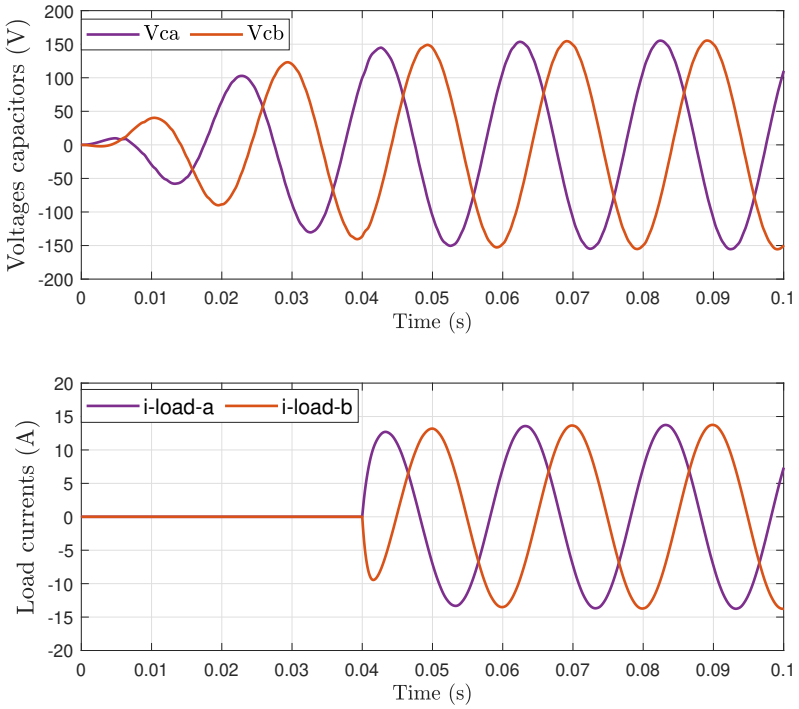

Figure 3.16: Voltages and load currents during a power variation from 0 to 3.2 kW with the AC bus effective voltage regulated at 110 V.

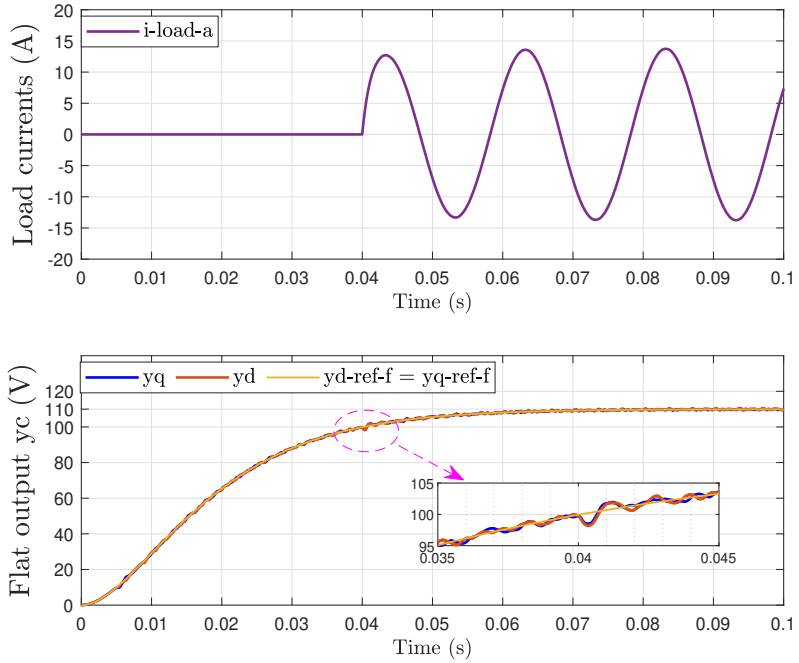

Figure 3.17: Behavior of the flat outputs y_d and y_q during a power variation from 0 to 3.2 kW,110 V.

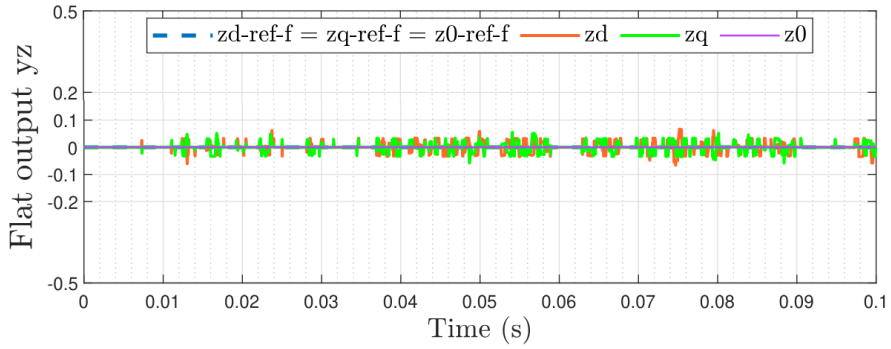

Figure 3.18: Behavior of flat outputs z_d, z_q, and z_0 during a load power variation from 0 to 3.2 kW for a regulated AC bus effective voltage of 110 V.

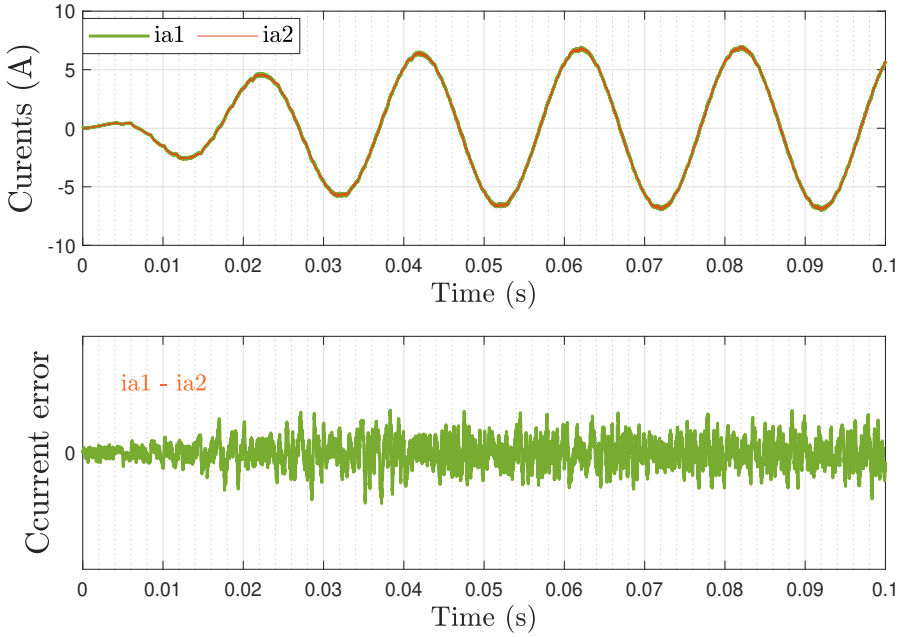

Figure 3.19: Line currents of phases a_1 and a_2, as well as their difference during a change in the physical inductance L_2, $P_{Load} = 3.2$ kW.

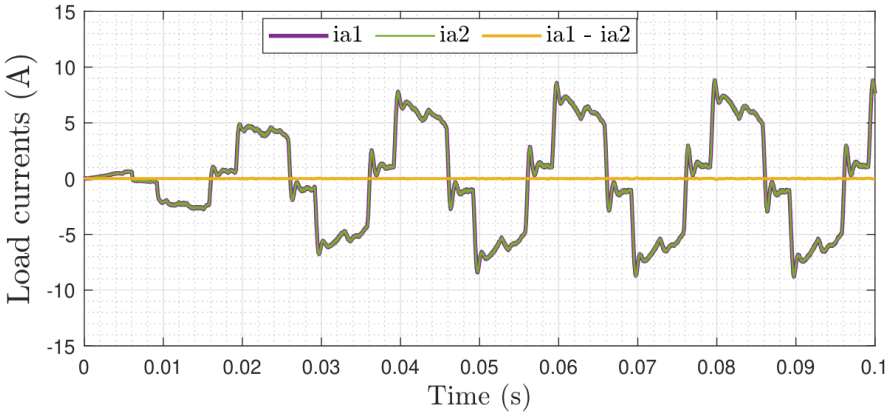

Figure 3.20: Phase line currents a_1 and a_2, along with their difference.

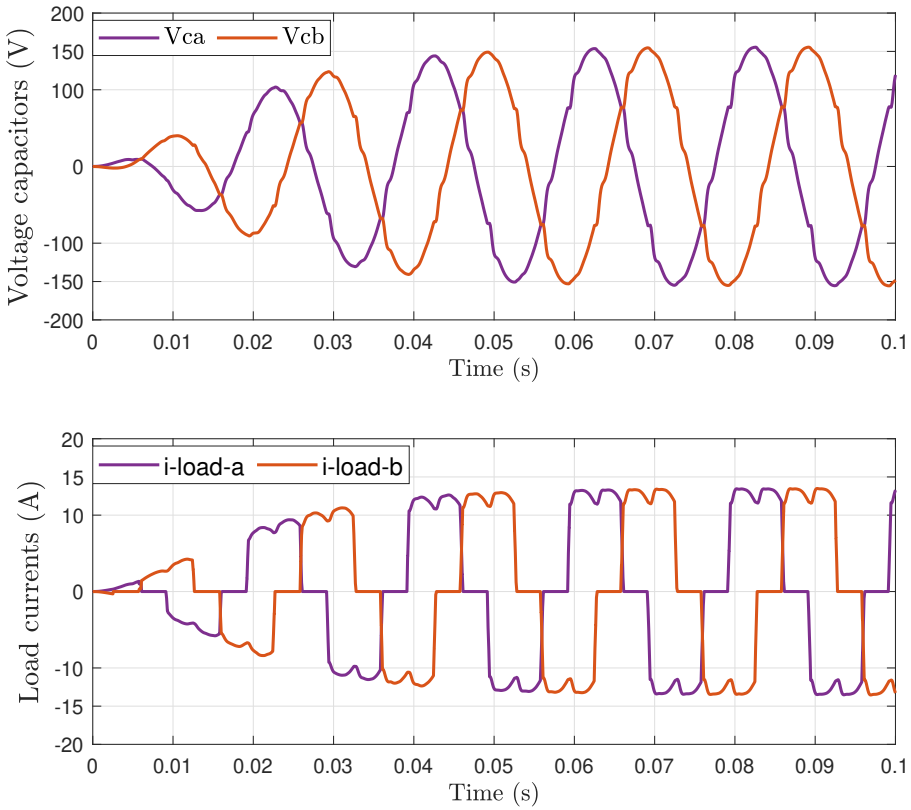

Figure 3.21: Non-linear load case, $P_{\text{Load}} = 3.2$ kW.Load voltages and currents.

3.4 Conclusion

This chapter introduces a parallel system comprising N three-phase inverters equipped with an LC filter. A novel energy control strategy leveraging flatness properties is proposed. The system's flatness is established, ensuring global stability under diverse operating conditions. The reference trajectories are meticulously designed to adhere to power supply constraints.

Moreover, the parallel system is augmented with a current balancing regulator to address requirements such as minimizing circulating currents and achieving balanced currents between the parallel inverters. Experimental results affirm the efficacy of the proposed Flatness-Based Control (FBC) method in regulating the output AC bus voltages and minimizing circulating currents.

To further validate the proposed control strategy, extensive simulations were conducted using Simulink. The main results derived from the simulations can be summarized as follows:

- The system exhibits excellent power quality.
- Trajectory planning enables a smooth and healthy startup of the installation.
- The residual current remains below ± 0.05A for all tested load conditions.
- The response time for load disturbance rejection is impressively short, being less than 0.1 s.

These results underscore the robustness and efficacy of the proposed control strategy in managing parallel inverter systems, ensuring both stability and high performance under various operating conditions. The integration of theoretical analysis and simulation provides a comprehensive validation of the Flatness-Based Control method, paving the way for its application in advanced power electronic systems.

General Conclusion

This dissertation focuses on implementing flatness-based control strategies in AC microgrids (MGs), particularly targeting inverters and multiple inverter systems. The primary objectives are to ensure high-quality energy delivery, achieve superior dynamic performance, and maintain robustness against parametric variations and modeling imperfections. This study highlights the critical role of flatness-based controls in enhancing the stability and efficiency of MGs.

In the opening chapter, we introduced essential concepts concerning MGs, starting with their definitions and categorizations. We also covered the various advantages and disadvantages of these systems, explored different types of inverters, and examined the control strategies employed in managing MGs.

In Chapter 2, the control of a three-phase inverter connected to an LC filter was established. Firstly, we ensured that our system is flat, proving that it possesses a specific structural property that allows for more straightforward control design and trajectory planning,to evaluate the control performance, we employed an open-loop, flatness-based implementation to observe the system's intrinsic response without feedback influences. By simulating the system in open loop, we compared the theoretical predictions with the actual behavior of the system. This helped ensure that the model accurately represents the physical system.

After discussing the open-loop system, we implemented a feedback mechanism to enhance performance. Specifically, we developed a closed-loop system with trajectory tracking to demonstrate the approach's potential. subsequent tests validated the control model under various conditions, Including assessments of energy quality, we conducted the first test under the presence of a 1 kW resistive and nonlinear load. Remarkably, the system performed well. To quantify the energy quality, we measured the Total Harmonic Distortion (THD) of the output voltage and current,our measurements revealed that the THD was equal to 0.05% This low THD indicates

effective mitigation of harmonic distortions,the low value of voltage THD in the case of flatness controller is mainly due to the use of reference reaction instead of disturbance reaction.
In the second test, we applied a heavy sudden load for 0.1 seconds to test the system's response in terms of voltage and current. The simulation results showed that the system stabilized very quickly, within milliseconds,to further validate our control approach, we conducted a third test that had two parts. In the first part, we varied the filter parameters, changing the capacitance and the inductance than we applied a load ranging from 0 kW (no load) to 12 kW (full load). This rapid change mimics real-world scenarios where power demand fluctuates quickly,the results of both parts showed that the control approach effectively handles these dynamic load changes, demonstrating its robustness and adaptability.

In the third chapter, we expanded on the results of controlling a single inverter to develop and control multiple inverters in parallel using the FBC strategy. We defined one inverter as the master to impose the output voltage, while the others were designated as slaves, regulating only current or power.

The main focus was addressing the problems of circulating current caused by parallel inverters and ensuring effective load sharing between them.

To ensure successful implementation of this control strategy, we conducted several critical tests. These tests included evaluating load sharing accuracy, assessing circulating current mitigation, and measuring overall system stability.

In the third chapter, we expanded on the results of controlling a single inverter to develop and control multiple inverters in parallel using the FBC strategy. We defined one inverter as the master to impose the output voltage, while the others were designated as slaves, regulating only current or power. The main focus was addressing circulating current problems and ensuring effective load sharing between inverters.We conducted several critical tests to validate this control strategy. The results demonstrated that our approach significantly reduced circulating currents, As demonstrated through simulation in MATLAB Simulink with SimPowerSystems, our analysis of two parallel inverters underscores the efficacy of our approach.where the flat output followed its trajectory effectively. Under conditions of non-identical inverters with delay and parameter mismatch, the system maintained residual currents below ± 0.3 A. Additionally, tests confirmed that the yz vector components followed their reference trajectories accurately.Further

tests measured capacitive voltages and load currents in steady state with $P_{\text{Charge}} = 3.2$ kW and a regulated AC bus voltage of 110 V, showing a Total Harmonic Distortion (THD) of only 0.25. We also ensured precise load sharing, with the two inverters equally distributing active power.These findings validate the FBC strategy's effectiveness and reliability in managing multiple inverters in parallel, ensuring precise load distribution and robust system stability under various conditions.

Bibliography

[1] Amjad Anvari-Moghaddam. *Microgrid Design and Operation: Toward Smart Energy in Cities*. Springer, 2020.

[2] Amjad Anvari-Moghaddam et al. A comprehensive review on microgrid technology. *International Journal of Electrical Power & Energy Systems*, 83:372–383, 2017.

[3] S. Bacha, I. Munteanu, and A. I. Bratcu. *Power Electronic Converters Modeling and Control - with Case Studies*. Advanced Textbooks in Control and Signal Processing. Springer, September 2013.

[4] Ahmed Bouraiou, Ammar Neçaibia, Nadir Boutasseta, Saad Mekhilef, Rachid Dabou, Aberrezzaq Ziane, Nordine Sahouane, Issam Attoui, Mohammed Mostefaoui, and Oussama Touaba. Status of renewable energy potential and utilization in algeria. *Journal of Cleaner Production*, page 119011, 2020. Journal Pre-proof.

[5] B. Cougo, T. Meynard, and G. Gateau. Parallel three-phase inverters: Optimal pwm method for flux reduction in intercell transformers. *IEEE Transactions on Power Electronics*, 26(8):2184–2191, August 2011.

[6] M. Dehghan, M. Doraghi, and H. Mokhtari. A novel robust decentralized control strategy for parallel-connected inverters in microgrids under islanding and grid-connected modes. *IEEE Transactions on Power Electronics*, 26(3):876–885, 2011.

[7] Michel Fliess, Jean Lévine, Philippe Martin, and Pierre Rouchon. Flatness and defect of non-linear systems: introductory theory and examples. *International Journal of Control*, 61(6):1327–1361, 1995.

[8] A. Gensior, J. Rudolph, and H. Güldner. Flatness based control of three-phase boost rectifiers. In *Proc.11th European Conference on Power Electronics and Applications, EPE 2005, Dresden, Germany*, Sep. 2005.

[9] A. Gensior, O. Woywode, J. Rudolph, and H. Güldner. Boost converter control: comparison of pi-passivity-based and flatness-based methods. In *Power Electronics and Motion Control Rec, EPE-PEMC 2004, Riga, Latvia*, Sep. 2004.

[10] Tim C Green and Marc Prodanovic. A review of key power system stability challenges for future grid inertia scenarios. *Renewable and Sustainable Energy Reviews*, 104:108–118, 2020.

[11] Josep M Guerrero, Jayakrishnan Vasquez, Juan Matas, Luis Garcia de Vicuna, and Mohammad Z Alrifai. Microgrids: Architectures and control. *IEEE Transactions on Industrial Electronics*, 58(10):878–897, 2011.

[12] M. A. Hannan, J. C. Ho, M. S. H. Lipu, and A. Hussain. Review of power sharing control strategies for ac microgrids with renewable energy sources. *IEEE Transactions on Industrial Electronics*, 64(7):5026–5034, 2017.

[13] Nikos Hatziargyriou. Microgrids: Benefits, challenges, and key issues. *IEEE Power and Energy Magazine*, 12(4):35–44, 2014.

[14] A. Houari, A. Battiston, and J.P. Martin. Flatness-based-control for parallel operation of n voltage-source inverters. In *2013 15th European Conference*. IEEE, 2013.

[15] J.-S. Kim, J.-H. Choi, G.-H. Cho, and J.-H. Jeon. Load sharing control of parallel inverters in islanded microgrids using virtual impedance loop. *IEEE Transactions on Power Electronics*, 26(3):886–893, 2011.

[16] Alexis Kwasinski, Srdjan Krstic, Albert Kwasinski, and Svetlana Krstic. Review of microgrid studies and issues toward development of microgrid policy. *IEEE Transactions on Power Systems*, 35(4):897–911, 2020.

[17] James A Momoh. Microgrid energy management systems. *IEEE Power and Energy Society General Meeting*, 2012.

[18] M. Narimani and G. Moschopoulos. Improved method for paralleling reduced switch vsi modules: Harmonic content and circulating current. *IEEE Transactions on Power Electronics*, 29(7):3308–3317, July 2014.

[19] Yelun Peng and John Shen. Multilevel dynamic master-slave control strategy for resilience enhancement of networked microgrids. *Energies*, 15(10):3698, 2022.

[20] J. Purhonen and A. Houari. Title of the paper. *Journal Name*, xx(xx):xx–xx, 2014.

[21] Taoufik Qoria. *Grid-forming Control to Achieve a 100% Power Electronics Interfaced Power Transmission Systems*. Phd thesis, HESAM Université, 2020. ffNNT: 2020HESAE041, fftel-03078479f.

[22] Malek Ramezani, Shuhui Li, and Yang Sun. Dq-reference-frame based impedance and power control design of islanded parallel voltage source converters for integration of distributed energy resources. *Electrical and Computer Engineering Department, University of Alabama, Tuscaloosa, AL, USA*, 2018.

[23] Surya Santoso and H. Wayne Beaty, editors. *Standard Handbook for Electrical Engineers*. McGraw-Hill Education, New York, 17 edition, 2020.

[24] G. Séguier and F. Labrique. *Power Electronic Converters: DC-AC Conversion*. Springer Science & Business Media, 2012.

[25] Hebertt Sira-Ramírez and S.K. Agrawal. *Differentially Flat Systems*. Marcel Dekker Inc., 2004.

[26] United Nations Environment Programme. Emissions gap report 2022: The closing window – climate crisis calls for rapid transformation of societies, 2022.

[27] Y. Wang, Y. Li, and Y. Li. A novel control strategy for parallel inverters based on an improved virtual impedance loop. *Nature Communications*, 14(1):1–10, 2023.